SUPPLEMENTARY RESULTS

Constructing Fan Charts from the Ragged Edge of SPF Forecasts*

Todd E. Clark,[1] Gergely Ganics,[2] and Elmar Mertens[3]

[1]Federal Reserve Bank of Cleveland, [2]Banco de España, [3]Deutsche Bundesbank.

September 3, 2024

Abstract

This online appendix provides results and descriptions that supplement our paper.

Contents

*The views expressed herein are solely those of the authors and do not necessarily reflect the views of the Federal Reserve Bank of Cleveland, the Federal Reserve System, the Banco de España, the Deutsche Bundesbank, or the Eurosystem. Replication files are available at https://github.com/elmarmertens/ClarkGanicsMertensSPFfancharts.

List of Tables

List of Figures

I SPF data and measurements

This appendix provides further information about the survey data used in our paper and obtained from the Survey of Professional Forecasters (SPF) for the US. In addition, this appendix describes additional details about the mapping between the survey data and the model. Finally, this appendix assesses potential inconsistencies between observed SPF forecasts for quarterly and annual forecast targets and the potential for such inconsistencies to generate excessively volatile imputations in our model's term structure of expectation, when assuming that both quarterly and annual forecasts are observed without error.

I(a) Data availability

As described in the paper, we use SPF forecasts for four variables: growth in real GDP, the unemployment rate, and inflation in CPI and GDP prices. For these variables, the SPF provides fairly long samples of data, albeit with differing availabilities of forecasts at different forecast horizons. The availability of forecasts at different horizons for each of the four variables is listed in Table A.1. All forecast data listed in the table is used for our analysis (of course, for our out-of-sample analysis, the data is used only subject to real-time availability).

In principle, to track forecasts for up to three calendar years ahead, our model's state vector should need to track (latent) quarterly forecasts, $F_t y_{t+h}$, for up to $h = 15$ quarters ahead. However, as described in Section 4 of the paper, the paucity of quarterly forecast data at longer horizons allows us to discipline our models by assuming that forecasts converge to a common

Table A.1: Availability of SPF point forecasts

		Fixed-horizon	Fixed-event calendar years		
Variable	Mnemonic	Quarters 0 – 4	next	2-year	3-year
Real GDP	RGDP	1968Q4	1981Q3	2009Q2	2009Q2
Unemployment rate	UNRATE	1968Q4	1981Q3	2009Q2	2009Q2
GDP price index	PGDP	1968Q4	1981Q3	NA	NA
CPI inflation	CPI	1981Q3	1981Q3	2005Q3	NA

Note: The table reports the first quarters in which SPF predictions become available in our data set for the stated variables and horizons. NA stands for not available. Prior to 1992, RGDP corresponds to real GNP, while PGDP corresponds to the GNP implicit deflator. The SPF's published data files include point forecasts for RGDP and PGDP in levels, which we convert to continuously compounded growth rates. The SPF also provides current year predictions that are, however, disregarded in our analysis due to overlap with the quarterly fixed-horizon predictions.

Table A.2: Choice of maximal H in term-structure vector $\boldsymbol{Y_t}$

Variable	Samples	H
RGDP	prior 2009Q2	5
	since 2009Q2	12
UNRATE	prior 2009Q2	5
	since 2009Q2	12
PGDP	entire sample	5
CPI	prior 2005Q4	5
	since 2005Q4	8

trend level sooner than for 15 quarters ahead. We denote the maximal horizon for which we track deviations from trend by H. We generally choose H such that when the forecast origin is in Q1, H points to the first quarter of the farthest annual horizon covered by the SPF forecasts. An exception is made for data covering only SPF forecasts up to the next year, where H is set to 5 (instead of 4), since the observed fixed-horizon SPF forecasts already extend through $h = 4$. As part of our out-of-sample forecast analysis, models are (re-)estimated over different sub-samples of data, and we adjust H accordingly. Reflecting the availability of long-horizon SPF data for different variables, we set H as listed in Table A.2. Note that, even though the state vector ends with $F_t y_{t+H}$ and H is no larger than 12, our endpoint assumption indicated in the paper allows us to simulate forecast densities arbitrarily far ahead, and we report densities up to 16 quarters ahead for all variables throughout.

I(b) Measurement equations

This subsection provides examples of the measurement vector and the loading matrix introduced in Section 4.4 of the main paper, defined as

$$\boldsymbol{Z_t} = \begin{bmatrix} \boldsymbol{Z_{q,t}} \\ \boldsymbol{Z_{a,t}} \end{bmatrix}, \tag{A.1}$$

$$\boldsymbol{C_t} = \begin{bmatrix} \boldsymbol{C_{q,t}} \\ \boldsymbol{C_{a,t}} \end{bmatrix}, \tag{A.2}$$

respectively, where the subscripts (q and a) reflect the partition of the arrays according to the quarterly or annual horizons, and the time index t highlights that these objects vary over time as a function of the available measurements. In the following examples, we take $t = 2024Q1$ as the first forecast origin, and then illustrate how the corresponding elements change when we move to the next quarter, $t = 2024Q2$. Before illustrating the measurement equations with examples for each variable and at different forecasting origins, we review the data definitions used throughout the paper for outcome variables and SPF data.

I(b.1) Data definitions

As indicated in the paper, the (quarterly) outcome variable y_t refers to the following data definitions for each variable:

RGDP: We measure GDP growth by the annualized quarterly growth rate (400 times the log change) of real GDP.

UNRATE: The quarterly average level of the unemployment rate.

PGDP: We measure inflation in GDP prices by the annualized quarterly growth rate of the GDP deflator (as with RGDP, calculated as 400 times the quarterly log change).

CPI: For CPI inflation, we take the annualized simple growth rate of quarterly CPI levels.

For each variable, we denote quarterly outcomes as defined above by y_t.

Considering their treatment in the SPF, the variables listed above can broadly be categorized into two groups: Variables from the national income and product accounts (NIPA) and non-NIPA variables. The NIPA variables are GDP growth and GDP price inflation, while the non-NIPA variables are the unemployment rate and CPI inflation.

For the non-NIPA variables, the SPF provides forecasts for the data definitions stated above. In addition, for the non-NIPA variables, annual forecasts can be represented as four-quarter averages of y_t over the calendar year, whose realization we denote by $\bar{y}_t$, as defined in equation (11) of the paper:

$$\bar{y}_t = \frac{1}{4} \cdot \sum_{j=0}^{3} y_{t-j} \,. \tag{11}$$

For the unemployment rate, the annual forecast targets are defined as annual average levels. For CPI inflation the annual forecasts target Q4/Q4 growth, which we approximate by the arithmetic four-quarter mean of quarterly growth rates (so as to avoid further transformations of the SPF quarterly forecasts).

In contrast, for the NIPA variables, the SPF provides (in the publicly available data files) forecasts in levels. We convert these to log growth rates.[1] Moreover, SPF calendar-year forecasts for NIPA variables reflect annual-average levels. Denoting the quarterly level of a NIPA variable by I_t, growth in the annual-average level for the calendar year ending at quarter t is measured in equation (12) of our paper as follows:

$$\hat{y}_t \equiv 100 \times \log\left(\frac{I_t + I_{t-1} + I_{t-2} + I_{t-3}}{I_{t-4} + I_{t-5} + I_{t-6} + I_{t-7}}\right), \tag{12}$$

Of course, the definition of $\hat{y}_t$ is non-linear, and to capture annual forecasts for GDP growth (and inflation in GDP prices) we employ a log-linear approximation involving 7 quarterly growth rates. The approximation itself has been popularized by the work of Mariano and Murasawa (2003) on nowcasting, and its accuracy has been favorably evaluated in the context of SPF forecasts by (amongst others) Patton and Timmermann (2011). Moreover, the approximation is commonly used in the related literature on SPF forecasts, with notable examples provided by Aruoba (2020), Crump, et al. (2023), and Patton and Timmermann (2011). Specifically, this is a log-linear approximation, around a steady-state of zero growth, $I_t/I_{t-j} = 1$ for all j, and with $y_t \equiv 400 \cdot \log(I_t/I_{t-1})$, and is equation (13) of the paper we get:

$$\begin{aligned} \hat{y}_t &\approx \frac{100}{4} \cdot \left(\log\frac{I_t}{I_{t-4}} + \log\frac{I_{t-1}}{I_{t-5}} + \log\frac{I_{t-2}}{I_{t-6}} + \log\frac{I_{t-3}}{I_{t-7}}\right), \\ &= 1/16 \cdot (y_t + 2 \cdot y_{t-1} + 3 \cdot y_{t-2} + 4 \cdot y_{t-3} + 3 \cdot y_{t-4} + 2 \cdot y_{t-5} + y_{t-6}) \,. \end{aligned} \tag{13}$$

[1] Similar transformations are also applied, for example, by Aruoba (2020) and others.

The measurement equations of our model, described further below, use the approximation in (13) to relate the annual SPF forecasts measured as in (12) to forecasts (or lagged realizations) of y_t.

To recap, the SPF provides forecasts for targets y_{t+h}, $\bar{y}_{t+h}$ (annual forecasts of non-NIPA variables), and $\hat{y}_{t+h}$ (annual forecasts of NIPA variables). To match forecasts of annual average levels and their growth rates, $t+h$ should, of course, correspond to a date in Q4, so that $\bar{y}_{t+h}$ and $\hat{y}_{t+h}$ denote outcomes that are realized at the end of a calendar year. We denote the corresponding SPF forecasts collected at forecast origin t by $F_t y_{t+h}$, $F_t \bar{y}_{t+h}$, and $F_t \hat{y}_{t+h}$, respectively. At time t, we match observed forecasts from the SPF with measurement equations for $F_t y_{t+h}$, $F_t \bar{y}_{t+h}$, and/or $F_t \hat{y}_{t+h}$, for different (but separate) values of $h \geq 0$. We treat the calendar-year forecasts of the unemployment rate and CPI inflation as readings of $F_t \bar{y}_{t+h}$, while treating annual forecasts for growth in real GDP and GDP prices as data on $F_t \hat{y}_{t+h}$. The remainder of this appendix describes the details of this matching with specific examples for each variable.

I(b.2) Real GDP growth

In $\boldsymbol{Z}_{\boldsymbol{q},2024Q1}$, we have y_{2023Q4} (real GDP growth of 2023Q4) and quarterly SPF point forecasts (as of 2024Q1) targeting 2024Q1, 2024Q2, 2024Q3, 2024Q4 and 2025Q1, formally:

$$\boldsymbol{Z}_{\boldsymbol{q},2024Q1} = \left[y_{2023Q4}, F_{2024Q1} y_{2024Q1}, F_{2024Q1} y_{2024Q2}, F_{2024Q1} y_{2024Q3}, F_{2024Q1} y_{2024Q4}, F_{2024Q1} y_{2025Q1} \right]' . \tag{A.3}$$

In $\boldsymbol{Z}_{\boldsymbol{a},2024Q1}$, we have annual real GDP forecasts targeting 2025, 2026 and 2027 (note that annual forecasts are associated with the fourth quarter of the target year):

$$\boldsymbol{Z}_{\boldsymbol{a},2024Q1} = \left[F_{2024Q1} \hat{y}_{2025Q4}, F_{2024Q1} \hat{y}_{2026Q4}, F_{2024Q1} \hat{y}_{2027Q4} \right]' . \tag{A.4}$$

The loading matrix takes the following form:

$$\boldsymbol{C}_{2024\text{Q1}} = \left[\begin{array}{c} \boldsymbol{C}_{\boldsymbol{q},2024\text{Q1}} \\ \hline \boldsymbol{C}_{\boldsymbol{a},2024\text{Q1}} \end{array}\right] \tag{A.5}$$

$$= \left[\begin{array}{cccccccccccccc} 1 & 0 & 0 & 0 & 0 & 0 & 0 & 0 & 0 & 0 & 0 & 0 & 0 & 0 \\ 0 & 1 & 0 & 0 & 0 & 0 & 0 & 0 & 0 & 0 & 0 & 0 & 0 & 0 \\ 0 & 0 & 1 & 0 & 0 & 0 & 0 & 0 & 0 & 0 & 0 & 0 & 0 & 0 \\ 0 & 0 & 0 & 1 & 0 & 0 & 0 & 0 & 0 & 0 & 0 & 0 & 0 & 0 \\ 0 & 0 & 0 & 0 & 1 & 0 & 0 & 0 & 0 & 0 & 0 & 0 & 0 & 0 \\ 0 & 0 & 0 & 0 & 0 & 1 & 0 & 0 & 0 & 0 & 0 & 0 & 0 & 0 \\ \hline 0 & 0 & \frac{1}{16} & \frac{2}{16} & \frac{3}{16} & \frac{4}{16} & \frac{3}{16} & \frac{2}{16} & \frac{1}{16} & 0 & 0 & 0 & 0 & 0 \\ 0 & 0 & 0 & 0 & 0 & 0 & \frac{1}{16} & \frac{2}{16} & \frac{3}{16} & \frac{4}{16} & \frac{3}{16} & \frac{2}{16} & \frac{1}{16} & 0 \\ 0 & 0 & 0 & 0 & 0 & 0 & 0 & 0 & 0 & 0 & \frac{1}{16} & \frac{2}{16} & \frac{3}{16} & \frac{4}{16} \end{array}\right], \tag{A.6}$$

where the horizontal line marks the distinction between the mapping into quarterly (upper part) and annual average (lower part) growth rates. Also, note that the loading matrix reflects the assumption that the term structure of SPF-consistent forecasts is flat beyond $H = 12$. In other words, the gaps $\tilde{Y}_{t+H+j}$ are assumed to be zero for all $j > 0$ (thus $\tilde{Y}_{2027\text{Q2}} = \tilde{Y}_{2027\text{Q3}} = \cdots = 0$), and at those horizons only the trend loading matters, hence the forecasts are set identical to the trend, with zero gaps.

When we move to the next quarter, $t = 2024\text{Q2}$, in $\boldsymbol{Z}_{\boldsymbol{q},2024\text{Q2}}$ we have $y_{2024\text{Q1}}$ (real GDP growth of 2024Q1) and quarterly SPF point forecasts (as of 2024Q2) targeting 2024Q2, 2024Q3, 2024Q4, 2025Q1 and 2025Q2, formally:

$$\boldsymbol{Z}_{\boldsymbol{q},2024\text{Q2}} = \left[y_{2024\text{Q1}}, F_{2024\text{Q2}} y_{2024\text{Q2}}, F_{2024\text{Q2}} y_{2024\text{Q3}}, F_{2024\text{Q2}} y_{2024\text{Q4}}, F_{2024\text{Q2}} y_{2025\text{Q1}}, F_{2024\text{Q2}} y_{2025\text{Q2}}\right]', \tag{A.7}$$

hence compared to equation (A.3) all quarterly forecast targets (and the lagged realization) move ahead by one quarter.

In $\boldsymbol{Z}_{\boldsymbol{a},2024\text{Q2}}$, we have annual real GDP forecasts targeting 2025, 2026 and 2027, as before, but as annual forecasts are associated with the fourth quarter of the target year, the forecast horizons shrink by one quarter relative to equation (A.4):

$$\boldsymbol{Z}_{\boldsymbol{a},2024\text{Q2}} = \left[F_{2024\text{Q2}} \hat{y}_{2025\text{Q4}}, F_{2024\text{Q2}} \hat{y}_{2026\text{Q4}}, F_{2024\text{Q2}} \hat{y}_{2027\text{Q4}}\right]'. \tag{A.8}$$

The loading matrix, $\boldsymbol{C}_{2024\text{Q2}}$, has the following components:

$$\boldsymbol{C}_{\boldsymbol{q},2024\text{Q2}} = \begin{bmatrix} 1 & 0 & 0 & 0 & 0 & 0 & 0 & 0 & 0 & 0 & 0 & 0 & 0 & 0 \\ 0 & 1 & 0 & 0 & 0 & 0 & 0 & 0 & 0 & 0 & 0 & 0 & 0 & 0 \\ 0 & 0 & 1 & 0 & 0 & 0 & 0 & 0 & 0 & 0 & 0 & 0 & 0 & 0 \\ 0 & 0 & 0 & 1 & 0 & 0 & 0 & 0 & 0 & 0 & 0 & 0 & 0 & 0 \\ 0 & 0 & 0 & 0 & 1 & 0 & 0 & 0 & 0 & 0 & 0 & 0 & 0 & 0 \\ 0 & 0 & 0 & 0 & 0 & 1 & 0 & 0 & 0 & 0 & 0 & 0 & 0 & 0 \end{bmatrix}, \tag{A.9}$$

and

$$\boldsymbol{C}_{\boldsymbol{a},2024\text{Q2}} = \begin{bmatrix} 0 & \frac{1}{16} & \frac{2}{16} & \frac{3}{16} & \frac{4}{16} & \frac{3}{16} & \frac{2}{16} & \frac{1}{16} & 0 & 0 & 0 & 0 & 0 & 0 \\ 0 & 0 & 0 & 0 & 0 & \frac{1}{16} & \frac{2}{16} & \frac{3}{16} & \frac{4}{16} & \frac{3}{16} & \frac{2}{16} & \frac{1}{16} & 0 & 0 \\ 0 & 0 & 0 & 0 & 0 & 0 & 0 & 0 & 0 & \frac{1}{16} & \frac{2}{16} & \frac{3}{16} & \frac{4}{16} & \frac{3}{16} \end{bmatrix}. \tag{A.10}$$

with

$$\boldsymbol{C}_{2024\text{Q2}} = \begin{bmatrix} \boldsymbol{C}_{\boldsymbol{q},2024\text{Q2}} \\ \hline \boldsymbol{C}_{\boldsymbol{a},2024\text{Q2}} \end{bmatrix}. \tag{A.11}$$

Compared to $\boldsymbol{C}_{2024\text{Q1}}$ in equation (A.6), in equation (A.9) we see that $\boldsymbol{C}_{\boldsymbol{q},2024\text{Q2}} = \boldsymbol{C}_{\boldsymbol{q},2024\text{Q1}}$ (i.e., the loadings associated with the lagged realization and the fixed-horizon forecasts remain unchanged), while the non-zero elements of the first two rows of $\boldsymbol{C}_{\boldsymbol{a},2024\text{Q1}}$ in equation (A.10) shift to the left, and so does the third row, with the weight $\frac{3}{16}$ appearing as the last (bottom right) entry (i.e., the loadings associated with the fixed-event forecasts change, in line with shrinking forecast horizons).

In case of a forecast origin in Q3, the measurement vector and loadings can be constructed analogously to the previous examples. However, when the forecast origin is in Q4, we need to adapt the procedures, on account of the next-year growth rate being modeled as a linear combination of growth rates in several quarters that also comprise the 2nd quarter of the current year, i.e., y_{t-2}, whereas the state vector comprises only y_{t-1}, and $F_t y_{t+h}$ for $h \geq 0$. In principle, a measure of y_{t-2} is contained in the lagged state vector. However, in our measurements, the lagged realization of GDP growth contained in $\boldsymbol{Y_t}$ is informed by the first release data available at the time t round of the SPF. Instead, when t is in Q4, the reading of y_{t-2} relevant for

constructing $F_t\hat{y}_{t+4}$ should be provided by the time t vintage of GDP data. Thus, short of tracking data revisions in our state space, we adjust the data construction and measurement loading for $F_t\hat{y}_{t+4}$, when t is in Q4. Specifically, we define:

$$F^{Q4}_{t+4}\hat{y}_{t+4} \equiv \frac{16}{15} \cdot \left(F_{t+4}\hat{y}_{t+4} - \frac{y_{t-2}}{16}\right) \tag{A.12}$$

$$= \frac{1}{15}\left(y_{t+4} + 2 \cdot y_{t+3} + 3 \cdot y_{t+2} + 4 \cdot y_{t+1} + 3 \cdot y_t + 2 \cdot y_{t-1}\right). \tag{A.13}$$

Consider the example of $t = 2023\text{Q4}$.[2] The measurement vector and associated loadings for the SPF's quarterly fixed-horizon forecasts remains unchanged relative to our earlier examples for forecast origins in Q1 and Q2. However, considering the annual fixed-event forecasts, the measurement vector becomes

$$\boldsymbol{Z_a}_{,2023\text{Q4}} = \left[F^{Q4}_{2023\text{Q4}}\hat{y}_{2024\text{Q4}}, F_{2023\text{Q4}}\hat{y}_{2025\text{Q4}}, F_{2023\text{Q4}}\hat{y}_{2026\text{Q4}}\right]', \tag{A.14}$$

and the associated measurement loadings are as follows:

$$\boldsymbol{C_a}_{,2023\text{Q4}} = \begin{bmatrix} \frac{2}{15} & \frac{3}{15} & \frac{4}{15} & \frac{3}{15} & \frac{2}{15} & \frac{1}{15} & 0 & 0 & 0 & 0 & 0 & 0 & 0 & 0 \\ 0 & 0 & 0 & \frac{1}{16} & \frac{2}{16} & \frac{3}{16} & \frac{4}{16} & \frac{3}{16} & \frac{2}{16} & \frac{1}{16} & 0 & 0 & 0 & 0 \\ 0 & 0 & 0 & 0 & 0 & 0 & 0 & \frac{1}{16} & \frac{2}{16} & \frac{3}{16} & \frac{4}{16} & \frac{3}{16} & \frac{2}{16} & \frac{1}{16} \end{bmatrix}. \tag{A.15}$$

I(b.3) Unemployment rate

In $\boldsymbol{Z_q}_{,2024\text{Q1}}$, we have $y_{2023\text{Q4}}$ (unemployment rate in 2023Q4) and quarterly SPF point forecasts (as of 2024Q1) targeting 2024Q1, 2024Q2, 2024Q3, 2024Q4 and 2025Q1, formally:

$$\boldsymbol{Z_q}_{,2024\text{Q1}} = \left[y_{2023\text{Q4}}, F_{2024\text{Q1}}y_{2024\text{Q1}}, F_{2024\text{Q1}}y_{2024\text{Q2}}, F_{2024\text{Q1}}y_{2024\text{Q3}}, F_{2024\text{Q1}}y_{2024\text{Q4}}, F_{2024\text{Q1}}y_{2025\text{Q1}}\right]'. \tag{A.16}$$

In $\boldsymbol{Z_a}_{,2024\text{Q1}}$, we have annual average unemployment rate forecasts targeting 2025, 2026 and 2027 (note that annual forecasts are associated with the fourth quarter of the target year):

$$\boldsymbol{Z_a}_{,2024\text{Q1}} = \left[F_{2024\text{Q1}}\bar{y}_{2025\text{Q4}}, F_{2024\text{Q1}}\bar{y}_{2026\text{Q4}}, F_{2024\text{Q1}}\bar{y}_{2027\text{Q4}}\right]'. \tag{A.17}$$

[2] At the time of writing, the SPF has released only forecast data through 2024Q2. However, we would expect the same definitions to continue to apply also for the 2024Q4 release.

The loading matrix takes the following form:

$$\boldsymbol{C}_{2024\text{Q1}} = \left[\begin{array}{c} \boldsymbol{C}_{\boldsymbol{q},2024\text{Q1}} \\ \hline \boldsymbol{C}_{\boldsymbol{a},2024\text{Q1}} \end{array}\right] = \left[\begin{array}{cccccccccccccc} 1 & 0 & 0 & 0 & 0 & 0 & 0 & 0 & 0 & 0 & 0 & 0 & 0 & 0 \\ 0 & 1 & 0 & 0 & 0 & 0 & 0 & 0 & 0 & 0 & 0 & 0 & 0 & 0 \\ 0 & 0 & 1 & 0 & 0 & 0 & 0 & 0 & 0 & 0 & 0 & 0 & 0 & 0 \\ 0 & 0 & 0 & 1 & 0 & 0 & 0 & 0 & 0 & 0 & 0 & 0 & 0 & 0 \\ 0 & 0 & 0 & 0 & 1 & 0 & 0 & 0 & 0 & 0 & 0 & 0 & 0 & 0 \\ 0 & 0 & 0 & 0 & 0 & 1 & 0 & 0 & 0 & 0 & 0 & 0 & 0 & 0 \\ \hline 0 & 0 & 0 & 0 & 0 & \frac{1}{4} & \frac{1}{4} & \frac{1}{4} & \frac{1}{4} & 0 & 0 & 0 & 0 & 0 \\ 0 & 0 & 0 & 0 & 0 & 0 & 0 & 0 & 0 & \frac{1}{4} & \frac{1}{4} & \frac{1}{4} & \frac{1}{4} & 0 \\ 0 & 0 & 0 & 0 & 0 & 0 & 0 & 0 & 0 & 0 & 0 & 0 & 0 & \frac{1}{4} \end{array}\right], \tag{A.18}$$

where the horizontal line marks the distinction between the mapping into quarterly (upper part) and annual average (lower part) unemployment rates. Also, note that the loading matrix reflects the assumption that the term structure of SPF-consistent forecasts is flat beyond $H = 12$. In other words, the gaps $\tilde{Y}_{t+H+j}$ are assumed to be zero for all $j > 0$ (thus $\tilde{Y}_{2027\text{Q2}} = \tilde{Y}_{2027\text{Q3}} = \cdots = 0$), and at those horizons only the trend loading matters, hence the forecasts are set identical to the trend, with zero gaps.

When the forecast origin moves to the next quarter, $t = 2024\text{Q2}$, in $\boldsymbol{Z}_{\boldsymbol{q},2024\text{Q2}}$ we have $y_{2024\text{Q1}}$ (unemployment rate in 2024Q1) and quarterly SPF point forecasts (as of 2024Q2) targeting 2024Q2, 2024Q3, 2024Q4, 2025Q1 and 2025Q2, formally:

$$\boldsymbol{Z}_{\boldsymbol{q},2024\text{Q2}} = \left[y_{2024\text{Q1}}, F_{2024\text{Q2}} y_{2024\text{Q2}}, F_{2024\text{Q2}} y_{2024\text{Q3}}, F_{2024\text{Q2}} y_{2024\text{Q4}}, F_{2024\text{Q2}} y_{2025\text{Q1}}, F_{2024\text{Q2}} y_{2025\text{Q2}}\right]', \tag{A.19}$$

hence compared to equation (A.16) all quarterly forecast targets (and the lagged realization) move ahead by one quarter. In $\boldsymbol{Z}_{\boldsymbol{a},2024\text{Q2}}$, we have annual average unemployment rate forecasts targeting 2025, 2026 and 2027 as before, but as annual forecasts are associated with the fourth quarter of the target year, the forecast horizons shrink by one quarter relative to equation (A.17):

$$\boldsymbol{Z}_{\boldsymbol{a},2024\text{Q2}} = \left[F_{2024\text{Q2}} \bar{y}_{2025\text{Q4}}, F_{2024\text{Q2}} \bar{y}_{2026\text{Q4}}, F_{2024\text{Q2}} \bar{y}_{2027\text{Q4}}\right]'. \tag{A.20}$$

The loading matrix takes the following form:

$$\boldsymbol{C}_{2024\text{Q2}} = \left[\begin{array}{c} \boldsymbol{C}_{\boldsymbol{q},2024\text{Q2}} \\ \hline \boldsymbol{C}_{\boldsymbol{a},2024\text{Q2}} \end{array}\right] = \left[\begin{array}{cccccccccccccc} 1 & 0 & 0 & 0 & 0 & 0 & 0 & 0 & 0 & 0 & 0 & 0 & 0 & 0 \\ 0 & 1 & 0 & 0 & 0 & 0 & 0 & 0 & 0 & 0 & 0 & 0 & 0 & 0 \\ 0 & 0 & 1 & 0 & 0 & 0 & 0 & 0 & 0 & 0 & 0 & 0 & 0 & 0 \\ 0 & 0 & 0 & 1 & 0 & 0 & 0 & 0 & 0 & 0 & 0 & 0 & 0 & 0 \\ 0 & 0 & 0 & 0 & 1 & 0 & 0 & 0 & 0 & 0 & 0 & 0 & 0 & 0 \\ 0 & 0 & 0 & 0 & 0 & 1 & 0 & 0 & 0 & 0 & 0 & 0 & 0 & 0 \\ \hline 0 & 0 & 0 & 0 & \frac{1}{4} & \frac{1}{4} & \frac{1}{4} & \frac{1}{4} & 0 & 0 & 0 & 0 & 0 & 0 \\ 0 & 0 & 0 & 0 & 0 & 0 & 0 & 0 & \frac{1}{4} & \frac{1}{4} & \frac{1}{4} & \frac{1}{4} & 0 & 0 \\ 0 & 0 & 0 & 0 & 0 & 0 & 0 & 0 & 0 & 0 & 0 & 0 & \frac{1}{4} & \frac{1}{4} \end{array}\right]. \tag{A.21}$$

Compared to $\boldsymbol{C}_{2024\text{Q1}}$ in equation (A.18), in equation (A.21) we see that $\boldsymbol{C}_{\boldsymbol{q},2024\text{Q2}} = \boldsymbol{C}_{\boldsymbol{q},2024\text{Q1}}$ (i.e., the loadings associated with the lagged realization and the fixed-horizon forecasts remain unchanged), while the non-zero elements of the first two rows of $\boldsymbol{C}_{\boldsymbol{a},2024\text{Q1}}$ shift to the left, and so does the third row, with the weight $\frac{1}{4}$ appearing as the last (bottom right) entry (i.e., the loadings associated with the fixed-event forecasts change, in line with shrinking forecast horizons).

I(b.4) GDP price inflation

In $\boldsymbol{Z}_{\boldsymbol{q},2024\text{Q1}}$, we have $y_{2023\text{Q4}}$ (GDP price inflation of 2023Q4) and quarterly SPF point forecasts (as of 2024Q1) targeting 2024Q1, 2024Q2, 2024Q3, 2024Q4 and 2025Q1, formally:

$$\boldsymbol{Z}_{\boldsymbol{q},2024\text{Q1}} = \left[y_{2023\text{Q4}}, F_{2024\text{Q1}}y_{2024\text{Q1}}, F_{2024\text{Q1}}y_{2024\text{Q2}}, F_{2024\text{Q1}}y_{2024\text{Q3}}, F_{2024\text{Q1}}y_{2024\text{Q4}}, F_{2024\text{Q1}}y_{2025\text{Q1}}\right]'. \tag{A.22}$$

In $\boldsymbol{Z}_{\boldsymbol{a},2024\text{Q1}}$, we have annual GDP price inflation forecasts targeting 2025 (note that the annual forecast is associated with the fourth quarter of the target year):

$$\boldsymbol{Z}_{\boldsymbol{a},2024\text{Q1}} = \left[F_{2024\text{Q1}}\hat{y}_{2025\text{Q4}}\right]'. \tag{A.23}$$

The loading matrix takes the following form:

$$\boldsymbol{C}_{2024\text{Q1}} = \left[\begin{array}{c} \boldsymbol{C}_{\boldsymbol{q},2024\text{Q1}} \\ \hline \boldsymbol{C}_{\boldsymbol{a},2024\text{Q1}} \end{array}\right] = \left[\begin{array}{ccccccc} 1 & 0 & 0 & 0 & 0 & 0 & 0 \\ 0 & 1 & 0 & 0 & 0 & 0 & 0 \\ 0 & 0 & 1 & 0 & 0 & 0 & 0 \\ 0 & 0 & 0 & 1 & 0 & 0 & 0 \\ 0 & 0 & 0 & 0 & 1 & 0 & 0 \\ 0 & 0 & 0 & 0 & 0 & 1 & 0 \\ \hline 0 & 0 & \frac{1}{16} & \frac{2}{16} & \frac{3}{16} & \frac{4}{16} & \frac{3}{16} \end{array}\right], \tag{A.24}$$

where the horizontal line marks the distinction between the mapping into quarterly (upper part) and annual average (lower part) GDP price inflation rates. Also, note that the loading matrix reflects the assumption that the term structure of SPF-consistent forecasts is flat beyond $H = 5$. In other words, the gaps $\tilde{Y}_{t+H+j}$ are assumed to be zero for all $j > 0$ (thus $\tilde{Y}_{2025\text{Q3}} = \tilde{Y}_{2025\text{Q4}} = \cdots = 0$), and at those horizons only the trend loading matters, hence the forecasts are set identical to the trend, with zero gaps.

When the forecast origin moves to the next quarter, $t = 2024\text{Q2}$, in $\boldsymbol{Z}_{\boldsymbol{q},2024\text{Q2}}$ we have $y_{2024\text{Q1}}$ (GDP price inflation of 2024Q1) and quarterly SPF point forecasts (as of 2024Q2) targeting 2024Q2, 2024Q3, 2024Q4, 2025Q1 and 2025Q2, formally:

$$\boldsymbol{Z}_{\boldsymbol{q},2024\text{Q2}} = \left[y_{2024\text{Q1}}, F_{2024\text{Q2}}y_{2024\text{Q2}}, F_{2024\text{Q2}}y_{2024\text{Q3}}, F_{2024\text{Q2}}y_{2024\text{Q4}}, F_{2024\text{Q2}}y_{2025\text{Q1}}, F_{2024\text{Q2}}y_{2025\text{Q2}}\right]', \tag{A.25}$$

hence compared to equation (A.22) all quarterly forecast targets (and the lagged realization) move ahead by one quarter.

In $\boldsymbol{Z}_{\boldsymbol{a},2024\text{Q2}}$, we have annual GDP price inflation forecast targeting 2025 as before, but as annual forecasts are associated with the fourth quarter of the target year, the forecast horizon shrinks by one quarter relative to equation (A.23):

$$\boldsymbol{Z}_{\boldsymbol{a},2024\text{Q2}} = \left[F_{2024\text{Q2}}\hat{y}_{2025\text{Q4}}\right]'. \tag{A.26}$$

The loading matrix takes the following form:

$$\boldsymbol{C}_{2024\text{Q2}} = \left[\begin{array}{c} \boldsymbol{C}_{\boldsymbol{q},2024\text{Q2}} \\ \hline \boldsymbol{C}_{\boldsymbol{a},2024\text{Q2}} \end{array}\right] = \left[\begin{array}{ccccccc} 1 & 0 & 0 & 0 & 0 & 0 & 0 \\ 0 & 1 & 0 & 0 & 0 & 0 & 0 \\ 0 & 0 & 1 & 0 & 0 & 0 & 0 \\ 0 & 0 & 0 & 1 & 0 & 0 & 0 \\ 0 & 0 & 0 & 0 & 1 & 0 & 0 \\ 0 & 0 & 0 & 0 & 0 & 1 & 0 \\ \hline 0 & \frac{1}{16} & \frac{2}{16} & \frac{3}{16} & \frac{4}{16} & \frac{3}{16} & \frac{2}{16} \end{array}\right]. \tag{A.27}$$

Compared to $\boldsymbol{C}_{2024\text{Q1}}$ in equation (A.24), in equation (A.27) we see that $\boldsymbol{C}_{\boldsymbol{q},2024\text{Q2}} = \boldsymbol{C}_{\boldsymbol{q},2024\text{Q1}}$ (i.e., the loadings associated with the lagged realization and the fixed-horizon forecasts remain unchanged), while the non-zero elements of $\boldsymbol{C}_{\boldsymbol{a},2024\text{Q1}}$ shift to the left, with the weight $\frac{2}{16}$ appearing as the last (bottom right) entry (i.e., the loadings associated with the fixed-event forecast change, in line with shrinking forecast horizon).

In case of a forecast origin in Q3, the measurement vector and loadings can be constructed analogously to the previous examples. However, when the forecast origin is in Q4, such as $t = 2023\text{Q4}$, we need to amend the data definition and measurement loadings as described above in the case of RGDP, and the measurement loadings for the (sole) annual forecast becomes:

$$\boldsymbol{C}_{\boldsymbol{a},2023\text{Q4}} = \left[\begin{array}{ccccccc} \frac{2}{15} & \frac{3}{15} & \frac{4}{15} & \frac{3}{15} & \frac{2}{15} & \frac{1}{15} & 0 \end{array}\right]. \tag{A.28}$$

I(b.5) CPI inflation

In $\boldsymbol{Z}_{\boldsymbol{q},2024\text{Q1}}$, we have $y_{2023\text{Q4}}$ (CPI inflation of 2023Q4) and quarterly SPF point forecasts (as of 2024Q1) targeting 2024Q1, 2024Q2, 2024Q3, 2024Q4 and 2025Q1, formally:

$$\boldsymbol{Z}_{\boldsymbol{q},2024\text{Q1}} = \left[y_{2023\text{Q4}}, F_{2024\text{Q1}} y_{2024\text{Q1}}, F_{2024\text{Q1}} y_{2024\text{Q2}}, F_{2024\text{Q1}} y_{2024\text{Q3}}, F_{2024\text{Q1}} y_{2024\text{Q4}}, F_{2024\text{Q1}} y_{2025\text{Q1}}\right]'. \tag{A.29}$$

In $\boldsymbol{Z}_{\boldsymbol{a},2024\text{Q1}}$, we have annual Q4/Q4 CPI inflation forecasts targeting 2025 and 2026:

$$\boldsymbol{Z}_{\boldsymbol{a},2024\text{Q1}} = \left[F_{2024\text{Q1}} \bar{y}_{2025\text{Q4}}, F_{2024\text{Q1}} \bar{y}_{2026\text{Q4}}\right]'. \tag{A.30}$$

The loading matrix takes the following form:

$$\boldsymbol{C}_{2024\text{Q1}} = \left[\begin{array}{c} \boldsymbol{C}_{\boldsymbol{q},2024\text{Q1}} \\ \hline \boldsymbol{C}_{\boldsymbol{a},2024\text{Q1}} \end{array}\right] = \left[\begin{array}{cccccccccc} 1 & 0 & 0 & 0 & 0 & 0 & 0 & 0 & 0 & 0 \\ 0 & 1 & 0 & 0 & 0 & 0 & 0 & 0 & 0 & 0 \\ 0 & 0 & 1 & 0 & 0 & 0 & 0 & 0 & 0 & 0 \\ 0 & 0 & 0 & 1 & 0 & 0 & 0 & 0 & 0 & 0 \\ 0 & 0 & 0 & 0 & 1 & 0 & 0 & 0 & 0 & 0 \\ 0 & 0 & 0 & 0 & 0 & 1 & 0 & 0 & 0 & 0 \\ \hline 0 & 0 & 0 & 0 & 0 & \frac{1}{4} & \frac{1}{4} & \frac{1}{4} & \frac{1}{4} & 0 \\ 0 & 0 & 0 & 0 & 0 & 0 & 0 & 0 & 0 & \frac{1}{4} \end{array}\right], \tag{A.31}$$

where the horizontal line marks the distinction between the mapping into quarterly (upper part) and Q4/Q4 (lower part) CPI inflation rates. Also, note that the loading matrix reflects the assumption that the term structure of SPF-consistent forecasts is flat beyond $H = 8$. In other words, the gaps $\tilde{Y}_{t+H+j}$ are assumed to be zero for all $j > 0$ (thus $\tilde{Y}_{2026\text{Q2}} = \tilde{Y}_{2026\text{Q3}} = \cdots = 0$), and at those horizons only the trend loading matters, hence the forecasts are set identical to the trend, with zero gaps.

When the forecast origin moves to the next quarter, $t = 2024\text{Q2}$, in $\boldsymbol{Z}_{\boldsymbol{q},2024\text{Q2}}$ we have $y_{2024\text{Q1}}$ (CPI inflation of 2024Q1) and quarterly SPF point forecasts (as of 2024Q2) targeting 2024Q2, 2024Q3, 2024Q4, 2025Q1 and 2025Q2, formally:

$$\boldsymbol{Z}_{\boldsymbol{q},2024\text{Q2}} = \left[y_{2024\text{Q1}}, F_{2024\text{Q2}} y_{2024\text{Q2}}, F_{2024\text{Q2}} y_{2024\text{Q3}}, F_{2024\text{Q2}} y_{2024\text{Q4}}, F_{2024\text{Q2}} y_{2025\text{Q1}}, F_{2024\text{Q2}} y_{2025\text{Q2}}\right]', \tag{A.32}$$

hence compared to equation (A.29) all quarterly forecast targets (and the lagged realization) move ahead by one quarter.

In $\boldsymbol{Z}_{\boldsymbol{a},2024\text{Q2}}$, we have annual Q4/Q4 CPI inflation forecasts targeting 2025 and 2026 as before, but the forecast horizon shrinks by one quarter relative to equation (A.30):

$$\boldsymbol{Z}_{\boldsymbol{a},2024\text{Q2}} = \left[F_{2024\text{Q2}} \bar{y}_{2025\text{Q4}}, F_{2024\text{Q2}} \bar{y}_{2026\text{Q4}}\right]'. \tag{A.33}$$

The loading matrix, $\boldsymbol{C}_{2024\text{Q}2}$, has the following components:

$$\boldsymbol{C}_{\boldsymbol{q},2024\text{Q}2} = \begin{bmatrix} 1 & 0 & 0 & 0 & 0 & 0 & 0 & 0 & 0 & 0 \\ 0 & 1 & 0 & 0 & 0 & 0 & 0 & 0 & 0 & 0 \\ 0 & 0 & 1 & 0 & 0 & 0 & 0 & 0 & 0 & 0 \\ 0 & 0 & 0 & 1 & 0 & 0 & 0 & 0 & 0 & 0 \\ 0 & 0 & 0 & 0 & 1 & 0 & 0 & 0 & 0 & 0 \\ 0 & 0 & 0 & 0 & 0 & 1 & 0 & 0 & 0 & 0 \end{bmatrix}, \tag{A.34}$$

and

$$\boldsymbol{C}_{\boldsymbol{a},2024\text{Q}2} = \begin{bmatrix} 0 & 0 & 0 & 0 & \frac{1}{4} & \frac{1}{4} & \frac{1}{4} & \frac{1}{4} & 0 & 0 \\ 0 & 0 & 0 & 0 & 0 & 0 & 0 & 0 & \frac{1}{4} & \frac{1}{4} \end{bmatrix}, \tag{A.35}$$

with

$$\boldsymbol{C}_{2024\text{Q}2} = \begin{bmatrix} \boldsymbol{C}_{\boldsymbol{q},2024\text{Q}2} \\ \hline \boldsymbol{C}_{\boldsymbol{a},2024\text{Q}2} \end{bmatrix}. \tag{A.36}$$

Compared to $\boldsymbol{C}_{2024\text{Q}1}$ in equation (A.31), in equation (A.34) we see that $\boldsymbol{C}_{\boldsymbol{q},2024\text{Q}2} = \boldsymbol{C}_{\boldsymbol{q},2024\text{Q}1}$ (i.e., the loadings associated with the lagged realization and the fixed-horizon forecasts remain unchanged), while the non-zero elements of the first row of $\boldsymbol{C}_{\boldsymbol{a},2024\text{Q}1}$ in equation (A.34) shift to the left, and so does the second row, with the weight $\frac{1}{4}$ appearing as the last (bottom right) entry (i.e., the loadings associated with the fixed-event forecasts change, in line with shrinking forecast horizons).

I(c) Measurement error in annual forecasts

This appendix serves to motivate our choice for modeling data on annual SPF forecasts with measurement error. To preview the main arguments of this appendix:

- In general, the goal of this paper is to treat observed SPF data largely as is, and we maintain the assumption that treats quarterly fixed-horizon forecasts from the SPF as observed without error.
- However, when jointly using data on quarterly and annual forecasts from the SPF, overlap in their respective forecast targets raises the question of whether both types of readings are perfectly consistent with each other. In case of next-year forecasts collected in Q4, there is perfect overlap with fixed-horizon forecasts collected for $h = 1, 2, 3, 4$, and it is straightforward to check whether both readings are a perfect match. As illustrated below, quarterly forecasts collected in Q4 are indeed often close to the corresponding next-year forecast reported by the SPF. However, deviations have not been infrequent either, and at times even quite sizable.
- Moreover, as argued below, even small inconsistencies can lead to outsized effects on imputed quarterly forecasts at longer horizons, as quarterly forecasts for the near term are taken as given from the SPF.

I(c.1) Observed inconsistencies in next-year forecasts collected in Q4

In Q4, the SPF reports a set of quarterly forecasts for $h = 0, 1, 2, 3, 4$ as well as an annual forecast for the next year. Evidently, the quarterly forecasts perfectly overlap with the next-year forecast. Here we assess how well the reported next-year forecasts match what is implied by the observed quarterly SPF forecasts (and lagged data if necessary).

To match quarterly SPF forecasts with the next year forecast, recall that, in case of the unemployment rate the annual forecast is directly defined as the arithmetic average of unemployment over the four quarters of the year. In case of CPI, the same holds approximately (since the annual forecast is to reflect Q4/Q4 inflation, measured as a simple growth rate). As discussed above in Appendix I(b), for the NIPA variables (GDP growth and inflation in GDP prices), the annual forecast reflects an (approximate) linear combination of growth in the four quarters of the targeted year, as well as the last three quarters of the previous year. Thus,

Figure A.1: Observed inconsistencies between quarterly and next-year forecasts collected in Q4

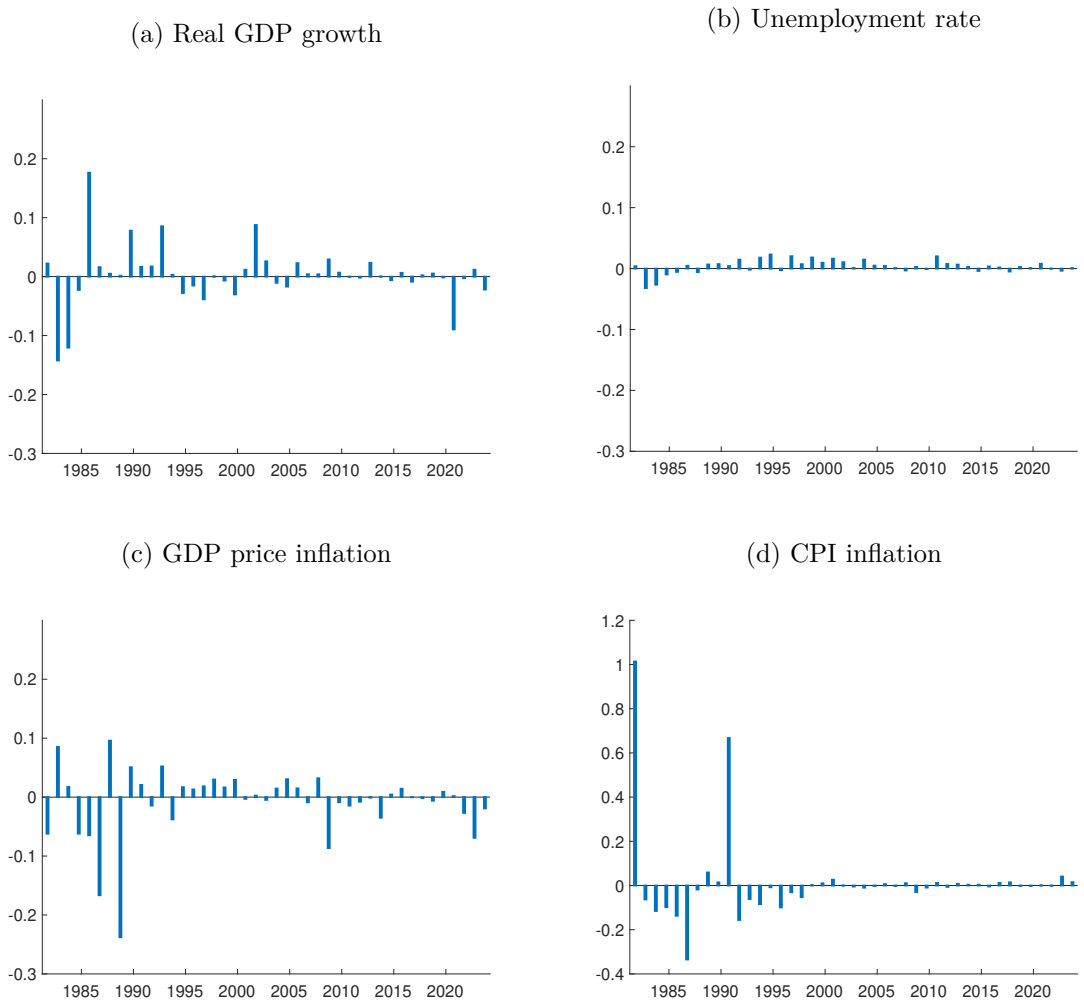

Notes: Difference between actual and implied SPF annual forecasts for next year collected in Q4. Implied SPF forecasts constructed from available quarterly forecast for one to four-quarters ahead, as well as lagged data (as needed for GDP growth and GDP price inflation). Only Q4 observations since 1981Q4. (The SPF began reporting next-year forecasts in 1981Q3.)

in the case of NIPA variables, when matching the next-year forecasts with quarterly forecasts collected in Q4, we also need to utilize the nowcast, as well as two lags of data.

Figure A.1 plots the difference between next year forecasts collected in Q4, and what is implied for the same forecast target by the SPF's quarterly fixed-horizon forecast that were collected jointly with the annual forecast. All data definitions follow the procedures employed in our model estimates, as described in Appendix I(b) above. Formally, according to the data definitions employed in our paper, annual forecast targets are linear combinations of quarterly

values, and we can generically write:

$$\hat{y}_t = \sum_{j=0}^{J-1} w_j y_{t-j}\,, \tag{A.37}$$

with $J = 7$ and $w_0 = 1/16$, $w_1 = 2/16$, $w_2 = 3/16$, $w_3 = 4/16$, $w_4 = 3/16$, $w_5 = 2/16$, and $w_6 = 1/16$ in case of GDP growth and GDP price inflation, and $J = 4$ and $w_j = 1/4$ in case of the unemployment rate and CPI inflation.[3] Figure A.1 then plots the difference between the actual next-year forecast, denoted $F_t^o \hat{y}_{t+4}$, and the implied value constructed from the quarterly forecasts, $F_t \hat{y}_{t+4} \equiv \sum_{j=0}^{J-1} w_j F_t^o y_{t+4-j}$. The superscript "'o" in F_t^o denotes observed SPF data (or, if needed, lagged realized data known by the SPF respondents in real time).[4]

Overall, Figure A.1 shows that there are indeed some differences between the actual next-year forecast from the SPF and what is implied by the corresponding quarterly SPF predictions. For many observations of all variables, the differences are quite small (less than 10 basis points (bp) in absolute value), but there are also cases when the differences are much larger than that. The occurrence of sizable differences varies across variables. For the unemployment rate, differences are always well below 5bp. For CPI inflation, there are notable differences in the 1980s and 1990s, with two particularly large outliers in 1981 and 1990, of about 100 and 70 basis points, respectively. For GDP growth, and GDP price inflation, differences do not exceed 30bp in absolute value, but there are still some observations with differences of 20bp or more, in particular prior to 1990. All in all, this suggests that there are some measurement issues and that these are quite unevenly distributed across time and variables. As we will argue next, even small inconsistencies can lead to outsized effects on imputed quarterly forecasts at longer horizons, as quarterly forecasts for the near term are taken as given from the SPF.

Consider the case of a forecast origin in Q3, henceforth denoted t. In this case, there is large overlap between the observed SPF forecast for next year, $F_t^o \hat{y}_{t+5}$, and what is covered by the equally observed quarterly forecasts, $F_t^o y_{t+h}$ for $h = 0, 1, 2, 3, 4$. In fact, quarterly forecasts for $h \leq 4$ (and lagged data) account for every component of $F_t \hat{y}_{t+5}$ except for the forecast of Q4 next year, $F_t y_{t+5}$. In this case, a measurement equation of the form in (A.37) already determines the imputed value for $F_t \hat{y}_{t+5}$ without any further need for modeling the stochastic

[3] The notation adopted here generalizes a little the more specific notation for $\hat{y}_t$ and $\bar{y}_t$ as adopted in the paper. At slight abuse of our earlier notation, we denote here annual forecasts for all variables simply by $\hat{y}_t$, without distinguishing further between $\hat{y}_t$ and $\bar{y}_t$.

[4] Lagged realized data is needed to construct $F_t \hat{y}_{t+4}$ in case of GDP growth and GDP price inflation, for which we have $J = 7$. Real time vintages that correspond to SPF rounds are obtained from the Philadelphia Fed.

evolution of data and SPF:

$$\hat{F}_t y_{t+5} = \frac{1}{w_0} \cdot \left(F_t \hat{y}^o_{t+5} - \sum_{j=1}^{J-1} w_j F^o_t y_{t+5-j} \right) , \qquad \text{when } t \text{ in Q3}\,, \tag{A.38}$$

where the "hat" in $\hat{F}_t$ denotes an imputed value. If the assumption is correct that annual SPF forecasts map into the SPF's quarterly forecasts without error, an imputation as in (A.38) should hold exactly. However, as we have seen in Figure A.1 for the case when t is in Q4, this is not always the case, casting doubt over the applicability of (A.38) when t is in Q3.

Instead, consider the case where the observed annual forecast is measured only with some (potentially) small error, while we maintain the assumption that quarterly forecasts are observed without error (so that $F_t y_{t+j} = F^o_t y_{t+j}$ for $j \leq 4$). In this case, we can write the measurement equation for the annual forecast as follows:

$$F^o_t \hat{y}_{t+5} = \sum_{j=0}^{J-1} w_j F_t y_{t+5-j} + n_t. \tag{A.39}$$

But, application of an imputation, as in (A.38), that assumes the absence of measurement error distorts the imputed value by the measurement error:

$$\Rightarrow \quad \hat{F}_t y_{t+5} = \frac{1}{w_0} \cdot \left(F_t \hat{y}^o_{t+5} - \sum_{j=1}^{J-1} w_j F^o_t y_{t+5-j} \right) , \qquad \text{when } t \text{ in Q3}, \tag{A.40}$$

$$= F_t y_{t+5} + \frac{1}{w_0} n_t\,. \tag{A.41}$$

With $1/w_0 = 16$ (for GDP growth and GDP inflation) or $1/w_0 = 4$ (for the unemployment rate and CPI inflation), even small measurement errors in the annual forecast can lead to large distortions in the imputed value for the forecast made in Q3 this year (t) for the quarterly outcome in Q4 next year.

By a similar logic, observations in Q1 and Q2 for the SPF's next-year and quarterly forecasts directly restrict a weighted average of imputed values for the quarterly forecasts for the next year. When the imputations are made based on an error-free measurement equation as in (A.37), while the actual data is affected by measurement error, these restrictions on imputed values are

again distorted by measurement error:

$$\text{When } t \text{ in Q2:} \quad \hat{\alpha}_{t,5:6} \equiv \frac{1}{w_0} \cdot \left(F_t \hat{y}^o_{t+6} - \sum_{j=2}^{J-1} w_j F^o_t y_{t+6-j} \right) \tag{A.42}$$

$$= \frac{w_0 F_t y_{t+6} + w_1 F_t y_{t+5}}{w_0 + w_1} + \frac{n_t}{w_0 + w_1} \,. \tag{A.43}$$

$$\text{And, when } t \text{ in Q1:} \quad \hat{\alpha}_{t,5:7} = \frac{1}{w_0} \cdot \left(F_t \hat{y}^o_{t+7} - \sum_{j=3}^{J-1} w_j F^o_t y_{t+7-j} \right) \tag{A.44}$$

$$= \frac{w_0 F_t y_{t+7} + w_1 F_t y_{t+6} + w_2 F_t y_{t+5}}{w_0 + w_1 + w_2} + \frac{n_t}{w_0 + w_1 + w_2} \,. \tag{A.45}$$

Notably, the weight on the measurement error in these calculations is increasing for imputations made later in a given calendar year.

For simplicity, we call $\hat{F}_t y_{t+5}$, $\hat{\alpha}_{t,5:6}$, and $\hat{\alpha}_{t,5:7}$ "naive" imputations. Figure A.2 plots these naive imputations against data for realized outcomes and the observed next-year SPF. Overall, the naive imputations appear to track (or predict) the data fairly well. Of note, $\hat{\alpha}_{t,5:6}$, and $\hat{\alpha}_{t,5:7}$ should reflect (weighted) averages of quarterly outcomes, which could be expected to be less volatile than quarterly outcomes or forecasts thereof. Indeed, imputations made in Q3 (yellow diamonds) tend to stand out more often than those made in Q1 and Q2 (orange squares and blue circles, respectively). More importantly, Figure A.2 shows some patterns that are reminiscent of what is shown in Figure A.1 for inconsistencies between observed and implied values for the next-year forecast at Q4 origins (which are a direct reflection of measurement error): While the naive imputations track the data particularly well for the unemployment rate and CPI inflation, imputations made in Q3 for GDP growth and GDP inflation show notable outliers, which could be indicative of the measurement error term in (A.41), and with decreasing effect for values constructed in Q2 and Q1, as predicted by equations (A.43) and (A.45).

I(c.2) Excessively volatile imputations when treating annual forecasts without error

Of course, the arguments presented so far can only highlight the particular risk of distortions in imputed values when annual forecasts are not perfectly consistent with quarterly forecasts. And, the results shown in Figures A.1 and A.2 are at best indicative of the extent to which such inconsistencies may be relevant in the data. At least for SPF rounds in Q4, the data suggests that inconsistencies cannot always be neglected.

As such, we evaluated models that allow for measurement error in annual forecasts, as

Figure A.2: Naive imputations of quarterly forecasts at longer horizons

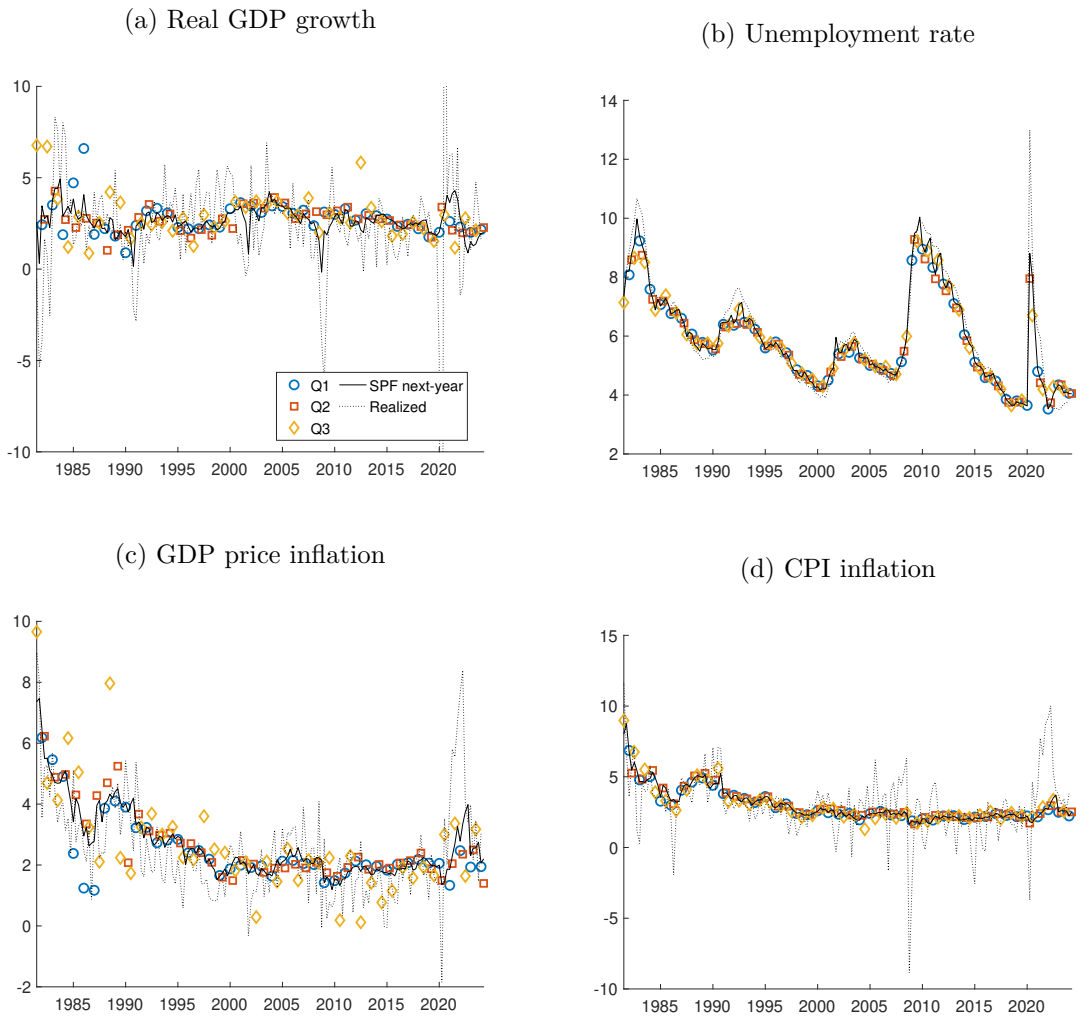

Notes: "Naive" imputations, $\hat{F}_t y_{t+5}$, $\hat{\alpha}_{t,5:6}$, and $\hat{\alpha}_{t,5:7}$, of quarterly forecasts at longer horizons as defined in equations (A.41), (A.43), and (A.45), respectively. Imputations made in Q1, Q2, and Q3 as indicated. Observations since 1981Q3, which is when the SPF reported its first next-year forecast. For sake of readability of SPF information, COVID-19 outliers in realized data are not shown.

described in Section 4 of the paper, as well as versions that assume all SPF data are observed without error. The latter case was also the basis for earlier versions of our manuscript. In light of Figure A.1, we drop Q4 observations from the estimation data for models that assume annual forecasts are observed without error.[5]

Strikingly, term structures of SPF-consistent forecasts that we imputed from models without measurement error are notably more volatile than those imputed from models that allow for measurement error in annual forecasts. This is particularly true for GDP growth and GDP price inflation, where the volatility of imputed forecasts at longer horizons is much higher in models that assume no measurement error in annual forecasts. Of course, these findings support the argument that even small inconsistencies between quarterly and annual forecasts can lead to outsized effects on imputed quarterly forecasts at longer horizons, as quarterly forecasts for the near term are taken as given from the SPF. Moreover, in feedback received from forecasting practitioners, the more "wiggly" imputations obtained from models that omit measurement error were considered to be less credible. In a similar vein, Table A.3 shows that one-step ahead forecasts of SPF data generated by a version of our model that assumes no measurement error in annual forecasts are dramatically worse in predicting future survey data than our baseline model which does assume measurement error (with results shown in Table 1 of the paper and restated as Table A.4 below).

All told, these results lead us to prefer — and adopt in the revised paper — models that allow for measurement error in observed annual SPF forecasts. Given the occasional nature of inconsistencies that are directly detectable (Figure A.1) and related patterns in naive imputations made in different quarters of the year (Figure A.2), we chose (1) to specify separate measurement error processes for data observed in different quarters of the year, and (2) to adopt fat-tailed specifications for the measurement errors, which place much mass a priori on errors being zero, while retaining the flexibility to fit occasionally sizable occurrences of errors. Details of the measurement error specifications are described in Section 4 of the paper and Appendix II below. Throughout, we maintain the specification that quarterly SPF forecasts are observed without error, in keeping with the goal of this paper to treat observed SPF data largely as is.

Figures A.3 through A.6 report time series of estimates of the measurement noise in annual forecasts — specifically, posterior medians in observed SPF forecasts for the next calendar year

[5] In results not shown, we also evaluated models that drop Q4 observations from the estimation data for models that allow for measurement error in annual forecasts. The results were largely similar to those presented in the paper.

ahead up through three years ahead (for variables with forecasts at these horizons), for both the MDS and VAR specifications. These estimates show that, in keeping with our choice of a horseshoe specification of the shocks' distributions, the noise shocks are usually small, but very occasionally large. This pattern is especially stark for the next-year forecasts. The relatively very large noise shocks in Figure A.3 tend to occur in the instances of large inconsistencies between quarterly and next-year forecasts indicated in Figure A.1, which are primarily early in the sample and to a lesser extent around the time of the outbreak of the COVID-19 pandemic. However, in keeping with the logic described above with imputation issues, the size of the noise shocks tends to be generally larger than the size of the inconsistencies; this naturally stems from the large weights that some quarters of forecasts can get due to the weights of the Mariano-Murasawa approximation of annual GDP growth and GDP price inflation. Another evident pattern in the estimates is that, except in the case of the unemployment rate (for which noise shocks are generally small) the noise shocks tend to be larger (in absolute value) at the year-ahead horizon than longer horizons. To the extent that the measurement error is linked to inconsistencies in annual and observed quarterly forecasts, this is to be expected, given that quarterly forecasts are only observed at shorter horizons and therefore consistency is only an issue for the year-ahead forecasts. Finally, the estimated shocks are similar for the MDS and VAR specifications, most clearly and strongly for the year-ahead horizon.

Figure A.3: Estimated noise in SPF next-year forecasts (MDS, 2024Q1)

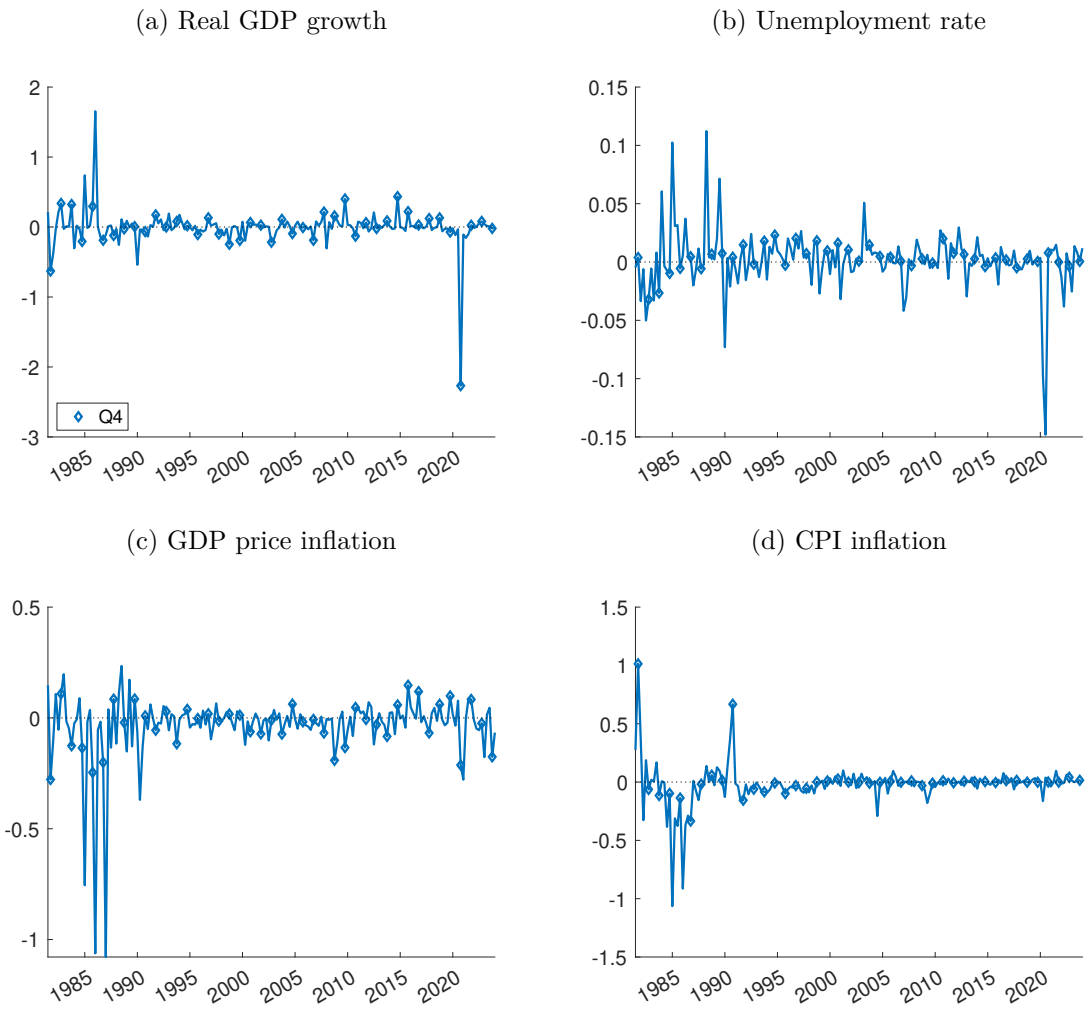

Notes: Posterior medians of noise levels in observed SPF forecasts for the next calendar year ahead. Q4 observations marked by a diamond. Estimates from the MDS model using data through 2024Q1.

Figure A.4: Estimated noise in SPF next-year forecasts (VAR, 2024Q1)

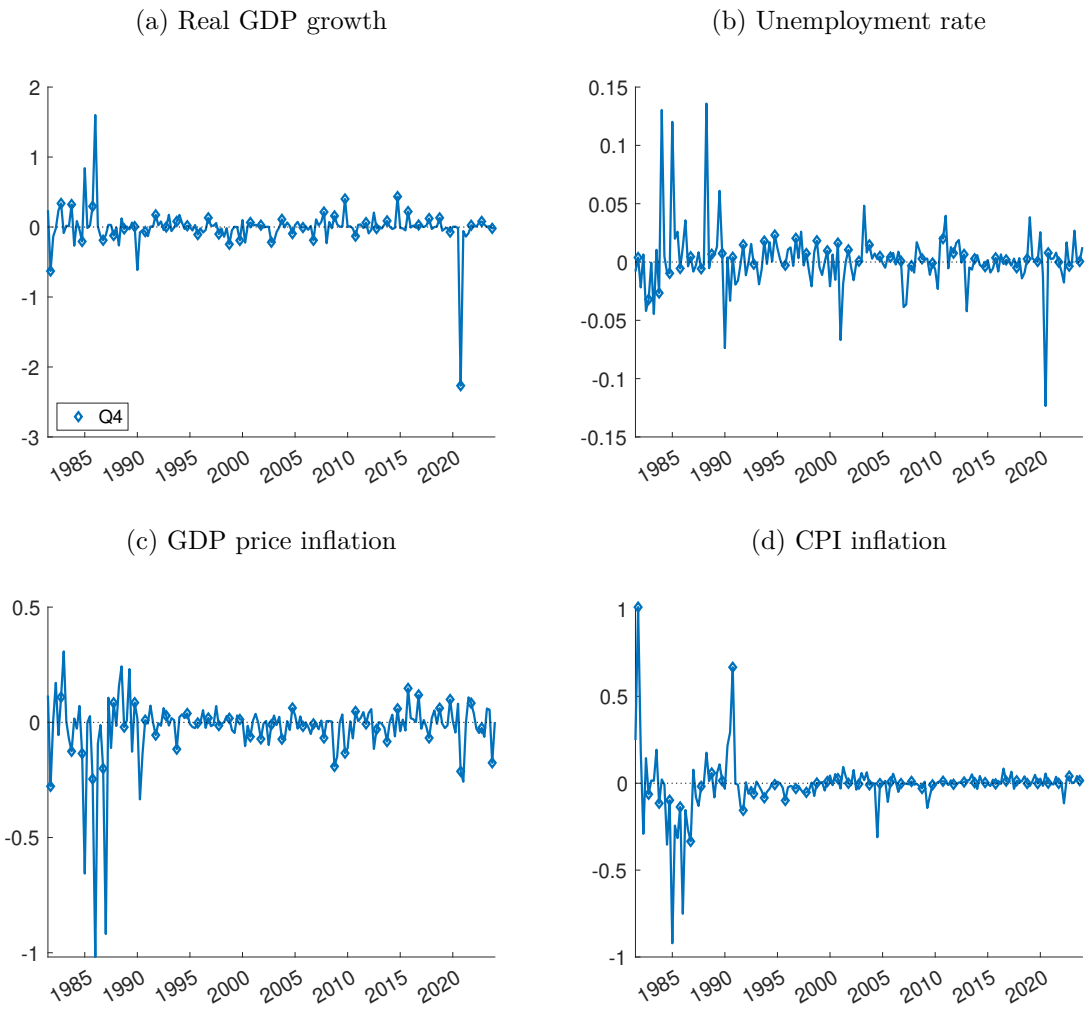

Notes: Posterior medians of noise levels in observed SPF forecasts for the next calendar year ahead. Q4 observations marked by a diamond. Estimates from the VAR model using data through 2024Q1.

Figure A.5: Estimated noise in SPF two-years ahead forecasts (2024Q1)

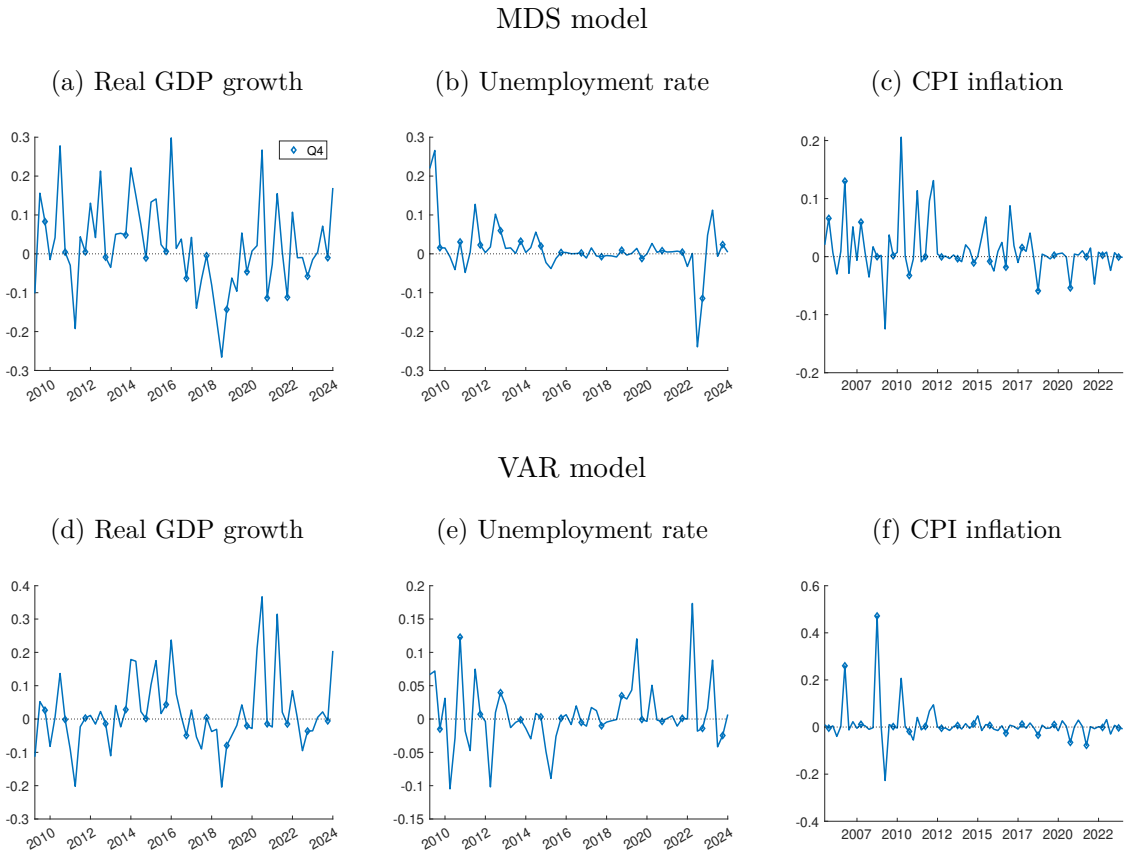

Notes: Posterior medians of noise levels in observed SPF forecasts for the next calendar year ahead. Q4 observations marked by a diamond. Estimates based on data through 2024Q1.

Figure A.6: Estimated noise in SPF three-years ahead forecasts (2024Q1)

MDS model

(a) Real GDP growth

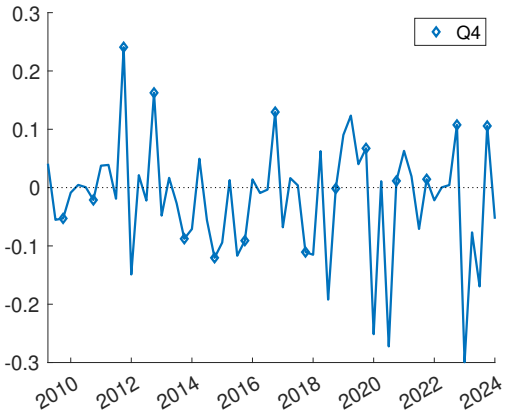

(b) Unemployment rate

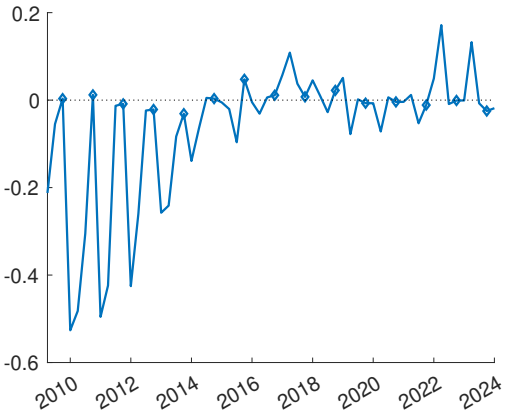

VAR model

(c) Real GDP growth

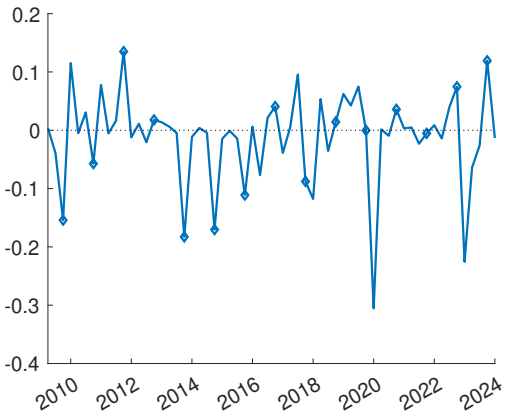

(d) Unemployment rate

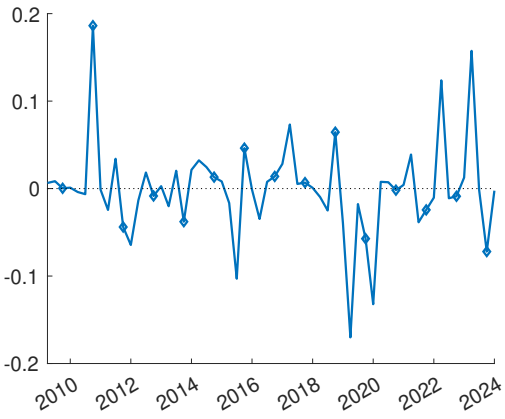

Notes: Posterior medians of noise levels in observed SPF forecasts for the next calendar year ahead. Q4 observations marked by a diamond. Estimates based on data through 2024Q1.

I(c.3) Comparison of results from models with and without noise in annual forecasts

To show how including measurement error around published annual forecasts impacts our forecasts and results, Figures A.7 through A.10 report examples of term structures of (out-of-sample) quarterly forecasts from models with and without measurement noise. Note that these charts end with H as specified for each variable; to facilitate comparisons, we do not report the forecasts out to 16 steps ahead (recall that the point forecasts for $h = H + 1, \ldots, 16$ are equal to the forecasts for $h = H$). In addition, by construction, without noise on short-horizon forecasts, the forecasts for $h = 0, \ldots, 4$ are the same across the noise and no-noise models.

Focusing first on results from MDS specifications, without noise, the quarterly forecasts at longer horizons show more variation from quarter to quarter than do the forecasts from the model with measurement noise in annual forecasts. In particular, the forecasts from the model with noise avoid the tendency of the forecasts from the model without noise to change one way early on and then snap in the opposite direction in the following few quarters. In some instances — e.g., GDP price inflation in the 2024Q1 example and unemployment in the 2019Q4 example — the inclusion of noise in the model can impact the level of the longer-horizon quarterly forecasts as compared to the model without noise. It is also evident that the inclusion of measurement noise on annual forecasts can have some impact on the uncertainty around the estimated quarterly forecast at longer horizons. This is evident in the case of GDP price inflation, with greater uncertainty around the forecasts from the model without noise than the model with noise. However, as noted in the paper, uncertainty around the latent quarterly forecast estimates at longer horizons is small relative to the overall forecast uncertainty reflected in the size of historical forecast errors. While not shown in the interest of brevity, the inclusion of noise in the model does not have much impact on overall forecast uncertainty: The widths of forecast confidence bands are comparable for the with-noise and without-noise model specifications.

Patterns are very broadly similar in forecasts from VAR specifications that allow for bias in SPF forecasts. However, the inclusion of noise around published annual forecasts has a smaller impact with the VAR than the MDS specification. For example, the with-noise and without-noise forecasts of GDP growth are quite similar in the VAR case; the with-noise forecasts are not smoother than the without-noise forecasts as observed in the MDS case. In turn, the forecasts of GDP growth from the VAR (in both the with-noise and without-noise estimates) show more variability across quarters than do the forecasts from the MDS specification with noise.

Figure A.7: Term structures estimated with and without noise (MDS, 2024Q1)

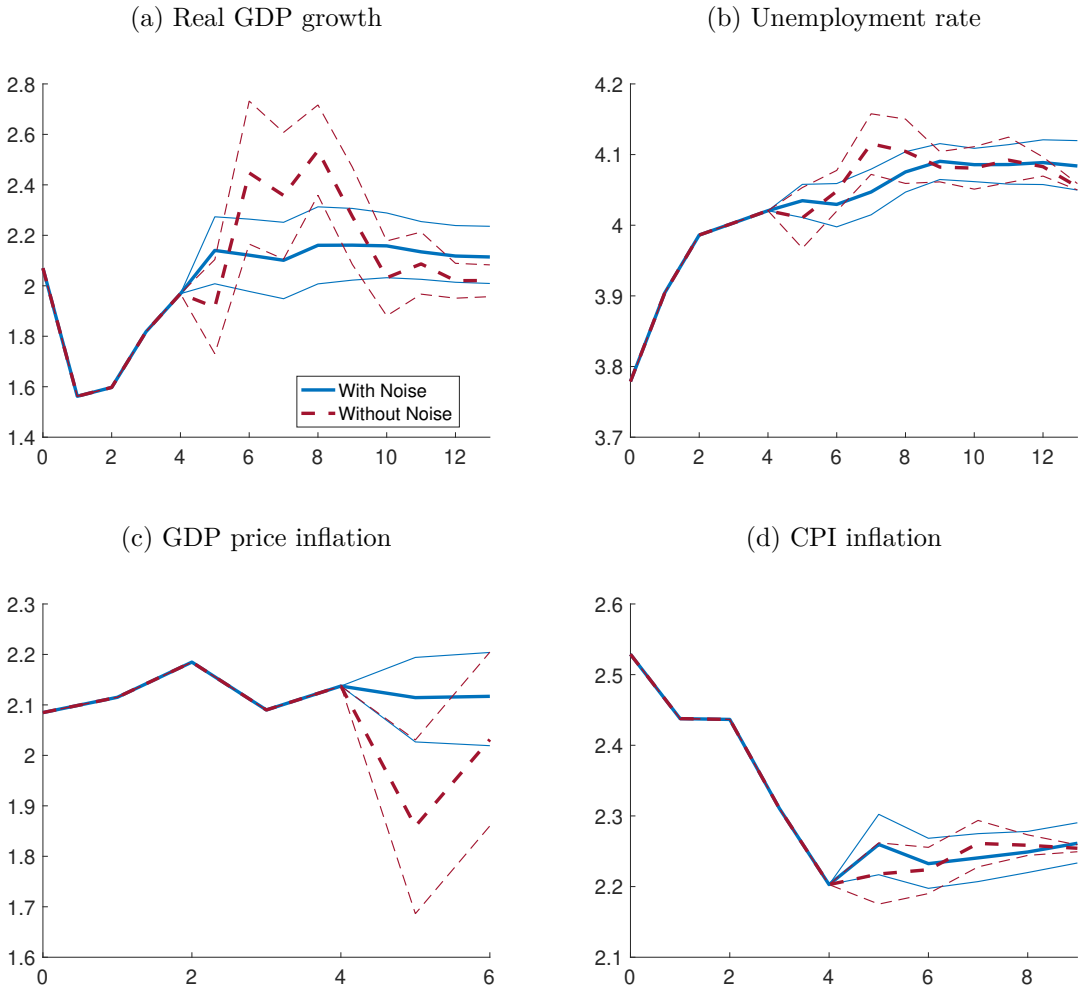

Notes: Posterior medians (and 68% bands) of term structures of SPF-consistent expectations, denoted $\boldsymbol{Y_t}$, obtained from the MDS model with or without noise in the observed SPF calendar-year forecasts. For estimation of the mode without noise, we drop Q4 observations for the next-year forecast (due to perfect overlap with the observed quarterly SPF forecasts.) Estimates based on data through 2024Q1.

Figure A.8: Term structures estimated with and without noise (VAR, 2024Q1)

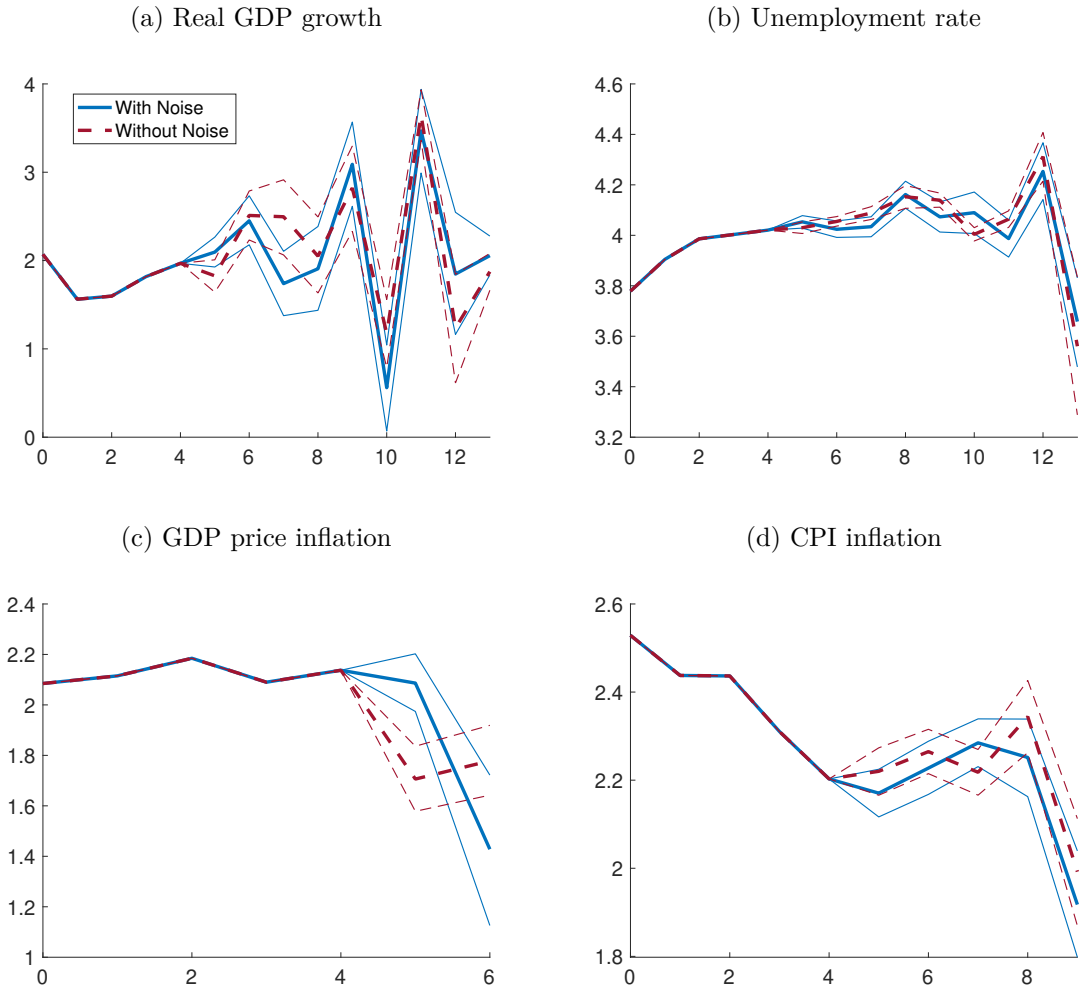

Notes: Posterior medians (and 68% bands) of term structures of SPF-consistent expectations, denoted $\boldsymbol{Y_t}$, obtained from the VAR model with or without noise in the observed SPF calendar-year forecasts. For estimation of the mode without noise, we drop Q4 observations for the next-year forecast (due to perfect overlap with the observed quarterly SPF forecasts.) Estimates based on data through 2024Q1.

Figure A.9: Term structures estimated with and without noise (MDS, 2019Q4)

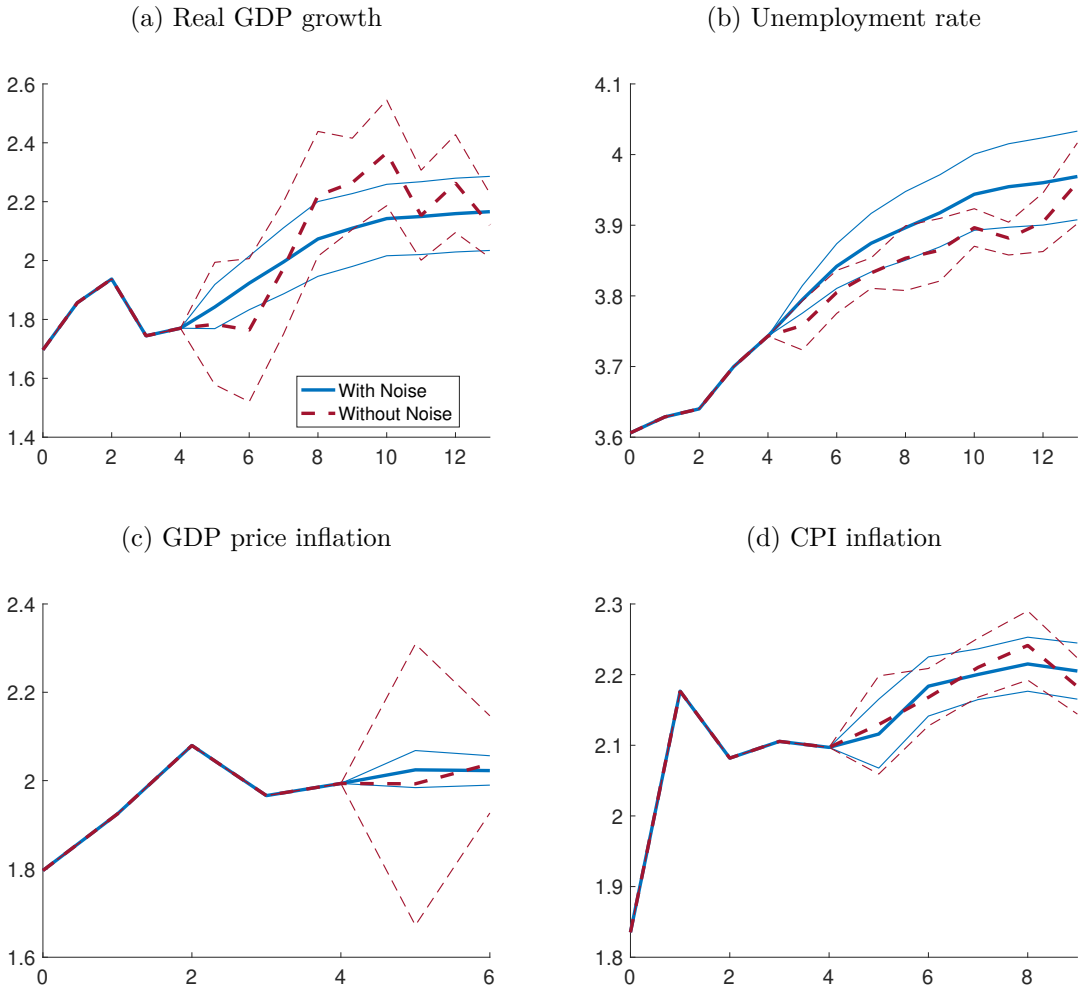

Notes: Posterior medians (and 68% bands) of term structures of SPF-consistent expectations, denoted $\boldsymbol{Y_t}$, obtained from the MDS model with or without noise in the observed SPF calendar-year forecasts. For estimation of the mode without noise, we drop Q4 observations for the next-year forecast (due to perfect overlap with the observed quarterly SPF forecasts.) Estimates based on data through 2019Q4.

Figure A.10: Term structures estimated with and without noise (VAR, 2019Q4)

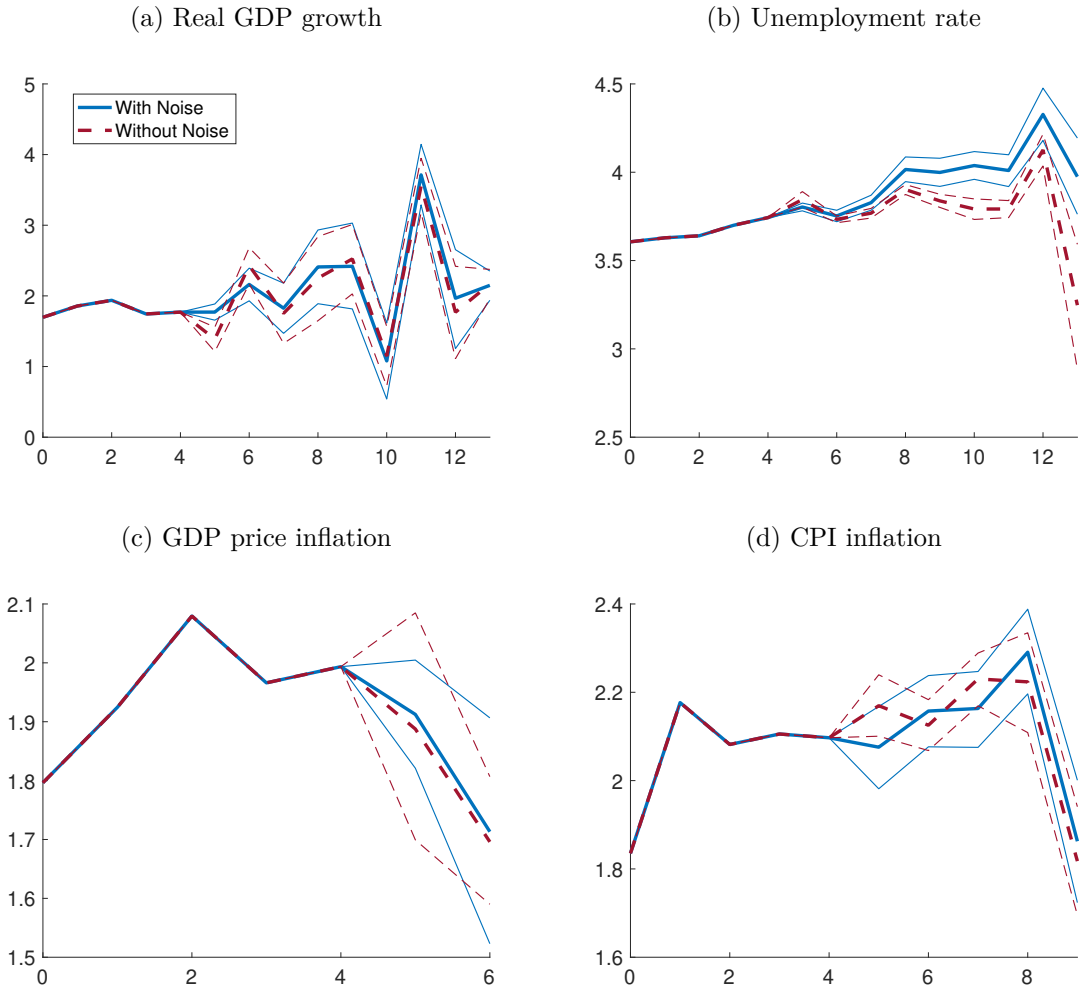

Notes: Posterior medians (and 68% bands) of term structures of SPF-consistent expectations, denoted $\boldsymbol{Y_t}$, obtained from the VAR model with or without noise in the observed SPF calendar-year forecasts. For estimation of the mode without noise, we drop Q4 observations for the next-year forecast (due to perfect overlap with the observed quarterly SPF forecasts.) Estimates based on data through 2019Q4.

Table A.3: Predictability of SPF point forecasts (noise-free model)

	intercept								slope							
	RGDP		UNRATE		PGDP		CPI		RGDP		UNRATE		PGDP		CPI	
Forecast	MDS	VAR	MDS	VAR	MDS	VAR	MDS	VAR	MDS	VAR	MDS	VAR	MDS	VAR	MDS	VAR
h = 0	-1.52	−1.17	0.81	0.91	−0.04	0.06	−0.33	−0.36	1.41	1.35	0.86	0.85	0.99	0.96	1.15	1.21
	(0.76)	(0.73)	(0.52)	(0.58)	(0.11)	(0.13)	(0.40)	(0.39)	(0.24)	(0.26)	(0.08)	(0.09)	(0.05)	(0.06)	(0.16)	(0.16)
h = 1	−0.11	−0.06	0.55	0.73	−0.08	0.04	−0.07	−0.07	1.02	1.02	0.91	0.88	1.02	0.98	1.01	1.03
	(0.28)	(0.25)	(0.43)	(0.48)	(0.09)	(0.09)	(0.15)	(0.13)	(0.09)	(0.08)	(0.06)	(0.08)	(0.04)	(0.04)	(0.07)	(0.06)
h = 2	−0.14	0.05	0.38	0.58	0.11	0.15	0.10	0.16	1.02	0.97	0.94	0.90	0.94	0.99	0.94	0.93
	(0.23)	(0.23)	(0.36)	(0.39)	(0.07)	(0.09)	(0.10)	(0.09)	(0.08)	(0.08)	(0.06)	(0.06)	(0.03)	(0.04)	(0.04)	(0.04)
h = 3	0.13	1.70	0.26	0.30	0.15	1.27	0.15	0.61	0.94	0.37	0.96	0.96	0.92	0.37	0.92	0.75
	(0.26)	(0.18)	(0.32)	(0.38)	(0.08)	(0.08)	(0.09)	(0.17)	(0.09)	(0.06)	(0.05)	(0.06)	(0.04)	(0.03)	(0.04)	(0.07)
h = 4	1.67	1.69	0.20	0.44	1.25	0.24	0.50	0.49	0.39	0.40	0.97	0.93	0.47	0.89	0.80	0.82
	(0.19)	(0.16)	(0.28)	(0.28)	(0.15)	(0.08)	(0.14)	(0.11)	(0.07)	(0.05)	(0.05)	(0.05)	(0.06)	(0.04)	(0.06)	(0.04)
y = 1	0.23	0.47	0.23	0.36	0.14	0.41	0.12	0.38	0.91	0.83	0.96	0.94	0.94	0.80	0.94	0.86
	(0.15)	(0.14)	(0.34)	(0.38)	(0.09)	(0.10)	(0.09)	(0.15)	(0.05)	(0.05)	(0.06)	(0.06)	(0.04)	(0.05)	(0.04)	(0.06)
y = 2	0.30	0.68	0.01	0.32	—	—	0.60	0.78	0.87	0.73	1.00	0.94	—	—	0.74	0.66
	(0.21)	(0.32)	(0.23)	(0.22)			(0.27)	(0.27)	(0.07)	(0.11)	(0.04)	(0.03)			(0.12)	(0.12)
y = 3	0.33	1.08	0.22	0.29	—	—	—	—	0.87	0.58	0.95	0.94	—	—	—	—
	(0.15)	(0.35)	(0.22)	(0.21)					(0.06)	(0.14)	(0.04)	(0.04)				

Notes: Estimated slope coefficients of Mincer-Zarnowitz regressions for model-based predictions of next-quarter's published values for SPF forecasts at different forecast horizons. Heteroskedasticity-consistent standard errors in brackets. Bold font distinguishes coefficient estimates significantly different from 0 (intercept) or 1 (slope) with a 10% confidence level. Evaluation window from 1990Q1 to 2023Q4 (and as far as data for SPF forecasts at the different horizons is available).

Table A.4: Predictability of SPF point forecasts (model w/noise)

	intercept								slope							
	RGDP		UNRATE		PGDP		CPI		RGDP		UNRATE		PGDP		CPI	
Forecast	MDS	VAR	MDS	VAR	MDS	VAR	MDS	VAR	MDS	VAR	MDS	VAR	MDS	VAR	MDS	VAR
h = 0	-1.52	−1.09	0.81	1.02	−0.04	0.04	−0.33	−0.31	1.41	1.32	0.86	0.83	0.99	0.98	1.15	1.19
	(0.76)	(0.71)	(0.52)	(0.60)	(0.11)	(0.12)	(0.40)	(0.37)	(0.24)	(0.25)	(0.08)	(0.10)	(0.05)	(0.06)	(0.16)	(0.15)
h = 1	−0.11	−0.04	0.55	0.82	−0.08	0.08	−0.07	0.04	1.02	1.02	0.91	0.86	1.02	0.99	1.01	1.00
	(0.28)	(0.27)	(0.43)	(0.51)	(0.09)	(0.09)	(0.15)	(0.13)	(0.09)	(0.09)	(0.06)	(0.08)	(0.04)	(0.04)	(0.07)	(0.06)
h = 2	−0.14	0.02	0.38	0.59	0.11	0.27	0.10	0.14	1.02	0.97	0.94	0.90	0.94	0.85	0.94	0.95
	(0.23)	(0.23)	(0.36)	(0.42)	(0.07)	(0.08)	(0.10)	(0.11)	(0.08)	(0.08)	(0.06)	(0.07)	(0.03)	(0.03)	(0.04)	(0.05)
h = 3	0.13	0.50	0.26	0.52	0.15	0.25	0.15	0.21	0.94	0.80	0.96	0.91	0.92	0.86	0.92	0.92
	(0.26)	(0.26)	(0.32)	(0.36)	(0.08)	(0.08)	(0.09)	(0.09)	(0.09)	(0.09)	(0.05)	(0.06)	(0.04)	(0.03)	(0.04)	(0.04)
h = 4	0.37	1.25	0.20	0.48	0.20	0.24	0.13	0.25	0.87	0.57	0.97	0.93	0.91	0.90	0.94	0.89
	(0.19)	(0.26)	(0.29)	(0.35)	(0.07)	(0.08)	(0.09)	(0.09)	(0.06)	(0.09)	(0.05)	(0.06)	(0.03)	(0.04)	(0.04)	(0.03)
y = 1	0.09	0.20	0.25	0.41	0.12	0.18	0.02	0.10	0.94	0.91	0.96	0.93	0.93	0.91	0.98	0.96
	(0.25)	(0.21)	(0.28)	(0.33)	(0.07)	(0.07)	(0.12)	(0.11)	(0.09)	(0.07)	(0.05)	(0.06)	(0.03)	(0.03)	(0.05)	(0.05)
y = 2	0.16	0.13	0.36	0.26	—	—	0.36	0.61	0.94	0.96	0.92	0.95	—	—	0.85	0.74
	(0.25)	(0.27)	(0.36)	(0.24)			(0.25)	(0.21)	(0.09)	(0.10)	(0.07)	(0.04)			(0.11)	(0.09)
y = 3	0.11	0.99	1.03	0.18	—	—	—	—	0.95	0.59	0.76	0.95	—	—	—	—
	(0.16)	(0.59)	(0.37)	(0.19)					(0.06)	(0.24)	(0.08)	(0.04)				

Notes: Estimated slope coefficients of Mincer-Zarnowitz regressions for model-based predictions of next-quarter's published values for SPF forecasts at different forecast horizons. Heteroskedasticity-consistent standard errors in brackets. Bold font distinguishes coefficient estimates significantly different from 0 (intercept) or 1 (slope) with a 10% confidence level. Evaluation window from 1990Q1 to 2023Q4 (and as far as data for SPF forecasts at the different horizons is available).

To further assess the role of measurement noise in our models and results, Tables A.3 and A.4 provide the estimated intercepts and slopes of Mincer-Zarnowitz regressions of SPF forecasts published in quarter $t+1$ on SPF forecasts estimated from our model using SPF forecasts up through quarter t. Table A.3 reports results from MDS and VAR specifications without measurement noise; Table A.4 provides corresponding results from specifications with measurement noise (the results also shown in the paper). In these results, the forecasts from models without noise are somewhat less efficient predictions of future SPF forecasts, in particular for annual SPF forecasts, as well as the four-quarters-ahead SPF. Overall, there are more rejections of slope coefficients of unity in the no-noise forecasts than the with-noise forecasts. Related, in some cases, the no-noise forecasts yield noticeably lower slope coefficients than the with-noise forecasts, especially with the VAR and less so with the MDS specification. For example, with GDP growth (PGDP inflation) at the four-quarters-ahead horizon ($h = 4$), the slope coefficient estimate is 0.39 (0.47) in the noise-free MDS forecasts and 0.87 (0.91) in the with-noise MDS forecasts. As another example, with GDP growth (PGDP inflation) at the one-year-ahead horizon ($y = 1$ in the table), the slope coefficient estimate is 0.83 (0.80) in the noise-free VAR forecasts and 0.91 (0.91) in the with-noise VAR forecasts.

While the specification with or without measurement error has some bearing on imputed SPF-consistent expectations, and the model's fit for SPF data, it has less effect on model-based predictive densities for the outcome variable. To illustrate the latter, Figure A.11–A.14 plot the probability integral transforms (PITs) of the forecasts of MDS and VAR models without noise against those from our baseline models with noise. As these figures show, both model variants generate fairly similar PITs. Likewise, the (realized) coverage rates for 68% and 90% predictive intervals generated from the model without noise, as reported in Table A.5, are quite similar to those from models with noise as reported in Tables A.11 and A.10 further below (as well as Table 3 in the paper).

While the specification of measurement error notably affects the imputed term structures of expectations (as shown in Figures A.7 through A.10), those effects change the imputed expectations by just about 10-20 basis points. In contrast, the predictive densities for the (quarterly) outcome variables are much wider; as reported in the paper, the width of their 68% bands regularly amounts to multiple percentage points. These differences in scales also explain the relative similarity in predictive densities obtained from models with and without noise, despite their differing impact on imputed term structures of expectations. All told, the

Table A.5: Coverage rates (model w/o noise, full sample)

	RGDP		UNRATE		PGDP		CPI	
h	68%	90%	68%	90%	68%	90%	68%	90%
PANEL A: MDS Model								
0	48.53***	80.15***	87.50***	96.32***	58.09**	84.56	66.91	91.91
1	54.07***	77.78***	82.96***	96.30***	60.00*	85.19	59.26**	85.19
2	52.99***	79.10***	79.85**	94.78*	60.45	82.09*	58.21**	85.07
3	50.38***	78.20**	75.94	93.98	60.15	85.71	63.16	83.46
4	56.06**	81.82*	71.97	91.67	57.58**	84.85	65.15	84.85
5	54.96**	85.50	69.47	90.08	62.60	87.02	64.89	82.44
6	62.31	85.38	66.92	88.46	69.23	93.08	66.92	84.62
7	66.67	88.37	66.67	89.92	68.22	93.02	65.89	86.05
8	69.53	84.38	66.41	89.06	70.31	93.75	65.62	85.94
9	71.65	84.25	64.57	88.98	70.87	92.91	66.93	87.40
10	70.63	87.30	61.90	88.10	70.63	92.86	67.46	88.10
11	69.60	87.20	64.00	88.00	72.00	92.00	70.40	87.20
12	68.55	87.90	63.71	87.10	75.00	91.13	69.35	87.10
13	69.92	88.62	61.79	87.80	75.61	92.68	69.92	87.80
14	69.67	87.70	60.66	86.89	76.23	94.26	68.03	88.52
15	67.77	88.43	61.16	86.78	76.03	94.21	71.07	87.60
16	71.67	88.33	59.17	87.50	75.83	93.33	71.67	89.17
PANEL B: VAR Model								
0	52.21***	82.35***	80.15***	94.12*	56.62***	84.56	67.65	91.18
1	56.30**	77.78***	82.22***	95.56**	62.96	82.96*	59.26*	85.93
2	56.72**	79.85***	79.10**	94.78*	67.16	85.82	63.43	83.58
3	54.89**	79.70**	78.95*	93.98	64.66	87.22	64.66	86.47
4	55.30**	84.85	72.73	91.67	64.39	86.36	67.42	87.88
5	58.78*	84.73	70.99	90.84	66.41	88.55	68.70	87.79
6	58.46*	84.62	67.69	90.00	66.15	90.00	66.15	86.92
7	58.14*	85.27	63.57	89.92	66.67	90.70	65.12	87.60
8	60.94	82.03	61.72	89.84	66.41	89.84	67.19	87.50
9	62.20	81.10	60.63	88.98	66.14	92.13	70.08	88.19
10	61.90	84.92	57.14	88.10	65.87	91.27	69.84	88.10
11	64.00	82.40	55.20**	88.00	68.00	89.60	68.00	89.60
12	66.13	84.68	54.84*	86.29	67.74	91.13	70.97	89.52
13	68.29	85.37	54.47*	84.55	66.67	91.06	73.17	89.43
14	66.39	84.43	53.28*	85.25	70.49	90.16	71.31	90.16
15	66.94	86.78	52.89*	85.12	73.55	90.91	73.55	89.26
16	66.67	87.50	53.33	85.83	74.17	91.67	72.50	90.00

Note: Coverage rates for uncertainty bands with nominal levels of 68% and 90% for out-of-sample forecasts at quarterly forecast horizons, h. Evaluation window from 1990Q1 through 2023Q4 (and as far as realized values are available). Reflecting the availability of annual SPF forecasts, forecasts for inflation in CPI and GDP prices are evaluated only up to $h = 12$, and $h = 8$, respectively. Significance assessed by Diebold-Mariano tests using Newey-West standard errors with $h + 1$ lags. ***, ** and * denote significance at the 1%, 5%, and 10% level, respectively.

Figure A.11: GDP growth PITs with and without noise

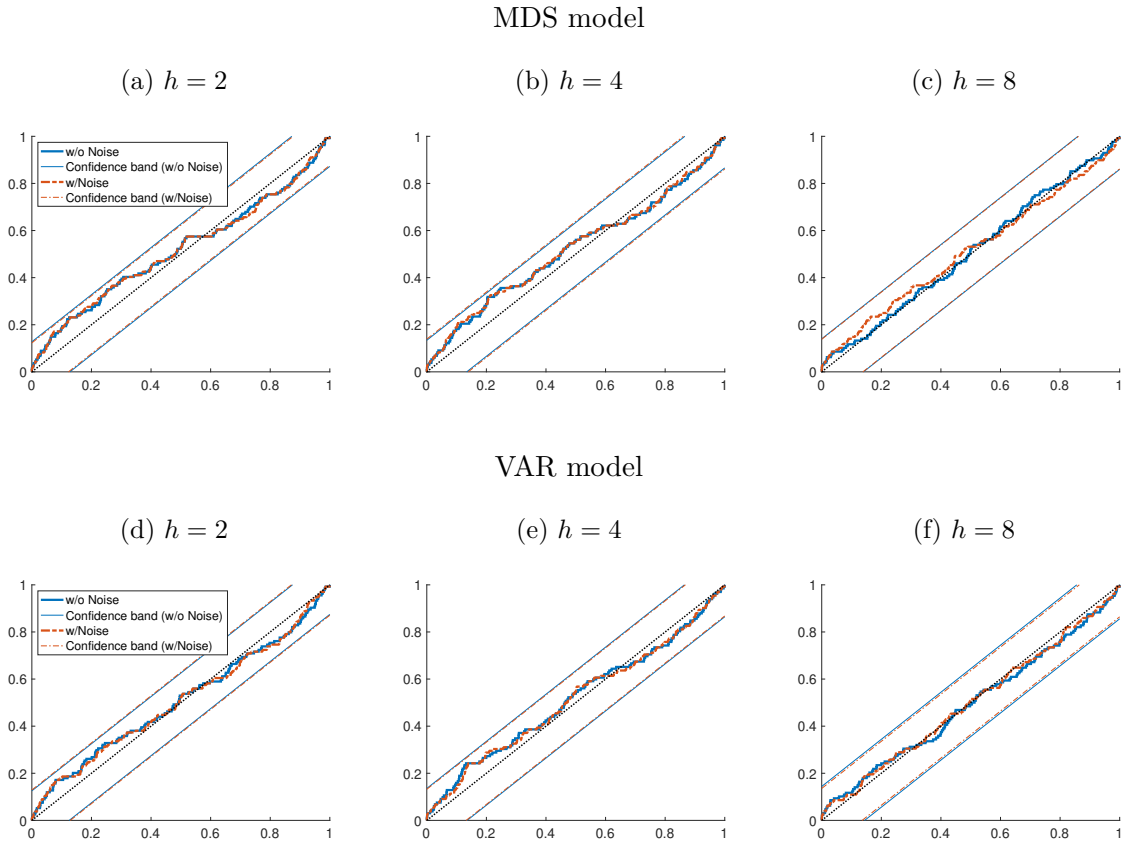

Notes: Empirical cumulative distributions of probability integral transforms (PITs) for GDP growth at selected quarterly forecast horizons. All forecasts are generated out of sample by our MDS and VAR models (with and without noise in measurement equations for annual forecasts), and evaluated over an evaluation window from 1990Q1 through 2023Q4 (and as far as realized values are available). 95% confidence bands for tests of correct calibration from Rossi and Sekhposyan (2019); computed separately for each model, but with nearly identical plot lines.

specification of measurement error for annual forecasts matters mainly for improving the model's fit for SPF data than for the outcome variable.

Figure A.12: Unemployment rate PITs with and without noise

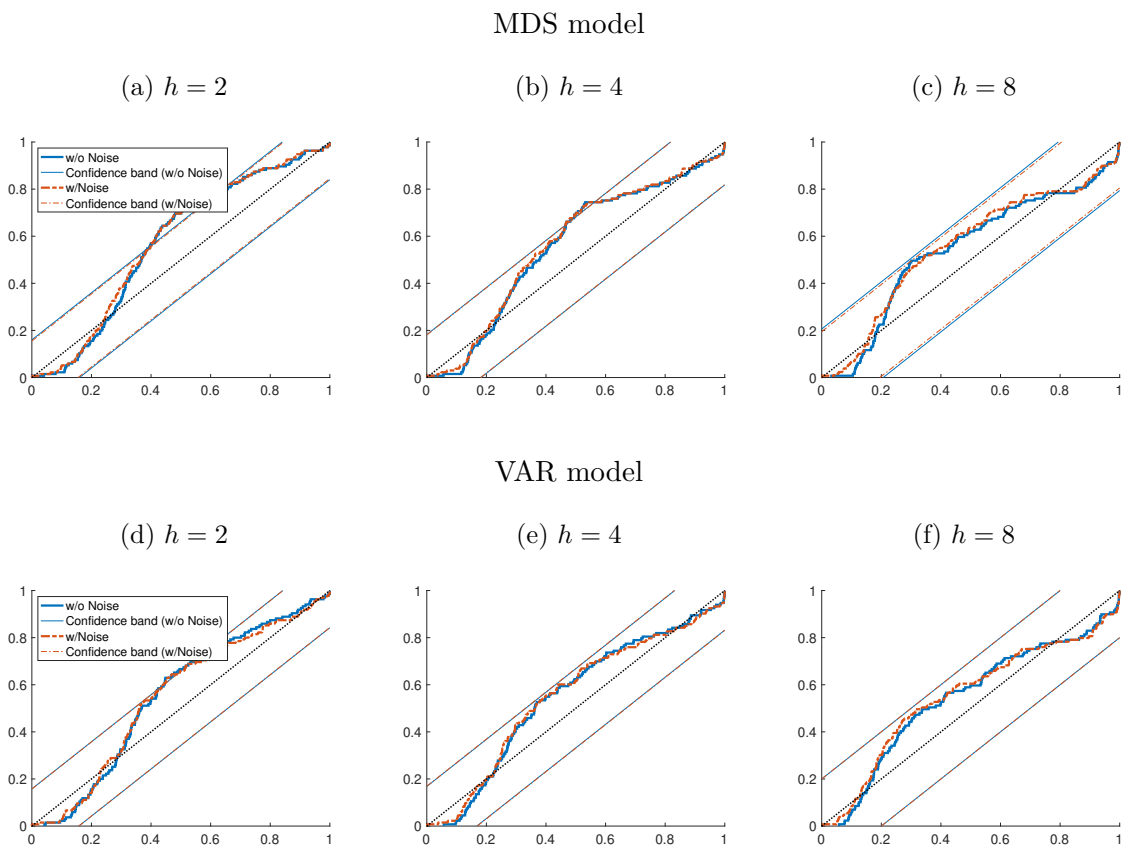

Notes: Empirical cumulative distributions of probability integral transforms (PITs) for Unemployment rate at selected quarterly forecast horizons. All forecasts are generated out of sample by our MDS and VAR models (with and without noise in measurement equations for annual forecasts), and evaluated over an evaluation window from 1990Q1 through 2023Q4 (and as far as realized values are available). 95% confidence bands for tests of correct calibration from Rossi and Sekhposyan (2019); computed separately for each model, but with nearly identical plot lines.

Figure A.13: GDP price inflation PITs with and without noise

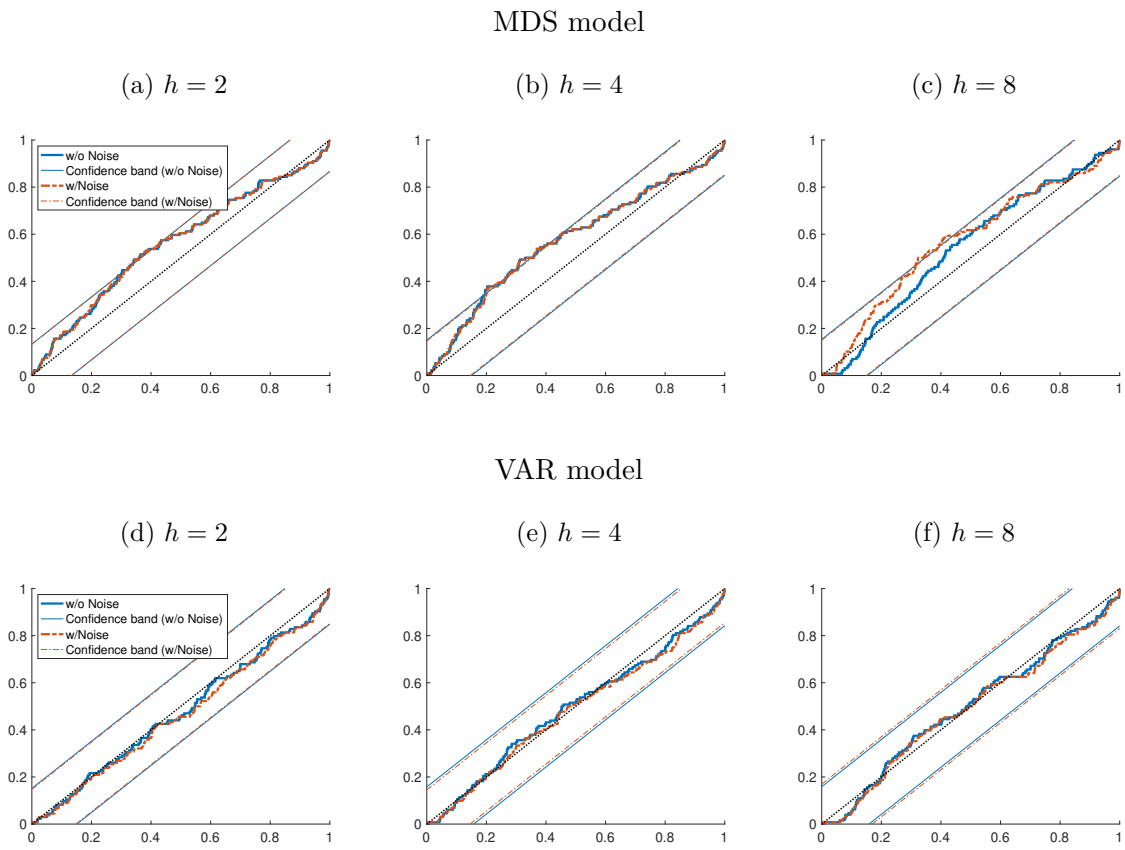

Notes: Empirical cumulative distributions of probability integral transforms (PITs) for GDP price inflation at selected quarterly forecast horizons. All forecasts are generated out of sample by our MDS and VAR models (with and without noise in measurement equations for annual forecasts), and evaluated over an evaluation window from 1990Q1 through 2023Q4 (and as far as realized values are available). 95% confidence bands for tests of correct calibration from Rossi and Sekhposyan (2019); computed separately for each model, but with nearly identical plot lines.

Figure A.14: CPI inflation PITs with and without noise

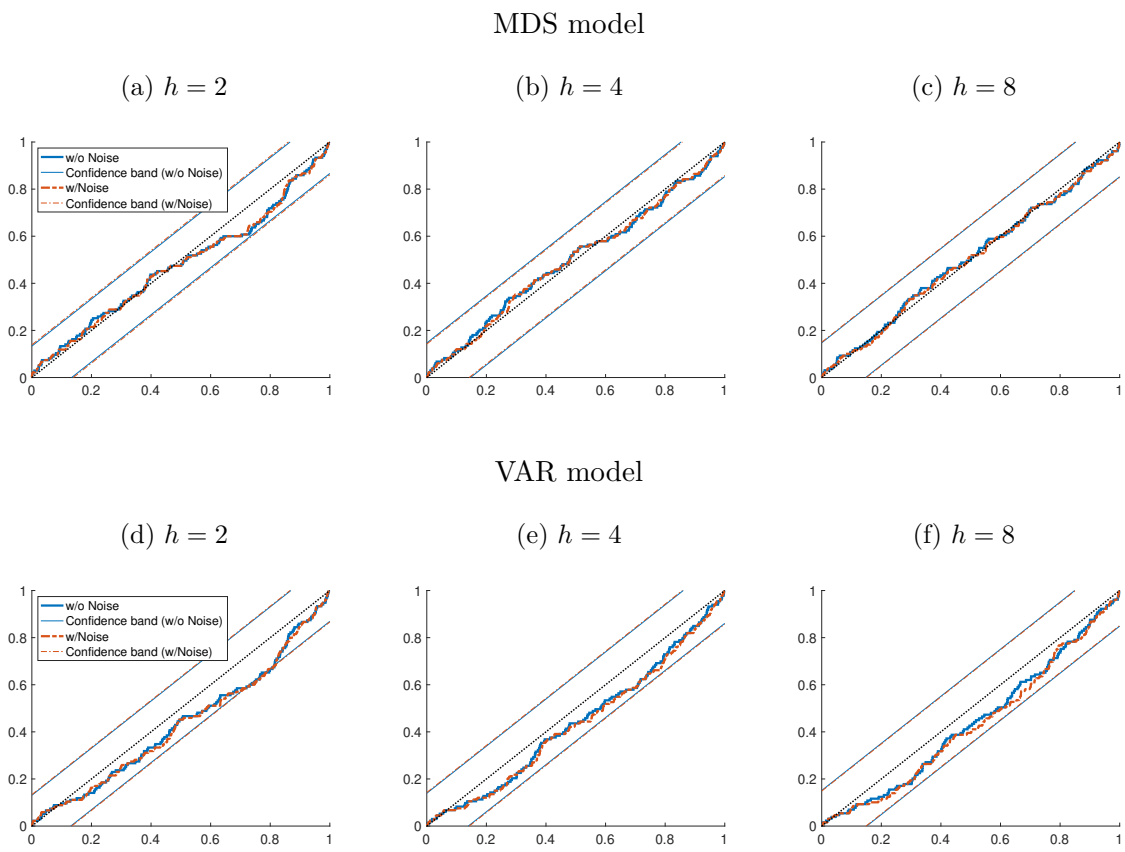

Notes: Empirical cumulative distributions of probability integral transforms (PITs) for CPI inflation at selected quarterly forecast horizons. All forecasts are generated out of sample by our MDS and VAR models (with and without noise in measurement equations for annual forecasts), and evaluated over an evaluation window from 1990Q1 through 2023Q4 (and as far as realized values are available). 95% confidence bands for tests of correct calibration from Rossi and Sekhposyan (2019); computed separately for each model, but with nearly identical plot lines.

II Details on Bayesian MCMC sampler and priors

II(a) Model summary, priors and MCMC steps

Before turning to a description of priors and MCMC sampling steps, we begin by restating the equations of our general model, with a VAR specification for forecast updates and unconditional bias, as detailed in Section 4 of the paper.

States: The model tracks a term structure of SPF-implied quarterly forecasts, denoted $\boldsymbol{Y_t}$ as detailed in equation (1) of the paper:

$$\boldsymbol{Y_t} \equiv \left[y_{t-1},\ F_t y_t,\ F_t y_{t+1}, \ldots, F_t y_{t+h}, \ldots, F_t y_{t+H} \right]' . \tag{1}$$

The dynamics of $\boldsymbol{Y_t}$ are characterized by the following trend-cycle decomposition:

$$\boldsymbol{Y_t} = \tilde{\boldsymbol{Y}}_{\boldsymbol{t}} + \mathbf{1} y_t^* , \tag{A.46}$$

$$y_t^* = y_{t-1}^* + w_t^* , \qquad w_t^* \sim \mathcal{N}(0, \omega_t^2) . \tag{A.47}$$

Section 4 of the paper, in equations (7), (9), and (10), derives the following law of motion for the gap vector:

$$\tilde{\boldsymbol{Y}}_{\boldsymbol{t}} = \left(\boldsymbol{I} - \tilde{\boldsymbol{\Psi}} \right) \bar{\boldsymbol{Y}} + \tilde{\boldsymbol{\Psi}} \tilde{\boldsymbol{Y}}_{\boldsymbol{t-1}} + \tilde{\boldsymbol{\eta}}_{\boldsymbol{t}} , \tag{7}$$

$$\text{and} \quad \tilde{\boldsymbol{\eta}}_{\boldsymbol{t}} = \tilde{\boldsymbol{\Pi}} \tilde{\boldsymbol{\eta}}_{\boldsymbol{t-1}} + \tilde{\boldsymbol{\varepsilon}}_{\boldsymbol{t}} , \text{ with } \tilde{\boldsymbol{\varepsilon}}_{\boldsymbol{t}} \sim \mathcal{N}(\mathbf{0}, \tilde{\boldsymbol{\Sigma}}_{\boldsymbol{t}}), \tag{9}$$

$$\Rightarrow \quad \tilde{\boldsymbol{Y}}_{\boldsymbol{t}} = \left(\boldsymbol{I} - \tilde{\boldsymbol{\Psi}} \right) \left(\boldsymbol{I} - \tilde{\boldsymbol{\Pi}} \right) \bar{\boldsymbol{Y}} + \left(\tilde{\boldsymbol{\Psi}} + \tilde{\boldsymbol{\Pi}} \right) \tilde{\boldsymbol{Y}}_{\boldsymbol{t-1}} - \left(\tilde{\boldsymbol{\Psi}} \tilde{\boldsymbol{\Pi}} \right) \tilde{\boldsymbol{Y}}_{\boldsymbol{t-2}} + \tilde{\boldsymbol{\varepsilon}}_{\boldsymbol{t}} , \tag{10}$$

where $\tilde{\boldsymbol{\Psi}}$ is a matrix of zeros and ones as described in equation (8) of the paper, $\tilde{\boldsymbol{\Pi}}$ a stable matrix to be estimated, and $\bar{\boldsymbol{Y}}$ a vector of average gap values, also to be estimated.

As discussed in the paper, the MDS version of our model is nested in the above, with the restrictions $\bar{\boldsymbol{Y}} = \mathbf{0}$ and $\tilde{\boldsymbol{\Pi}} = \mathbf{0}$.

The measurement equations are:

$$\boldsymbol{Z_t} = \begin{bmatrix} \boldsymbol{Z_{q,t}} \\ \boldsymbol{Z_{a,t}} \end{bmatrix} = \begin{bmatrix} \boldsymbol{C_{q,t}} \\ \boldsymbol{C_{a,t}} \end{bmatrix} \boldsymbol{Y_t} + \begin{bmatrix} \mathbf{0} \\ \boldsymbol{n_t} \end{bmatrix} , \quad n_{i,t} \sim \mathcal{N}(0, \sigma_{i,t}^2), \tag{A.48}$$

where $\boldsymbol{Z_{q,t}}$ contains the lagged realized value y_{t-1} and observed quarterly fixed-horizon forecasts from the SPF (all assumed to be measured without error) and $\boldsymbol{Z_{a,t}}$ consists of the observed fixed-event annual predictions from the SPF. Further details on $\boldsymbol{Z_{q,t}}$, $\boldsymbol{Z_{a,t}}$ and their measurement loadings $\boldsymbol{C_{q,t}}$ and $\boldsymbol{C_{a,t}}$ are described in Appendix I(b) above.

Shock distributions: Horseshoe models are applied to the time-varying variances of shocks to trend and noise, ω_t^2 and $\sigma_{i,t}^2$, as detailed further below in appendix II(b). As described in Section 4.5 of the paper, the time-varying second moment matrices of the gap shocks are modeled via the following two-block stochastic volatility (SV) process with fat tails. Restating the equations from the paper, we have:

$$\tilde{\boldsymbol{\varepsilon}}_{\boldsymbol{t}} = \begin{bmatrix} \tilde{\boldsymbol{\varepsilon}}_{\mathbf{1},\boldsymbol{t}} \\ \tilde{\boldsymbol{\varepsilon}}_{\mathbf{2},\boldsymbol{t}} \end{bmatrix} = \begin{bmatrix} \boldsymbol{I} & \tilde{\boldsymbol{K}} \\ \mathbf{0} & \boldsymbol{I} \end{bmatrix} \begin{bmatrix} \boldsymbol{\varepsilon}^*_{\mathbf{1},\boldsymbol{t}} \\ \boldsymbol{\varepsilon}^*_{\mathbf{2},\boldsymbol{t}} \end{bmatrix}, \quad \text{with} \begin{bmatrix} \boldsymbol{\varepsilon}^*_{\mathbf{1},\boldsymbol{t}} \\ \boldsymbol{\varepsilon}^*_{\mathbf{2},\boldsymbol{t}} \end{bmatrix} \sim \mathcal{N}\left(\begin{bmatrix} \mathbf{0} \\ \mathbf{0} \end{bmatrix}, \begin{bmatrix} \lambda_{1,t} \cdot \tilde{\boldsymbol{\Sigma}}_{\mathbf{11}} & \mathbf{0} \\ \mathbf{0} & \lambda_{2,t} \cdot \tilde{\boldsymbol{\Sigma}}_{\mathbf{22}} \end{bmatrix} \right), \tag{15}$$

in which $\tilde{\boldsymbol{K}}$ is a matrix (with dimension $4 \times (H-2)$) of coefficients to be estimated. This SV structure yields the following time-varying variance-covariance matrix of the cyclical shocks:

$$\tilde{\boldsymbol{\Sigma}}_{\boldsymbol{t}} = \begin{bmatrix} \boldsymbol{I} & \tilde{\boldsymbol{K}} \\ \mathbf{0} & \boldsymbol{I} \end{bmatrix} \begin{bmatrix} \lambda_{1,t} \cdot \tilde{\boldsymbol{\Sigma}}_{\mathbf{11}} & \mathbf{0} \\ \mathbf{0} & \lambda_{2,t} \cdot \tilde{\boldsymbol{\Sigma}}_{\mathbf{22}} \end{bmatrix} \begin{bmatrix} \boldsymbol{I} & \tilde{\boldsymbol{K}} \\ \mathbf{0} & \boldsymbol{I} \end{bmatrix}'. \tag{16}$$

The scalar factors $\lambda_{1,t}$ and $\lambda_{2,t}$ impart time variation and fat tails to the shock vector $\tilde{\boldsymbol{\varepsilon}}_{\boldsymbol{t}}$. Building on, among others, Carriero, et al. (2022b), Chan (2020), and Jacquier, Polson, and Rossi (2004), we model these factors as the products of *iid* inverse-gamma draws and persistent stochastic volatility processes:

$$\lambda_{i,t} = \phi_{i,t} \cdot \tilde{\lambda}_{i,t}, \qquad \forall\, i = 1, 2, \tag{17}$$

$$\text{with} \quad \phi_{i,t} \sim \mathcal{IG}\left(\frac{\nu_i}{2}, \frac{\nu_i}{2}\right), \qquad \log \tilde{\boldsymbol{\lambda}}_{\boldsymbol{t}} \equiv \begin{bmatrix} \log \tilde{\lambda}_{1,t} \\ \log \tilde{\lambda}_{2,t} \end{bmatrix} = \begin{bmatrix} \rho_1 & 0 \\ 0 & \rho_2 \end{bmatrix} \log \tilde{\boldsymbol{\lambda}}_{\boldsymbol{t-1}} + \boldsymbol{\epsilon}^{\boldsymbol{\lambda}}_{\boldsymbol{t}}, \tag{18}$$

and $\boldsymbol{\epsilon}^{\boldsymbol{\lambda}}_{\boldsymbol{t}} \sim \mathcal{N}(\mathbf{0}, \boldsymbol{\Phi})$. The *iid* inverse-gamma draws add fat tails in the form of a multivariate t distribution with ν_i degrees of freedom to each block. The vector SV process $\log \tilde{\boldsymbol{\lambda}}_{\boldsymbol{t}}$ has correlated shocks and is normalized to a mean of zero, obviating the need for normalizing assumptions on the constant-coefficient matrices $\tilde{\boldsymbol{\Sigma}}_{\mathbf{11}}$ and $\tilde{\boldsymbol{\Sigma}}_{\mathbf{22}}$.

Notation for state vectors, measurement vectors, and parameters: We collect all observed measurements, $\{\boldsymbol{Z_t}\}_{t=1}^{T}$, in the measurement vector $\boldsymbol{Z}$, and all values of $\{y_t^*\}_{t=0}^{T}$, $\{\tilde{\boldsymbol{Y}}_{\boldsymbol{t}}\}_{t=-1}^{T}$, and $\bar{\boldsymbol{Y}}$ in the (linear) state vector $\boldsymbol{Y}$, where $t = T$ denotes the end of the sample, and $t = -1, 0$ points to initial conditions.[6] Conditional on values for the time-varying second moment parameters, $\{\tilde{\boldsymbol{\Sigma}}_{\boldsymbol{t}}\}_{t=1}^{T}$, and $\{\omega_t^2\}_{t=1}^{T}$, the equations above describe a Gaussian state space, with measurements $\boldsymbol{Z}$ and state vector $\boldsymbol{Y}$. In addition, we collect the latent SV and t-mixture-representation states, $\tilde{\lambda}_{i,t}$ and $\phi_{t,i}$, in the vectors $\tilde{\boldsymbol{\lambda}}$, and $\boldsymbol{\phi}$, respectively, and collect the time-varying second moment parameters for trend and noise shocks in the vectors $\boldsymbol{\omega^2}$ and $\boldsymbol{\sigma^2}$. The remaining parameters of the model are the VAR coefficient matrix, $\tilde{\boldsymbol{\Pi}}$, fixed parameters of the block-SV model, $\boldsymbol{K}$, $\tilde{\boldsymbol{\Sigma}}_{\boldsymbol{11}}$, and $\tilde{\boldsymbol{\Sigma}}_{\boldsymbol{22}}$, the AR(1) coefficients of the cyclical SV processes, $\boldsymbol{\rho} = [\rho_1,\, \rho_2]'$, and associated variance-covariance matrix of shocks to the SV processes, $\boldsymbol{\Phi}$, as well as the degrees of freedom of the multivariate t distributions for cyclical shocks, $\boldsymbol{\nu} = [\nu_1,\, \nu_2]'$.

In our description of the MCMC sampler below, we denote the sets of constant parameters and time-varying second moment states as follows:

$$\boldsymbol{\Theta} \equiv \left\{\tilde{\boldsymbol{\Pi}}, \boldsymbol{K}, \tilde{\boldsymbol{\Sigma}}_{\boldsymbol{11}}, \tilde{\boldsymbol{\Sigma}}_{\boldsymbol{22}}, \boldsymbol{\rho}, \boldsymbol{\Phi}, \boldsymbol{\nu}\right\}, \tag{A.49}$$

$$\boldsymbol{\Omega} = \left\{\tilde{\boldsymbol{\lambda}}, \boldsymbol{\phi}, \boldsymbol{\omega}^2, \boldsymbol{\sigma}^2\right\}. \tag{A.50}$$

When referring to any of these sets while excluding one of its components, we simply refer to $\boldsymbol{\Theta}^{\dagger}$ or $\boldsymbol{\Omega}^{\dagger}$, where the excluded component shall be clear from the context. Moreover, we suppress notation for mixture states involved in the estimation of the SV processes based on the methods of Kim, Shephard, and Chib (1998) and Omori, et al. (2007), as well as mixture states used in the horsehoe representations of the shocks to trend and noise (with further details provided in Appendix II(b)).

We use the following priors for parameters and initial values of the states:

- $y_0^* \sim N\left(0, 100^2\right)$, which is an essentially diffuse prior for the initial value of the trend level.
- $\begin{bmatrix} \tilde{\boldsymbol{Y}}_{\boldsymbol{0}} \\ \tilde{\boldsymbol{Y}}_{\boldsymbol{-1}} \end{bmatrix} \sim N\left(\boldsymbol{0}, 25 \cdot \boldsymbol{I}\right)$, which is a fairly wide prior for the initial gap levels.

[6] Our reference to $\boldsymbol{Y}$ as state vector is understood conditional on trajectories for the time-varying second moment parameters, whose stochastic evolution is, of course, also needed to fully describe the state of the model.

- $\bar{\boldsymbol{Y}} \sim N(\mathbf{0}, \boldsymbol{D_Y})$ with $\boldsymbol{D_Y}$ a diagonal matrix with typical element $\text{Var}(\bar{Y}_j) = 25/j$ so as to imply shrinkage of (unconditional) bias towards zero that is increasing with forecast horizon.

- $\text{vec}(\tilde{\boldsymbol{\Pi}}) \sim N\left(\mathbf{0}, \boldsymbol{D}_{\tilde{\boldsymbol{\Pi}}}\right)$, where $\boldsymbol{D}_{\tilde{\boldsymbol{\Pi}}}$ is a diagonal matrix that implements the structure of a typical Minnesota prior on the VAR coefficients, with overall shrinkage $\text{Var}(\tilde{\Pi}_{i,i}) = \theta_1$ and cross-variable shrinkage $\text{Var}(\tilde{\Pi}_{i,j}) = \theta_1 \cdot \theta_2$ for $i \neq j$, and $\theta_1 = .2^2$ and $\theta_2 = .5^2$.

- $\log(\tilde{\lambda}_{j,0}) \sim \mathcal{N}(0, 100)$ for $j = 1, 2$, which is a fairly uninformative prior for the initial values of the SV factors.

- $\rho_j \sim \mathcal{N}(0.8, 0.2^2)$ for $j = 1, 2$ as in Clark and Ravazzolo (2015) and other studies.

- $\nu_j \sim U(3, 40)$ for $j = 1, 2$, and implemented over a grid of natural numbers as in Jacquier, Polson, and Rossi (2004).

- $\tilde{\boldsymbol{\Sigma}}_{\boldsymbol{jj}} \sim IW(N_j, 0.01 \cdot \boldsymbol{I})$ for $i = 1, 2$, where N_j is the number of elements of the j block of the SV model, so that the prior is relatively uninformative, and has no mean.

- $\text{vec}(\boldsymbol{K}) \sim N(\mathbf{0}, \boldsymbol{I})$.

- $\boldsymbol{\Phi} \sim IW(2, \boldsymbol{I})$, which is fairly uninformative since with as many degrees of freedom as there are SV shocks, this prior has no mean.

Note that the initial levels of trend and mean bias, y_0^* and $\bar{\boldsymbol{Y}}$, are not separately identifiable and could be normalized, for example by setting $y_0^* = 0$. We choose to estimate both, but report only statistics reflecting their joint effects, as the estimates with the normalization $y_0^* = 0$ displayed poorer convergence properties in our experiments.

Our MCMC sampler iterates over the following steps:

1. $p\left(\boldsymbol{Y} \middle| \boldsymbol{\Omega}, \boldsymbol{\Theta}, \boldsymbol{Z}\right)$. Draws from the latent vector of term-structure expectations can be obtained via standard sampling techniques for a linear Gaussian state space model. For computational efficiency, we build on the precision-based sampler developed by Mertens (2023), with details described below in Appendix II(c).

2. $p\left(\tilde{\boldsymbol{\Pi}} \middle| \boldsymbol{Y}, \boldsymbol{\Omega}, \boldsymbol{\Theta}^\dagger, \boldsymbol{Z}\right)$. We draw from the posterior of the VAR coefficients using a Bayesian updating with normal conjugate prior (and posteriors). Appendix II(d) provides details of

an efficient implementation that accounts for the heteroskedasticity in the VAR residuals while exploiting the two-block structure of the SV model. Rejection sampling is employed to ensure that the VAR coefficients remain within the unit circle.

3. $p\left(\boldsymbol{K}\middle|\boldsymbol{Y},\boldsymbol{\Omega},\boldsymbol{\Theta}^{\dagger},\boldsymbol{Z}\right)$ is a standard Bayesian vector regression with normal conjugate prior (and posterior), performed by regressing draws of $\tilde{\boldsymbol{\varepsilon}}_{\boldsymbol{1},\boldsymbol{t}}$ on $\tilde{\boldsymbol{\varepsilon}}_{\boldsymbol{2},\boldsymbol{t}}$ after scaling each by $\lambda_{1,t}$.

4. For $j = 1, 2$, draw $p\left(\tilde{\boldsymbol{\Sigma}}_{\boldsymbol{jj}}\middle|\boldsymbol{Y},\boldsymbol{\Omega},\boldsymbol{\Theta}^{\dagger},\boldsymbol{Z}\right)$, which are standard inverse-Wishart updates based on draws of $\boldsymbol{\varepsilon}^{*}_{\boldsymbol{j},\boldsymbol{t}}/\lambda_{j,t}$.

5. $p\left(\boldsymbol{\nu}\middle|\boldsymbol{Y},\boldsymbol{\Omega},\boldsymbol{\Theta}^{\dagger},\boldsymbol{Z}\right)$ the degrees of freedom for the multivariate student t distributions of the cyclical shocks are sampled over a uniform grid of natural numbers, as described by Jacquier, Polson, and Rossi (2004).

6. $p\left(\tilde{\boldsymbol{\phi}}\middle|\boldsymbol{Y},\boldsymbol{\Omega}^{\dagger},\boldsymbol{\Theta},\boldsymbol{Z}\right)$ which are the common inverse-gamma mixture states of the multivariate t distributions for the cyclical shock blocks, and are drawn as described, for example, by Chan (2020), exploiting the conjugacy of their (conditional) inverse Gamma priors.

7. $p\left(\tilde{\boldsymbol{\lambda}}\middle|\boldsymbol{Y},\boldsymbol{\Omega}^{\dagger},\boldsymbol{\Theta},\boldsymbol{Z}\right)$ which are the common SV processes of the cyclical shock blocks, and are drawn as described, for example, by Carriero, Clark, and Marcellino (2016) and Chan (2020), using the mixture-state SV sampler of Kim, Shephard, and Chib (1998), with a 10-point grid as recommended in Omori, et al. (2007), while following the advice of Del Negro and Primiceri (2015), regarding the correct ordering of steps in the mixture sampling.

8. $p\left(\boldsymbol{\rho}\middle|\boldsymbol{Y},\boldsymbol{\Omega},\boldsymbol{\Theta}^{\dagger},\boldsymbol{Z}\right)$ is a seemingly-unrelated Bayesian system regression with normal conjugate prior (and posterior), using draws of $\tilde{\lambda}_{j,t}$ for $j = 1, 2$, and which is conducted using rejection sampling to ensure that the AR(1) coefficients remain within the unit circle.

9. $p\left(\boldsymbol{\Phi}\middle|\boldsymbol{Y},\boldsymbol{\Omega},\boldsymbol{\Theta}^{\dagger},\boldsymbol{Z}\right)$ is a standard inverse-Wishart update based on draws of the shocks to the (log-)SV processes.

10. $p\left(\boldsymbol{\omega}^{2}\middle|\boldsymbol{Y},\boldsymbol{\Omega}^{\dagger},\boldsymbol{\Theta},\boldsymbol{Z}\right)$ and $p\left(\boldsymbol{\sigma}^{2}\middle|\boldsymbol{Y},\boldsymbol{\Omega}^{\dagger},\boldsymbol{\Theta},\boldsymbol{Z}\right)$ are independently sampled using the Gibbs sampling steps described by Makalic and Schmidt (2016) for the horseshoe model. (See also Appendix II(b)).

The MDS version of our model restricts $\bar{\boldsymbol{Y}}$ and $\tilde{\boldsymbol{\Pi}}$ to be zero, so that when estimating the model, we omit $\bar{\boldsymbol{Y}}$ from the state vector $\boldsymbol{Y}$ and drop the sampling step for $\tilde{\boldsymbol{\Pi}}$. In addition, we

can omit $\tilde{\boldsymbol{Y}}_{-\mathbf{1}}$ from the set of initial conditions, since the gap dynamics are fully determined by a VAR(1) (instead of a VAR(2)) in this case.

The remainder of this appendix describes details of the horseshoe specifications for the shocks to trend and noise, the precision-based sampler for the state space, and the sampling of VAR coefficients when heteroskedasticity in its residuals is described by a two-block SV model.

II(b) Horseshoe shock specifications

II(b.1) Horseshoe model for trend shocks

We model shocks to the trend and measurement errors via a horseshoe model. The horseshoe model has originally been proposed by Carvalho, Polson, and Scott (2010) for modeling sparse regressions, i.e. regressions with a priori potentially many regressors, many of whom are however expected to be irrelevant, with only a few attracting substantial mass a posteriori. As such, while the horseshoe prior places considerable mass on coefficient values of zero, it also has particularly fat tails to generate (few) significantly-sized coefficient estimates.

In our application, we apply the horseshoe model to sequences of shocks (in this case: the trend shocks), instead of regression coefficients where we suspect that most realizations are close to zero while some can also be sizable. In a similar spirit, Prüser (2021) applies a horseshoe model to the shocks of drifting coefficients in a VAR with time-varying parameters. The horseshoe has a conditionally Gaussian representation for the shocks:

$$w_t^* \sim \mathcal{N}\left(0, \omega_t^2\right) \tag{A.51}$$

and achieves its particular form with a hierarchical model for the conditional variance ω_t^2:

$$\Rightarrow \quad \omega_t^2 = \tau_\omega^2 \cdot \vartheta_{w,t}^2 \tag{A.52}$$

$$\text{with} \quad \tau_\omega^2 \sim \mathcal{C}^+(0,1)\,, \qquad \text{and} \quad \vartheta_{w,t}^2 \sim \mathcal{C}^+(0,1)\,, \tag{A.53}$$

where $\mathcal{C}^+(0,1)$ denotes the half-Cauchy distribution. In this horseshoe model, τ_w^2 denotes the global shrinkage (applicable to shocks, w_t^*, at all t) and $\vartheta_{w,t}^2$ denotes local shrinkage (that is specific to the time-t realization of w_t^*). For brevity, we denote the hierarchical model for ω_t^2 as

follows:

$$\omega_t^2 \sim \mathcal{HS}\left(\tau_\omega^2\right). \tag{A.54}$$

The horseshoe model can be represented via scale mixtures. Moreover, as shown by Makalic and Schmidt (2016), Bayesian estimation via Gibbs sampling becomes straightforward when auxiliary variables are used, and we follow their approach in sampling posterior values for ω_t^2. Estimated trend levels are reported in Appendix V further below.

II(b.2) Measurement error with horseshoe model

With similar motivation to the trend shocks, we apply (separate) horseshoe models to the measurement errors attached to annual SPF forecasts. Moreover, since we suspect that the size of measurement errors varies across quarters of the year, we apply separate horseshoe models to forecasts collected in different quarters of the year. For this purpose, let $q(t) \in \{1, 2, 3, 4\}$ denote a function that maps a time index t into the corresponding quarter of the year.

As described, the measurement error in the annual forecast i at time t by $n_{i,t}$ has a conditionally Gaussian distribution, and for each $q(t)$ we apply separate horseshoe models to the conditional variance of $n_{i,t}$:

$$n_{i,t} \sim \mathcal{N}(0, \sigma_{i,t}^2), \qquad \sigma_{i,t}^2 \sim \mathcal{HS}\left(\tau_{i,q(t)}^2\right) \tag{A.55}$$

$$\Rightarrow \quad \sigma_{i,t}^2 = \tau_{i,q(t)}^2 \cdot \vartheta_{i,t}^2, \qquad \tau_{i,q(t)}^2 \sim \mathcal{C}^+(0,1) \qquad \vartheta_{i,t}^2 \sim \mathcal{C}^+(0,1). \tag{A.56}$$

Estimated noise levels are reported in Appendix I(c).

II(c) Precision-based sampling from state space

Step 1 of the MCMC scheme outlined above involves drawing a vector of latent states, $\boldsymbol{Y}$, conditional on observables, $\boldsymbol{Z}$, and draws of model parameters (including time-varying second moment parameters). This sampling step involves a Gaussian signal extraction, which is efficiently implemented with a precision-based sampler, that extends methods detailed in Mertens (2023), and that is described here.

For ease of notation, we drop dependence of the sampling problem on the various model parameters. As before, $\boldsymbol{Y}$, denotes a vector of all values for $\boldsymbol{Y_t}$ for all t, stacked on top of each other, and likewise for $\boldsymbol{Z}$. In stacked form, the state space can be written as follows:

$$\boldsymbol{\mathcal{A}}\boldsymbol{Y} = \boldsymbol{Y_0} + \boldsymbol{\mathcal{B}}\,\boldsymbol{w_t}\,, \qquad \boldsymbol{w} \sim \mathcal{N}(\boldsymbol{0}, \boldsymbol{I})\,, \tag{A.57}$$

$$\boldsymbol{Z_q} = \boldsymbol{\mathcal{C}_q}\boldsymbol{Y}\,, \tag{A.58}$$

$$\boldsymbol{Z_a} = \boldsymbol{\mathcal{C}_a}\boldsymbol{Y} + \boldsymbol{\mathcal{D}}\boldsymbol{n}\,, \qquad \boldsymbol{n} \sim \mathcal{N}(\boldsymbol{0}, \boldsymbol{I})\,, \tag{A.59}$$

and $\boldsymbol{Z_q}$ and $\boldsymbol{Z_a}$ collecting measurement equations for, respectively, quarterly fixed-horizon data (without measurement error) and annual fixed-event data (with measurement error). Details of the mapping between a dynamic representation, such as the one described in Section 4 of the paper, and this stacked representation are illustrated, for example, in Mertens (2023).

Originally developed in Chib and Jeliazkov (2006) and then Chan and Jeliazkov (2009), precision-based samplers offer a computationally efficient alternative to sample latent states from linear Gaussian models as compared to recursive methods based on Kalman filtering and smoothing, such as the simulation smoother of Durbin and Koopman (2002). Precision-based samplers operate on the inverse variance of the state vector. However, in cases where the measurement vector is assumed to be observed without measurement error, as in (A.58), we face an ill-defined posterior precision:

$$\boldsymbol{\mathcal{C}_q}\,\mathrm{Var}\,(\boldsymbol{Y}|\boldsymbol{Z_q}) = \boldsymbol{0} \quad \Longrightarrow \quad |\,\mathrm{Var}\,(\boldsymbol{Y}|\boldsymbol{Z_q})| = 0\,, \tag{A.60}$$

which cannot be directly handled by conventional precision-based samplers. Mertens (2023) derives a precision-based sampler for the case when all measurement variables are observed without error, thus corresponding to the state space consisting solely of (A.57) and (A.58). The version of our model without error in all measurement equations is isomorphic to merely

sampling from $p(\boldsymbol{Y}|\boldsymbol{Z_q})$, but using $\boldsymbol{Z}$ in lieu of $\boldsymbol{Z_q}$, and, in this case, the sampling methods of Mertens (2023) can be directly applied.

To sample from the space consisting of (A.57) and (A.58) and (A.59), where some measurements, but not all, are observed without error, we build on the methods of Mertens (2023) as follows:

- Consider the posterior moments of $p(\boldsymbol{Y}|\boldsymbol{Z_q})$:
  - From a QR decomposition of $\boldsymbol{\mathcal{C}_q}$, obtain the following:

$$\boldsymbol{\mathcal{C}_q} = \boldsymbol{RQ} = \begin{bmatrix} \boldsymbol{R_1} & \boldsymbol{0} \end{bmatrix} \begin{bmatrix} \boldsymbol{Q_1} \\ \boldsymbol{Q_2} \end{bmatrix}, \qquad \boldsymbol{QQ'} = \boldsymbol{I}, \tag{A.61}$$

$$\boldsymbol{\mathcal{Y}} = \begin{bmatrix} \boldsymbol{\mathcal{Y}_1} \\ \boldsymbol{\mathcal{Y}_2} \end{bmatrix} \equiv \begin{bmatrix} \boldsymbol{Q_1} \\ \boldsymbol{Q_2} \end{bmatrix} \boldsymbol{Y}, \qquad \Leftrightarrow \quad \boldsymbol{Y} = \boldsymbol{Q_1'}\,\boldsymbol{\mathcal{Y}_1} + \boldsymbol{Q_2'}\,\boldsymbol{\mathcal{Y}_2}, \tag{A.62}$$

    where $\boldsymbol{R_1}$ is lower triangular, $\boldsymbol{\mathcal{Y}_1}$ describes linear combinations of the state vector $\boldsymbol{Y}$ that are perfectly described by $\boldsymbol{Z_q}$, and $\boldsymbol{\mathcal{Y}_2}$ collects the remaining linear combinations. Since $\boldsymbol{Y}$ is multivariate normal, so is also $\boldsymbol{\mathcal{Y}}$.
  - With $\boldsymbol{\mathcal{Y}_1} = \boldsymbol{R_1^{-1}}\boldsymbol{Z_q}$, the problem of describing $p(\boldsymbol{Y}|\boldsymbol{Z_q})$ boils down to

$$p(\boldsymbol{\mathcal{Y}_2}|\boldsymbol{Z_q}) \sim \mathcal{N}\left(\boldsymbol{\mu_{2|1}}, \boldsymbol{P_{22|1}^{-1}}\right). \tag{A.63}$$

    Derivations for the posterior mean, $\boldsymbol{\mu_{2|1}}$, and precision, $\boldsymbol{P_{22|1}}$, are detailed in Mertens (2023).

- For $p(\boldsymbol{\mathcal{Y}_2}|\boldsymbol{Z_q}, \boldsymbol{Z_a})$, set up a conventional precision-based sampling problem with measurement error.
  - The problem is isomorphic to sampling from $p(\boldsymbol{\mathcal{Y}_2}|\boldsymbol{Z_a})$, while using $\boldsymbol{\mu_{2|1}}$, and $\boldsymbol{P_{22|1}}$ as prior moments.
  - The transformed measurement equation is:

$$\boldsymbol{Z_a} = \boldsymbol{\mathcal{C}_a}\boldsymbol{Q_1'}\,\boldsymbol{R_1^{-1}}\boldsymbol{Z_q} + \boldsymbol{\mathcal{C}_a}\boldsymbol{Q_2'}\,\boldsymbol{\mathcal{Y}_2} + \boldsymbol{\mathcal{D}n} \tag{A.64}$$

$$\Rightarrow \quad \boldsymbol{\tilde{Z}_a} \equiv \boldsymbol{Z_a} - \boldsymbol{\mathcal{C}_a}\boldsymbol{Q_1'}\,\boldsymbol{R_1^{-1}}\boldsymbol{Z_q} \tag{A.65}$$

$$= \boldsymbol{\tilde{\mathcal{C}}_a}\,\boldsymbol{\mathcal{Y}_2} + \boldsymbol{\mathcal{D}n} \tag{A.66}$$

with $\tilde{\boldsymbol{\mathcal{C}}}_{\boldsymbol{a}} \equiv \boldsymbol{\mathcal{C}}_{\boldsymbol{a}} \boldsymbol{Q}_{\boldsymbol{2}}'$.

– Standard signal extraction formulas lead to the following posterior:

$$p\left(\boldsymbol{\mathcal{Y}}_{\boldsymbol{2}} | \boldsymbol{Z}_{\boldsymbol{q}}, \boldsymbol{Z}_{\boldsymbol{a}}\right) \sim \mathcal{N}\left(\boldsymbol{\mu}_{\boldsymbol{2}}, \boldsymbol{P}_{\boldsymbol{22}}^{-\boldsymbol{1}}\right), \tag{A.67}$$

$$\text{with} \quad \boldsymbol{P}_{\boldsymbol{22}} = \boldsymbol{P}_{\boldsymbol{22|1}} + \tilde{\boldsymbol{\mathcal{C}}}_{\boldsymbol{a}}' \left(\boldsymbol{\mathcal{D}}\boldsymbol{\mathcal{D}}'\right)^{-1} \tilde{\boldsymbol{\mathcal{C}}}_{\boldsymbol{a}}, \tag{A.68}$$

$$\text{and} \quad \boldsymbol{P}_{\boldsymbol{22}}\, \boldsymbol{\mu}_{\boldsymbol{2}} = \boldsymbol{P}_{\boldsymbol{22|1}}\, \boldsymbol{\mu}_{\boldsymbol{2|1}} + \tilde{\boldsymbol{\mathcal{C}}}_{\boldsymbol{a}}' \left(\boldsymbol{\mathcal{D}}\boldsymbol{\mathcal{D}}'\right)^{-1} \tilde{\boldsymbol{Z}}_{\boldsymbol{a}}. \tag{A.69}$$

- Given a draw from $p\left(\boldsymbol{\mathcal{Y}}_{\boldsymbol{2}} | \boldsymbol{Z}_{\boldsymbol{q}}, \boldsymbol{Z}_{\boldsymbol{a}}\right)$ we can construct a draw from $p\left(\boldsymbol{Y} | \boldsymbol{Z}_{\boldsymbol{q}}, \boldsymbol{Z}_{\boldsymbol{a}}\right)$ from

$$\boldsymbol{Y} = \boldsymbol{Q}_{\boldsymbol{1}}'\, \boldsymbol{R}_{\boldsymbol{1}}^{-\boldsymbol{1}} \boldsymbol{Z}_{\boldsymbol{q}} + \boldsymbol{Q}_{\boldsymbol{2}}'\, \boldsymbol{\mathcal{Y}}_{\boldsymbol{2}}. \tag{A.70}$$

II(d) Sampling of VAR coefficients with two-block SV model

Step 2 of the MCMC scheme outlined above involves drawing the VAR coefficients, $\tilde{\boldsymbol{\Pi}}$, conditional on the latent states, $\boldsymbol{Y}$, and draws of model parameters (including time-varying second moment parameters). As described in the paper, we employ a two-block SV model for the cyclical shocks. In our VAR specification, these cyclical shocks drive the VAR in the detrended SPF forecast updates, given by equation (9) of the paper (and restated above). Estimation of the VAR coefficients for the updates to (detrended) forecasts requires us to account for this source of heteroskedasticity. In general, estimation of VAR models with SV can be computationally intensive, and Carriero, et al. (2022a) and Carriero, Clark, and Marcellino (2019) derive an efficient Gibbs sampling procedure for this case. We build on their sampler, and we develop a variant of it that exploits the specific two-block structure of the SV model. As such Step 2 of the MCMC sampler described above involves multiple steps, which we detail here:

- We condition on draws for $\{\tilde{\boldsymbol{\eta}}_{\boldsymbol{t}}\}_{t=0}^{T}$, as well as $\tilde{\boldsymbol{K}}$, $\tilde{\boldsymbol{\Sigma}}_{\boldsymbol{ii}}$, $\{\lambda_{i,t}\}_{t=1}^{T}$ $\forall\, i = 1, 2$ and seek to sample the slope coefficients $\tilde{\boldsymbol{\Pi}}$ in the following regression, which restates the regressors of (9) in terms of $\boldsymbol{x}_{\boldsymbol{t}} \equiv \tilde{\boldsymbol{\eta}}_{\boldsymbol{t-1}}$:

$$\tilde{\boldsymbol{\eta}}_{\boldsymbol{t}} = \tilde{\boldsymbol{\Pi}} \boldsymbol{x}_{\boldsymbol{t}} + \tilde{\boldsymbol{\varepsilon}}_{\boldsymbol{t}}, \tag{A.71}$$

where $\tilde{\boldsymbol{\varepsilon}}_{\boldsymbol{t}}$ is the vector of cyclical shocks described in (15). With a multivariate normal prior on $\tilde{\boldsymbol{\Pi}}$ and since the shock vector, $\tilde{\boldsymbol{\varepsilon}}_{\boldsymbol{t}}$ is multivariate normal, the posterior for $\tilde{\boldsymbol{\Pi}}$

is multivariate normal as well.[7] Thus, we can equivalently work with a linearly rotated matrix of VAR slopes, which will be convenient to do, as will be shown in the following steps.

- Following the two-block structure of the SV specification, we partition the vector regression into two sets of equations:

$$\begin{bmatrix} \tilde{\boldsymbol{\eta}}_{\mathbf{1},t} \\ \tilde{\boldsymbol{\eta}}_{\mathbf{2},t} \end{bmatrix} = \begin{bmatrix} \tilde{\boldsymbol{\Pi}}_{\mathbf{1}} \\ \tilde{\boldsymbol{\Pi}}_{\mathbf{2}} \end{bmatrix} \boldsymbol{x}_{\boldsymbol{t}} + \begin{bmatrix} \boldsymbol{I} & \tilde{\boldsymbol{K}} \\ \mathbf{0} & \boldsymbol{I} \end{bmatrix} \begin{bmatrix} \boldsymbol{\varepsilon}^{*}_{\mathbf{1},t} \\ \boldsymbol{\varepsilon}^{*}_{\mathbf{2},t} \end{bmatrix}, \tag{A.72}$$

  where $\boldsymbol{\varepsilon}^{*}_{\boldsymbol{i},\boldsymbol{t}} \sim \mathcal{N}(\mathbf{0}, \lambda_{i,t} \cdot \tilde{\boldsymbol{\Sigma}}_{\boldsymbol{ii}})$ for $i = 1, 2$ (as in (15)).

- When $\tilde{\boldsymbol{K}} \neq \mathbf{0}$, the VAR shocks are correlated across blocks and it is convenient to rotate the system into a decoupled form:

$$\text{Let} \quad \begin{bmatrix} \boldsymbol{\eta}^{*}_{\mathbf{1},t} \\ \boldsymbol{\eta}^{*}_{\mathbf{2},t} \end{bmatrix} \equiv \begin{bmatrix} \boldsymbol{I} & \tilde{\boldsymbol{K}} \\ \mathbf{0} & \boldsymbol{I} \end{bmatrix}^{-1} \begin{bmatrix} \tilde{\boldsymbol{\eta}}_{\mathbf{1},t} \\ \tilde{\boldsymbol{\eta}}_{\mathbf{2},t} \end{bmatrix}, \quad \text{and} \quad \begin{bmatrix} \boldsymbol{\Pi}^{*}_{\mathbf{1}} \\ \boldsymbol{\Pi}^{*}_{\mathbf{2}} \end{bmatrix} \equiv \begin{bmatrix} \boldsymbol{I} & \tilde{\boldsymbol{K}} \\ \mathbf{0} & \boldsymbol{I} \end{bmatrix}^{-1} \begin{bmatrix} \tilde{\boldsymbol{\Pi}}_{\mathbf{1}} \\ \tilde{\boldsymbol{\Pi}}_{\mathbf{2}} \end{bmatrix} \tag{A.73}$$

$$\text{and we obtain} \quad \begin{bmatrix} \boldsymbol{\eta}^{*}_{\mathbf{1},t} \\ \boldsymbol{\eta}^{*}_{\mathbf{2},t} \end{bmatrix} = \begin{bmatrix} \boldsymbol{\Pi}^{*}_{\mathbf{1}} \\ \boldsymbol{\Pi}^{*}_{\mathbf{2}} \end{bmatrix} \boldsymbol{x}_{\boldsymbol{t}} + \begin{bmatrix} \boldsymbol{\varepsilon}^{*}_{\mathbf{1},t} \\ \boldsymbol{\varepsilon}^{*}_{\mathbf{2},t} \end{bmatrix}. \tag{A.74}$$

$$\text{Since} \quad \begin{bmatrix} \boldsymbol{I} & \tilde{\boldsymbol{K}} \\ \mathbf{0} & \boldsymbol{I} \end{bmatrix}^{-1} = \begin{bmatrix} \boldsymbol{I} & -\tilde{\boldsymbol{K}} \\ \mathbf{0} & \boldsymbol{I} \end{bmatrix}, \tag{A.75}$$

  we have $\boldsymbol{\varepsilon}^{*}_{\mathbf{2},t} = \tilde{\boldsymbol{\varepsilon}}_{\mathbf{2},t}$, $\boldsymbol{\varepsilon}^{*}_{\mathbf{1},t} = \tilde{\boldsymbol{\eta}}_{\mathbf{1},t} - \tilde{\boldsymbol{K}}\tilde{\boldsymbol{\eta}}_{\mathbf{2},t}$, $\boldsymbol{\Pi}^{*}_{\mathbf{2}} = \tilde{\boldsymbol{\Pi}}_{\mathbf{2}}$, $\boldsymbol{\Pi}^{*}_{\mathbf{1}} = \tilde{\boldsymbol{\Pi}}_{\mathbf{1}} - \tilde{\boldsymbol{K}}\tilde{\boldsymbol{\Pi}}_{\mathbf{2}}$.

- If the priors for $\boldsymbol{\Pi}^{*}_{\mathbf{1}}$ and $\boldsymbol{\Pi}^{*}_{\mathbf{2}}$ are independent, both blocks of the decoupled VAR system in (A.74) could be separately estimated. However, this is generally not the case. In fact, in a typical application (including ours), a researcher might specify independent priors for $\tilde{\boldsymbol{\Pi}}_{\mathbf{1}}$ and $\tilde{\boldsymbol{\Pi}}_{\mathbf{2}}$. In that case, and with $\tilde{\boldsymbol{K}} \neq \mathbf{0}$, the priors for the rotated slopes, $\boldsymbol{\Pi}^{*}_{\mathbf{1}}$ and $\boldsymbol{\Pi}^{*}_{\mathbf{2}}$, will generally be correlated.

- Below, we derive a two-step Gibbs algorithm with the following steps:

[7] The shock vector is multivariate normal conditional on $\boldsymbol{K}$, $\tilde{\boldsymbol{\Sigma}}_{\boldsymbol{ii}}$, $\{\lambda_{i,t}\}_{t=1}^{T}$ $\forall\, i = 1, 2$.

1. $p\left(\mathbf{\Pi_1^*}|\mathbf{\Pi_2^*},\boldsymbol{\mathcal{I}}\right)$ with prior $p\left(\mathbf{\Pi_1^*}|\mathbf{\Pi_2^*}\right)$
2. $p\left(\mathbf{\Pi_2^*}|\mathbf{\Pi_1^*},\boldsymbol{\mathcal{I}}\right)$ with prior $p\left(\mathbf{\Pi_2^*}|\mathbf{\Pi_1^*}\right)$,

where $\boldsymbol{\mathcal{I}} = \{\{\tilde{\boldsymbol{\eta}}_{\boldsymbol{t}}\}_{t=0}\}_{t=1}^{T}, \tilde{\boldsymbol{K}}, \tilde{\boldsymbol{\Sigma}}_{\boldsymbol{ii}}, \{\lambda_{i,t}\}_{t=1}^{T}\ \forall\, i = 1,2\}$. These Gibbs steps are similar to the triangular algorithm of Carriero, et al. (2022a), but specialized to the two-block case, and they proceed by operating on the rotated slopes (and their priors), rather than by adjusting the VAR equations with additional regressors (as in Carriero, et al. (2022a)). Of course, for full estimation of our state space model, these two Gibbs steps are to be wrapped into a larger Gibbs sampler with additional steps for inference on the latent states, SV processes, etc. and as described elsewhere in our paper (or its appendix).

- In the general case, with $\tilde{\boldsymbol{K}} \neq \mathbf{0}$, we generally have $p\left(\mathbf{\Pi_1^*}|\mathbf{\Pi_2^*}\right) \neq p\left(\mathbf{\Pi_1^*}\right)$ and $p\left(\mathbf{\Pi_2^*}|\mathbf{\Pi_1^*}\right) \neq p\left(\mathbf{\Pi_2^*}\right)$ and these conditional priors are reevaluated at each step of the Gibbs sampler as described further below.[8]

- Apart from deriving $p\left(\mathbf{\Pi_i^*}, \mathbf{\Pi_{j\neq i}^*}|\boldsymbol{\mathcal{I}}\right)\ \forall\, i,j = 1,2$, each of the two Gibbs steps amounts to a standard Gaussian vector regression subject to a scalar SV factor, $\lambda_{i,t}$, and can be efficiently sampled with standard methods.

- A given set of draws for $\mathbf{\Pi_1^*}$ and $\mathbf{\Pi_2^*}$ can then swiftly be transformed into draws for $\tilde{\mathbf{\Pi}}_\mathbf{1}$ and $\tilde{\mathbf{\Pi}}_\mathbf{2}$ by using (A.73). The joint draw for $\tilde{\mathbf{\Pi}}_\mathbf{1}$ and $\tilde{\mathbf{\Pi}}_\mathbf{2}$ is accepted only if the resulting transition matrix for the VAR, $\tilde{\mathbf{\Pi}}$, is stable.

Derivation of priors for the rotated slopes: To derive the conditional priors, $p\left(\mathbf{\Pi_i^*}, \mathbf{\Pi_{j\neq i}^*}|\boldsymbol{\mathcal{I}}\right)$, we begin with the (given) prior for the original VAR slopes, $\tilde{\mathbf{\Pi}}$. Since $\tilde{\mathbf{\Pi}}$ is a matrix (its sub-blocks $\tilde{\mathbf{\Pi}}_\mathbf{1}$ and $\tilde{\mathbf{\Pi}}_\mathbf{2}$ are also matrices), we consider priors for their vectorized forms. To keep better track of the system's block structure, it is convenient to express the prior in terms of vectorizing the transposed slopes matrix, $\tilde{\mathbf{\Pi}}'$:[9]

$$\text{vec}\left(\tilde{\mathbf{\Pi}}'\right) = \begin{bmatrix} \text{vec}\left(\tilde{\mathbf{\Pi}}_\mathbf{1}{}'\right) \\ \text{vec}\left(\tilde{\mathbf{\Pi}}_\mathbf{2}{}'\right) \end{bmatrix}. \tag{A.76}$$

[8] Note: For the case of $\tilde{\boldsymbol{K}} = \mathbf{0}$, we have $p\left(\mathbf{\Pi_1^*}|\mathbf{\Pi_2^*}\right) = p\left(\mathbf{\Pi_1^*}\right)$ and $p\left(\mathbf{\Pi_2^*}|\mathbf{\Pi_1^*}\right) = p\left(\mathbf{\Pi_2^*}\right)$, and the system is perfectly decoupled. A single iteration over both steps generates a direct draw from the joint distribution of $p\left(\mathbf{\Pi_1^*}, \mathbf{\Pi_2^*}|\boldsymbol{\mathcal{I}}\right)$.

[9] Expressing the slopes' prior in terms of $\tilde{\mathbf{\Pi}}'$ also corresponds to much of the general literature on VAR systems, including Kadiyala and Karlsson (1997), and Carriero, Clark, and Marcellino (2019).

Throughout, we assume a Gaussian prior for $\text{vec}\left(\tilde{\boldsymbol{\Pi}}'\right)$ that is mean zero and has a (block-) diagonal variance-covariance matrix. Expressed in terms of precision matrices (i.e. inverse variance-covariance matrices), the prior has the following form:[10]

$$\begin{bmatrix} \text{vec}\left(\tilde{\boldsymbol{\Pi}}_{\boldsymbol{1}}'\right) \\ \text{vec}\left(\tilde{\boldsymbol{\Pi}}_{\boldsymbol{2}}'\right) \end{bmatrix} \sim \mathcal{N}\left(\begin{bmatrix} \boldsymbol{0} \\ \boldsymbol{0} \end{bmatrix}, \begin{bmatrix} \boldsymbol{P}_{\boldsymbol{11}}^{-\boldsymbol{1}} & \boldsymbol{0} \\ \boldsymbol{0} & \boldsymbol{P}_{\boldsymbol{22}}^{-\boldsymbol{1}} \end{bmatrix} \right). \tag{A.77}$$

The vector of rotated slopes is related to the vector of the original slopes as follows:[11]

$$\text{vec}\left(\boldsymbol{\Pi}^{*\prime}\right) = \left(\begin{bmatrix} \boldsymbol{I} & -\tilde{\boldsymbol{K}} \\ \boldsymbol{0} & \boldsymbol{I} \end{bmatrix} \otimes \boldsymbol{I} \right) \text{vec}\left(\tilde{\boldsymbol{\Pi}}'\right) \tag{A.78}$$

$$= \begin{bmatrix} \boldsymbol{I} & -\boldsymbol{\mathcal{K}} \\ \boldsymbol{0} & \boldsymbol{I} \end{bmatrix} \text{vec}\left(\tilde{\boldsymbol{\Pi}}'\right), \qquad \text{with} \quad \boldsymbol{\mathcal{K}} \equiv \tilde{\boldsymbol{K}} \otimes \boldsymbol{I} \tag{A.79}$$

$$\Rightarrow \quad \text{vec}\left(\boldsymbol{\Pi}_{\boldsymbol{1}}^{*\prime}\right) = \text{vec}\left(\tilde{\boldsymbol{\Pi}}_{\boldsymbol{1}}'\right) - \boldsymbol{\mathcal{K}}\,\text{vec}\left(\tilde{\boldsymbol{\Pi}}_{\boldsymbol{2}}'\right), \qquad \text{vec}\left(\boldsymbol{\Pi}_{\boldsymbol{2}}^{*\prime}\right) = \text{vec}\left(\tilde{\boldsymbol{\Pi}}_{\boldsymbol{2}}'\right). \tag{A.80}$$

The joint prior for $\boldsymbol{\Pi}_{\boldsymbol{1}}^{*}$ and $\boldsymbol{\Pi}_{\boldsymbol{2}}^{*}$ can then be expressed (and again using precision matrices) as

$$\begin{bmatrix} \text{vec}\left(\boldsymbol{\Pi}_{\boldsymbol{1}}^{*\prime}\right) \\ \text{vec}\left(\boldsymbol{\Pi}_{\boldsymbol{2}}^{*\prime}\right) \end{bmatrix} \sim \mathcal{N}\left(\begin{bmatrix} \boldsymbol{0} \\ \boldsymbol{0} \end{bmatrix}, \begin{bmatrix} \boldsymbol{P}_{\boldsymbol{11}}^{*} & \boldsymbol{P}_{\boldsymbol{12}}^{*} \\ \boldsymbol{P}_{\boldsymbol{21}}^{*} & \boldsymbol{P}_{\boldsymbol{22}}^{*} \end{bmatrix}^{-1} \right), \tag{A.81}$$

$$\text{where} \quad \begin{bmatrix} \boldsymbol{P}_{\boldsymbol{11}}^{*} & \boldsymbol{P}_{\boldsymbol{12}}^{*} \\ \boldsymbol{P}_{\boldsymbol{21}}^{*} & \boldsymbol{P}_{\boldsymbol{22}}^{*} \end{bmatrix} = \begin{bmatrix} \boldsymbol{I} & \boldsymbol{\mathcal{K}} \\ \boldsymbol{0} & \boldsymbol{I} \end{bmatrix}' \begin{bmatrix} \boldsymbol{P}_{\boldsymbol{11}} & \boldsymbol{0} \\ \boldsymbol{0} & \boldsymbol{P}_{\boldsymbol{22}} \end{bmatrix} \begin{bmatrix} \boldsymbol{I} & \boldsymbol{\mathcal{K}} \\ \boldsymbol{0} & \boldsymbol{I} \end{bmatrix} \tag{A.82}$$

$$= \begin{bmatrix} \boldsymbol{P}_{\boldsymbol{11}} & \boldsymbol{P}_{\boldsymbol{11}}\boldsymbol{\mathcal{K}} \\ \boldsymbol{\mathcal{K}}'\boldsymbol{P}_{\boldsymbol{11}} & \boldsymbol{\mathcal{K}}'\boldsymbol{P}_{\boldsymbol{11}}\boldsymbol{\mathcal{K}} + \boldsymbol{P}_{\boldsymbol{22}} \end{bmatrix}, \tag{A.83}$$

and, using standard signal-extraction formulas, the conditional priors then follow as:

$$\text{vec}\left(\boldsymbol{\Pi}_{\boldsymbol{1}}^{*\prime}\right) \,\big|\, \text{vec}\left(\boldsymbol{\Pi}_{\boldsymbol{2}}^{*\prime}\right) \sim \mathcal{N}\left(-\boldsymbol{\mathcal{K}}\,\text{vec}\left(\boldsymbol{\Pi}_{\boldsymbol{2}}^{*\prime}\right), \boldsymbol{P}_{\boldsymbol{11}}^{-\boldsymbol{1}}\right), \tag{A.84}$$

$$\text{vec}\left(\boldsymbol{\Pi}_{\boldsymbol{2}}^{*\prime}\right) \,\big|\, \text{vec}\left(\boldsymbol{\Pi}_{\boldsymbol{1}}^{*\prime}\right) \sim \mathcal{N}\left(-\boldsymbol{P}_{\boldsymbol{22}}^{-\boldsymbol{1}}\boldsymbol{\mathcal{K}}'\boldsymbol{P}_{\boldsymbol{11}}\,\text{vec}\left(\boldsymbol{\Pi}_{\boldsymbol{1}}^{*\prime}\right), \left(\boldsymbol{\mathcal{K}}'\boldsymbol{P}_{\boldsymbol{11}}\boldsymbol{\mathcal{K}} + \boldsymbol{P}_{\boldsymbol{22}}\right)^{-1}\right). \tag{A.85}$$

For MCMC estimation, an additional step is added to the sampler described above for the

[10] Typical Minnesota-style priors, like the one used in our application, have diagonal variance-covariance matrices, thus also diagonal precision matrices $\boldsymbol{P}_{\boldsymbol{11}}$ and $\boldsymbol{P}_{\boldsymbol{22}}$. The extension to non-diagonal priors and variance-covariance matrices is straightforward.

[11] Throughout, each use of $\boldsymbol{I}$ denotes an identity matrix of conformable size, so that repeated uses of $\boldsymbol{I}$ need not refer to identically-sized identity matrices.

MDS version of the SV model. Between steps 1 and 2 of the sampler, we draw from

$$p\left(\tilde{\mathbf{\Pi}}|\boldsymbol{Z},\boldsymbol{Y},\boldsymbol{\lambda},\sigma_*^2,\tilde{\mathbf{\Sigma}},\sigma_\nu^2\right)=p\left(\tilde{\mathbf{\Pi}}|\boldsymbol{Y},\boldsymbol{\lambda},\tilde{\mathbf{\Sigma}}\right),$$

which is a standard conjugate-normal Bayesian regression update. (Furthermore, $\tilde{\mathbf{\Pi}}$ is added to the conditioning sets of the other steps).

III Coibion-Gorodnichenko slopes implied by VAR model

This appendix describes our calculations of model-implied slopes for regressions testing the efficiency of SPF forecasts known from the work of Coibion and Gorodnichenko (2015). We derive these slopes within our VAR model for forecast updates. To restate relevant parts of the model, we denote the vector of forecast updates (including the lagged nowcast error, and change in long-run forecast) by $\boldsymbol{\eta}_t$, and the VAR model with SV specifies the following:

$$\boldsymbol{\eta_t} \equiv F_t \begin{bmatrix} y_{t-1} \\ y_t \\ y_{t+1} \\ \vdots \\ y_{t+H-1} \\ y_{t+H} \end{bmatrix} - F_{t-1} \begin{bmatrix} y_{t-1} \\ y_t \\ y_{t+1} \\ \vdots \\ y_{t+H-1} \\ y_{t+H-1} \end{bmatrix} \tag{A.86}$$

$$= \tilde{\boldsymbol{\eta}}_{\boldsymbol{t}} + \mathbf{1}w_t^* + \bar{\boldsymbol{\eta}}\,, \tag{A.87}$$

$$\text{with} \quad \tilde{\boldsymbol{\eta}}_{\boldsymbol{t}} = \tilde{\mathbf{\Pi}}\,\tilde{\boldsymbol{\eta}}_{\boldsymbol{t-1}} + \tilde{\boldsymbol{\varepsilon}}_{\boldsymbol{t}}\,, \tag{A.88}$$

$$\text{and} \quad \tilde{\boldsymbol{\varepsilon}}_{\boldsymbol{t}} \sim N(\mathbf{0}, \tilde{\mathbf{\Sigma}}_{\boldsymbol{t}})\,, \tag{A.89}$$

$$w_t^* \sim N(0, \omega_t^2)\,. \tag{A.90}$$

Since the SPF is assumed to know the lagged realized value, we have $F_t y_{t-1} = y_{t-1}$, and the top element of $\boldsymbol{\eta_t}$ is identical to $e_{t-1} = y_{t-1} - F_{t-1}y_{t-1}$. The VAR's transition matrix, $\tilde{\mathbf{\Pi}}$, is required to be stable (i.e. all eigenvalues inside the unit circle).

For each MCMC draw of the model parameters, we derive regression slopes from the population moments of the model. For the time-varying variance parameters, $\tilde{\mathbf{\Sigma}}_{\boldsymbol{t}}$ and ω_t^2, we use fixed values (per MCMC draw) as follows: For the trend shocks, that are generated from a

horseshoe model, $\omega_t^2 \sim \mathcal{HS}(\tau_w^2)$, we use the global scale parameter τ_w^2. This choice is motivated by the notion that the local scale parameter represents occasional shifts in trend levels that are ignored for sake of computing CG slopes. In lieu of $\tilde{\boldsymbol{\Sigma}}_{\boldsymbol{t}}$, at a given MCMC draw, we use the median values over the sampled (time-series) paths for $\lambda_{1,t}$ and $\lambda_{2,t}$ to construct the corresponding (constant) value for $\tilde{\boldsymbol{\Sigma}}$.

III(a) CG regressions in population

Given values for $\tilde{\boldsymbol{\Sigma}}$, ω^2, and $\tilde{\boldsymbol{\Pi}}$, we can solve for the variance of the unconditional (or steady-state) variance of $\boldsymbol{\eta_t}$ as follows:

$$\text{Var}\,(\boldsymbol{\eta_t}) \equiv \boldsymbol{\Gamma} = \tilde{\boldsymbol{\Gamma}} + \mathbf{1}\mathbf{1}'\omega\,, \qquad \text{with} \quad \tilde{\boldsymbol{\Gamma}} = \tilde{\boldsymbol{\Pi}}\,\tilde{\boldsymbol{\Gamma}}\,\tilde{\boldsymbol{\Pi}}' + \tilde{\boldsymbol{\Sigma}}\,, \tag{A.91}$$

where the second equation is a standard Lyapunov equation. Given a (positive definite) solution for $\tilde{\boldsymbol{\Gamma}}$, autocovariances of $\boldsymbol{\eta_t}$ follow as $\text{Cov}\,(\boldsymbol{\eta}_{t+h}, \boldsymbol{\eta_t}) = \tilde{\boldsymbol{\Pi}}^h\,\tilde{\boldsymbol{\Gamma}}\ \forall h > 0$.[12]

Based on the population variances $\text{Var}\,(\boldsymbol{\eta_t})$ and autocovariances $\text{Cov}\,(\boldsymbol{\eta}_{t+h}, \boldsymbol{\eta_t})$, we want to compute regression slopes, b_h, for the following "CG" regression known from Coibion and Gorodnichenko (2015):

$$(1 - F_t)y_{t+h} = a_h + b_h \cdot (F_t - F_{t-1})y_{t+h} + e_{t+h} \tag{A.92}$$

for horizons $h = 0, 1, 2, \ldots$ etc., with

$$b_h = \frac{\text{Cov}\,((1 - F_t)y_{t+h}, (F_t - F_{t-1})y_{t+h})}{\text{Var}\,((F_t - F_{t-1})y_{t+h})}. \tag{A.93}$$

The regressor of the CG regression represents a sum of forecast updates at different points in time:[13]

$$(1 - F_t)y_{t+h} = \sum_{k=0}^{h}(F_{t+k+1} - F_{t+k})y_{t+h}\,. \tag{A.94}$$

Let $\boldsymbol{e}(k)$ denote a selection vector, defined for $k = -1, 0, 1 \ldots, H$, that selects the $(k+2)$th

[12] Equation (A.91) is a standard Lyapunov equation and can be solved analytically. The solution exists since $\tilde{\boldsymbol{\Pi}}$ is stable, and it is positive definite since $\tilde{\boldsymbol{\Sigma}}$ is.

[13] Recall that $F_{t+h+1}y_{t+h} = y_{t+h}$.

element of a vector of length $H+2$ so that $(F_t - F_{t-1})y_{t+k} = \boldsymbol{e}(k)'\,\boldsymbol{\eta_t}$ $(\forall\, k < H)$, and we get:

$$\operatorname{Cov}\left((1-F_t)y_{t+h}, (F_t - F_{t-1})y_{t+h}\right) = \sum_{k=0}^{h} \operatorname{Cov}\left(F_{t+k+1} - F_{t+k})y_{t+h}, (F_t - F_{t-1})y_{t+h}\right) \tag{A.95}$$

$$= \left(\sum_{k=0}^{h} \boldsymbol{e}(h-k-1)'\tilde{\boldsymbol{\Pi}}^{k+1}\right) \tilde{\boldsymbol{\Gamma}}\, \boldsymbol{e}(h)\,, \tag{A.96}$$

$$\text{and} \quad \operatorname{Var}\left((F_t - F_{t-1})y_{t+h}\right) = \boldsymbol{e}(h)'\,\boldsymbol{\Gamma}\,\boldsymbol{e}(h) \tag{A.97}$$

$$= \boldsymbol{e}(h)'\,\tilde{\boldsymbol{\Gamma}}\,\boldsymbol{e}(h) + \omega^2 \tag{A.98}$$

and the CG slope can be computed as follows:

$$b_h = \frac{\left(\sum_{k=0}^{h} \boldsymbol{e}(h-k-1)'\tilde{\boldsymbol{\Pi}}^{k+1}\right) \tilde{\boldsymbol{\Gamma}}\, \boldsymbol{e}(h)}{\boldsymbol{e}(h)'\,\tilde{\boldsymbol{\Gamma}}\,\boldsymbol{e}(h) + \omega^2}\,. \tag{A.99}$$

When pooling the CG slopes across $j = 0, 2, \ldots, h$, the pooled slope is:[14]

$$\bar{b}_{0:h} = \frac{\sum_{j=1}^{h}\left[\left(\sum_{k=0}^{j} \boldsymbol{e}(h-k-1)'\tilde{\boldsymbol{\Pi}}^{k+1}\right) \tilde{\boldsymbol{\Gamma}}\, \boldsymbol{e}(j)\right]}{\sum_{j=1}^{h}\left[\boldsymbol{e}(j)'\,\tilde{\boldsymbol{\Gamma}}\,\boldsymbol{e}(j)\right] + h\cdot\omega^2}\,. \tag{A.100}$$

Since the common trend is a martingale (and thus an efficient forecast), the CG coefficients will be smaller the larger the trend-shock variance, ω^2.

III(b) Estimated CG slopes

Table A.6 reports the slopes of Coibion-Gorodnichenko regressions for each variable implied by our VAR specifications fit to SPF forecasts. We compute the population slopes, as described above, for each draw of model parameters obtained from Bayesian MCMC estimation of the VAR model and report the posterior moments of the pooled slopes, $\bar{b}_{0:h}$, for $h = 3$. The horizons considered correspond to what is available in terms of observed SPF fixed-horizon forecasts, and thus commonly used in empirical work.[15]

These estimates are generally in line with the literature that finds positive coefficients of small-to-modest magnitudes, indicating some departures from full rationality in professional forecasts. For the sample of forecasts through 2023Q4, across variables the posterior medians range from 0.11 (RGDP) to 0.24 (CPI inflation), with 90 percent credible sets that do not

[14] See, for example, Chapter 4 of Hayashi (2000).

[15] Note that the right-hand side of (A.92) involves a forecast for $h+1$ steps ahead, so that computation of $\bar{b}_{0:3}$ involves all observable fixed-horizon forecasts.

Table A.6: Slopes of Coibion-Gorodnichenko regressions

	2019Q4			2023Q4		
Variable	5%	50%	95%	5%	50%	95%
RGDP	0.01	0.11	0.22	0.02	0.12	0.23
UNRATE	0.08	0.18	0.30	0.06	0.15	0.27
PGDP	0.00	0.13	0.29	0.04	0.18	0.35
CPI	0.11	0.22	0.33	0.14	0.25	0.36

Notes: Posterior moments of model-implied slopes, b_h, in predictability regressions of Coibion and Gorodnichenko (2015), $(1 - F_t)y_{t+h} = b_h \cdot (F_t - F_{t-1})y_{t+h} + e_{t+h}$, pooled for $h = 0, 1, 2, 3$. Estimated from our VAR model, using full-sample data through 2019Q4 and 2023Q4, respectively.

include 0, except in the case of the unemployment rate. Quantitatively, our estimates are broadly comparable to those in surveys such as Angeletos, Huo, and Sastry (2021).[16] Based on this evidence, it appears that our VAR model of SPF forecasts can capture reasonably well the empirical extent of non-rationality emphasized by Coibion and Gorodnichenko and subsequent studies.

[16] For example, for a sample of (SPF) unemployment and inflation forecasts for 1984-2017 at a horizon of $h = 3$, these authors report a coefficient of 0.292 (their Table 1).

IV Model-implied IMA representation for outcome process

Our state space model embeds a process for the outcome variable, y_t, that is driven by multiple shocks, most of which represent expectational updates at various horizons. As described in Clark, McCracken, and Mertens (2020), such a representation can emerge from a wide class of models with multiple drivers, including DSGE models, that have a (conditionally linear) state-space representation. For ease of reference, we can also describe the model-implied process for y_t in terms of a univariate representation driven by innovations defined relative to the history of y_t alone:

$$\varepsilon_t \equiv y_t - E(y_t|y^{t-1})\,, \qquad \text{with} \quad y^{t-1} \equiv \{y_{t-1}, y_{t-2}, \ldots\}\,. \tag{A.101}$$

Here we show that our MDS model implies a univariate IMA$(1, H)$ process for y_t, which can be derived from the innovations representation of our state space model. Further below, we also show that, due to the added persistence in its forecast updates, the VAR model implies a univariate IMA$(1, \infty)$ representation.

In this context, the conditional expectations operator, $E(\cdot|y^{t-1})$, is understood to condition also on given values for the model's parameters (like $\tilde{\boldsymbol{\Sigma}}_{\mathbf{11}}$, $\tilde{\boldsymbol{\Sigma}}_{\mathbf{22}}$, $\tilde{\boldsymbol{K}}$, and τ_w^2, or $\tilde{\boldsymbol{\Pi}}$ in the case of the VAR model). For simplicity, we derive a time-invariant process of y_t that abstracts from variations in stochastic volatility. To do so, and similar to our derivation of CG slopes in Appendix III(b), we work with a time-invariant representation of our state space model, obtained by holding fixed the time-varying second moments of the model, $\tilde{\boldsymbol{\Sigma}}_{\boldsymbol{t}}$ and ω_t^2. All computations are performed draw-by-draw from the model's MCMC output. As in Appendix III(b), at every MCMC draw, we employ a fixed value for $\tilde{\boldsymbol{\Sigma}}_{\boldsymbol{t}}$ that is constructed using the median values over the sampled (time-series) paths for $\lambda_{1,t}$ and $\lambda_{2,t}$, and we replace $\omega_t^2 \sim \mathcal{HS}(\tau_w^2)$ by the corresponding draw of the global scale parameter τ_w^2.

IV(a) Univariate process for y_t implied by MDS model

The MDS model is characterized by the following state equations (and assuming constant variances, as discussed above):

$$\tilde{\boldsymbol{Y}}_{\boldsymbol{t}} = \tilde{\boldsymbol{\Psi}}\tilde{\boldsymbol{Y}}_{\boldsymbol{t-1}} + \tilde{\boldsymbol{\eta}}_{\boldsymbol{t}}\,, \qquad \tilde{\boldsymbol{\eta}}_{\boldsymbol{t}} \sim \mathcal{N}(\boldsymbol{0}, \tilde{\boldsymbol{\Sigma}})\,, \tag{A.102}$$

$$y_t^* = y_{t-1}^* + w_t^*\,, \qquad w_t^* \sim \mathcal{N}(0, \tau_w^2)\,. \tag{A.103}$$

We derive an innovations representation based on the following univariate measurement equation:

$$y_t = \boldsymbol{e_1}\tilde{\boldsymbol{Y}}_{\boldsymbol{t+1}} + y_{t+1}^*\,, \tag{A.104}$$

where $\boldsymbol{e_1}$ is a row vector that selects the first element of $\tilde{\boldsymbol{Y}}_{\boldsymbol{t+1}}$.[17] To derive the innovations process for y^t, we need to define the projections of state variables onto y^t:

$$\tilde{\boldsymbol{Y}}_{\boldsymbol{t+1|t}} \equiv E\left(\tilde{\boldsymbol{Y}}_{\boldsymbol{t+1}} \mid y^t\right) = \tilde{\boldsymbol{\Psi}}\tilde{\boldsymbol{Y}}_{\boldsymbol{t|t-1}} + \tilde{\boldsymbol{\kappa}}\,\varepsilon_t\,, \tag{A.105}$$

$$= \left(\boldsymbol{I} - \tilde{\boldsymbol{\Psi}}L\right)^{-1}\tilde{\boldsymbol{\kappa}}\,\varepsilon_t\,, \tag{A.106}$$

and $$y_{t+1|t}^* \equiv E\left(y_{t+1}^* \mid y^t\right) = y_{t|t-1}^* + \kappa^*\,\varepsilon_t\,, \tag{A.107}$$

$\Leftrightarrow$ $$(1-L)\,y_{t+1|t}^* = \kappa^*\,\varepsilon_t\,, \tag{A.108}$$

where $\tilde{\boldsymbol{\kappa}}$ and κ^* are steady-state Kalman gains for each component of the state vector. The lag operator L is understood to shift both the timing and conditioning sets of the projections, as in $L\cdot\tilde{\boldsymbol{Y}}_{\boldsymbol{t|t}} = \tilde{\boldsymbol{Y}}_{\boldsymbol{t-1|t-1}}$ and analogously for $y_{t|t}^*$ and ε_t. To derive the steady-state Kalman gains, consider the following state space:

$$\boldsymbol{\mathcal{S}}_{\boldsymbol{t+1}} = \begin{bmatrix} \tilde{\boldsymbol{Y}}_{\boldsymbol{t+1}} \\ y_{t+1}^* \end{bmatrix} = \boldsymbol{\mathcal{A}}\boldsymbol{\mathcal{S}}_{\boldsymbol{t}} + \boldsymbol{\mathcal{B}}\boldsymbol{w}_{\boldsymbol{t+1}}\,, \qquad \boldsymbol{w}_{\boldsymbol{t}} \sim \mathcal{N}(\boldsymbol{0}, \boldsymbol{I})\,, \tag{A.109}$$

$$y_t = \boldsymbol{\mathcal{C}}\boldsymbol{\mathcal{S}}_{\boldsymbol{t+1}}\,, \tag{A.110}$$

[17] Reflecting the timing assumptions in our state space model, y_t is captured only by $t+1$ state variables. These assumption reflect the data flow of economic data releases relative to the SPF at time $t+1$.

with

$$\boldsymbol{\mathcal{A}} = \begin{bmatrix} \tilde{\boldsymbol{\Psi}} & \mathbf{0} \\ \mathbf{0} & 1 \end{bmatrix}, \qquad \boldsymbol{\mathcal{B}} = \begin{bmatrix} \tilde{\boldsymbol{\Sigma}}^{1/2} & 0 \\ 0 & \tau_w \end{bmatrix}, \qquad \boldsymbol{\mathcal{C}} = \begin{bmatrix} \boldsymbol{e_1} & 1 \end{bmatrix}. \tag{A.111}$$

And the Kalman gains are obtained as follows:

$$\boldsymbol{\kappa} = \begin{bmatrix} \tilde{\boldsymbol{\kappa}} \\ \kappa^* \end{bmatrix} = \boldsymbol{\mathcal{V}}\boldsymbol{\mathcal{C}}' \left(\boldsymbol{\mathcal{C}}\,\boldsymbol{\mathcal{V}}\,\boldsymbol{\mathcal{C}}'\right)^{-1}, \tag{A.112}$$

where $\boldsymbol{\mathcal{V}}$ solves the following Riccati equation:

$$\boldsymbol{\mathcal{V}} = \boldsymbol{\mathcal{A}}\left(\boldsymbol{\mathcal{V}} - \boldsymbol{\mathcal{V}}\boldsymbol{\mathcal{C}}' \left(\boldsymbol{\mathcal{C}}\,\boldsymbol{\mathcal{V}}\,\boldsymbol{\mathcal{C}}'\right)^{-1} \boldsymbol{\mathcal{C}}\,\boldsymbol{\mathcal{V}}\right) \boldsymbol{\mathcal{A}}' + \boldsymbol{\mathcal{B}}\,\boldsymbol{\mathcal{B}}'. \tag{A.113}$$

To derive the univariate innovations process for y_t, note that the state equations imply $\tilde{\boldsymbol{Y}}_{\boldsymbol{t+1|t}} = \tilde{\boldsymbol{\Psi}}\tilde{\boldsymbol{Y}}_{\boldsymbol{t|t-1}}$ and $y^*_{t+1|t} = y^*_{t|t-1}$. With $y_t = \varepsilon_t + \boldsymbol{e_1}\,\tilde{\boldsymbol{\Psi}}\,\tilde{\boldsymbol{Y}}_{\boldsymbol{t|t-1}} + y^*_{t|t-1}$, we obtain:

$$(1-L)y_t = \left(1 - (1-\kappa^*)\,L + (1-L)\,\boldsymbol{e_1}\tilde{\boldsymbol{\Psi}}\left(\boldsymbol{I} - \tilde{\boldsymbol{\Psi}}L\right)^{-1}\tilde{\boldsymbol{\kappa}}\,L\right)\varepsilon_t. \tag{A.114}$$

To determine the number of MA lags on the right-hand side of (A.114), it is useful to note that for $\tilde{\boldsymbol{\Psi}}$ as defined in equation (8) of the paper, we have $\tilde{\boldsymbol{\Psi}}^{H+1+j} = \mathbf{0}$ for all $j > 0$:[18]

$$\left(\boldsymbol{I} - \tilde{\boldsymbol{\Psi}}L\right)^{-1} = \sum_{j=0}^{H+1} (\tilde{\boldsymbol{\Psi}}\,L)^i \quad \Rightarrow \quad \tilde{\boldsymbol{\Psi}}\left(\boldsymbol{I} - \tilde{\boldsymbol{\Psi}}L\right)^{-1} L = \sum_{j=1}^{H+1} \tilde{\boldsymbol{\Psi}}^j\,L^j. \tag{A.115}$$

In total, it follows that there are $H+2$ MA lags on the right-hand side of (A.114), and the process of y_t is an integrated moving-average (IMA) process with integration order of one and H MA lags, or, in short, IMA$(1, H+2)$. As discussed above, there is some choice in selecting the length, H, of the cyclical state vector, $\tilde{\boldsymbol{Y}}_{\boldsymbol{t}}$, used to track the term structure of SPF consistent forecasts. As shown here, this choice of H is reflected in the number of MA lags in the model-implied univariate process for y_t.

Moreover, it is straightforward to verify that for all $j < H+2$ we have $\boldsymbol{e_1}\tilde{\boldsymbol{\Psi}}^j = \boldsymbol{e_{j+1}}$, where $\boldsymbol{e_j}$ is an $H+2$ dimensional row vector that selects the jth row.[19] Denoting the jth element of

[18] Recall that $\boldsymbol{Y_t}$ contains not only forecasts for horizons $h = 1, 2, \ldots, H$ but also the nowcast and the lagged realized value, y_{t-1}, so that $\boldsymbol{Y_t}$ has $H+2$ elements, and the transition matrix $\tilde{\boldsymbol{\Psi}}$ is of dimension $(H+2)\times(H+2)$.

[19] Reflecting differences in context, the definitions of selection vectors $\boldsymbol{e_j}$ here and $\boldsymbol{e}(h)$ in Section III(b) are similar, but differ in that $\boldsymbol{e}(h)$ is a column vector selecting the $(k+2)th$ element.

the Kalman gain vector $\tilde{\boldsymbol{\kappa}}$ by $\tilde{\kappa}_j \equiv \boldsymbol{e_j}\tilde{\boldsymbol{\kappa}}$, the IMA representation simplifies as follows:

$$(1-L)y_t = \left(1-(1-\kappa^*)\cdot L + \sum_{j=1}^{H+1} \boldsymbol{e_1}\,\tilde{\boldsymbol{\Psi}}^j\,\tilde{\boldsymbol{\kappa}}\cdot(L^j - L^{j+1})\right)\cdot\varepsilon_t \tag{A.116}$$

$$= \left(1-(1-\kappa^*)\cdot L + \sum_{j=1}^{H+1} \tilde{\kappa}_{j+1}\cdot(L^j - L^{j+1})\right)\cdot\varepsilon_t\,. \tag{A.117}$$

In the MDS model, the moving average coefficients in the IMA representation of y_t thus correspond to the Kalman gains involved in forming projections of trend and cyclical states that track SPF-consistent expectations at different forecast horizons. When the trend gain, κ^*, is close to zero, the unit-root factor $(1-L)$ nearly cancels on both sides of (A.117). Of course, the case of $\kappa^* \approx 0$ corresponds to situations where the trend shock variance is negligible relative to the variability of cyclical shocks in the model, and y_t is essentially a stationary variable, and its process is close to an MA$(H-1)$. In terms of the level of y_t we can also write:

$$y_t = \left(1+\sum_{j=1}^{H+1}\tilde{\kappa}_{j+1}\cdot L^j\right)\cdot\varepsilon_t + y^*_{t-1|t-1}\,, \tag{A.118}$$

$$\text{with}\quad y^*_{t|t} = \kappa^*\cdot\sum_{j=0}^{\infty}\varepsilon_{t-j}. \tag{A.119}$$

IV(b) Univariate process for y_t implied by VAR model

The derivation of a univariate innovations representation for y_t in the VAR model is similar to the steps described above for the MDS case. The main difference is that (ignoring constants) the gap process for $\tilde{\boldsymbol{Y_t}}$ has a richer VMA representation:

$$\tilde{\boldsymbol{Y_t}} = \tilde{\boldsymbol{\Phi}}(L)^{-1}\,\tilde{\boldsymbol{\varepsilon_t}}\,, \qquad \text{with}\quad \tilde{\boldsymbol{\Phi}}(L) = \left(\boldsymbol{I}-\tilde{\boldsymbol{\Pi}}L\right)\left(\boldsymbol{I}-\tilde{\boldsymbol{\Psi}}L\right). \tag{A.120}$$

The roots of $\tilde{\boldsymbol{\Phi}}(L)$ are the union of the roots of $(\boldsymbol{I}-\tilde{\boldsymbol{\Pi}}L)$ and $(\boldsymbol{I}-\tilde{\boldsymbol{\Psi}}L)$, and the former are generally non-zero so that the VMA lags of $\tilde{\boldsymbol{\Phi}}(L)^{-1}$ vanish only asymptotically. Nevertheless, the derivation of the process for y_t is isomorphic for the MDS case and results in the following IMA$(1,\infty)$ representation:[20]

[20] To derive the Kalman gains for the VAR model, we use the following augmented state space matrices:

$$\boldsymbol{\mathcal{A}} = \begin{bmatrix} \tilde{\boldsymbol{\Psi}}+\tilde{\boldsymbol{\Pi}} & -\tilde{\boldsymbol{\Psi}}\,\tilde{\boldsymbol{\Pi}} & \boldsymbol{0} \\ \boldsymbol{I} & \boldsymbol{0} & \boldsymbol{0} \\ \boldsymbol{0} & \boldsymbol{0} & 1 \end{bmatrix}, \qquad \boldsymbol{\mathcal{B}} = \begin{bmatrix} \tilde{\boldsymbol{\Sigma}}^{1/2} & \boldsymbol{0} \\ \boldsymbol{0} & \boldsymbol{0} \\ \boldsymbol{0} & \tau_w \end{bmatrix}, \qquad \boldsymbol{\mathcal{C}} = \begin{bmatrix} \boldsymbol{e_1} & \boldsymbol{0} & 1 \end{bmatrix}. \tag{A.121}$$

$$(1-L)y_t = \left(1-(1-\kappa^*)\ L + (1-L)\,\boldsymbol{e_1}\left(\tilde{\boldsymbol{\Pi}}+\tilde{\boldsymbol{\Psi}}\right)\ \tilde{\boldsymbol{\Phi}}(L)^{-1}\tilde{\boldsymbol{\kappa}}\,L\right)\varepsilon_t\,. \tag{A.122}$$

$$y_t = \left(1+\boldsymbol{e_1}\left(\tilde{\boldsymbol{\Pi}}+\tilde{\boldsymbol{\Psi}}\right)\ \tilde{\boldsymbol{\Phi}}(L)^{-1}\tilde{\boldsymbol{\kappa}}\,L\right)\cdot\varepsilon_t + y^*_{t|t-1}\,. \tag{A.123}$$

IV(c) Estimates of the IMA process for y_t

To illustrate estimates of the IMA process for y_t, we compute impulse responses of y_t in response to an innovation of the IMA process (denoted ε_t in the derivations above). Figures A.15 through A.18 report these impulse responses for each variable, based on estimates from MDS and VAR models and using data through 2019Q4 or 2024Q1. The estimates differ mainly across variables, and are fairly unchanged when including or excluding data since the onset of the COVID-19 pandemic. The general contours of the estimated impulse responses for each variable are also quite similar using the MDS or VAR models.

By construction, all responses are equal to 1 on impact. For GDP growth and CPI and GDP price inflation, the estimated responses then return within a couple of quarters to the (new) steady state, which is barely changed for GDP growth and GDP price inflation. Even for CPI inflation, a unit surprise in the realized data raises the endpoint of the term structure of expectations by no more than 10 basis points. Of course, all three of these variables measure rates of change, and the relatively low persistence embodied in their estimated impulse responses is consistent with that. In contrast, the unemployment is a more persistent variable, which is also borne out by the estimated hump shape in its impulse responses. In both the MDS and VAR models, the unemployment rate response peaks about three quarters after impact and at responses that exceed the impact value by about one to two fifths. For the MDS model, the peak of its hump-shaped response is followed by a relatively gradual decline, that declines below 0.6 after only about 8 quarters. In contrast, the VAR model generates a sharper peak in the unemployment rate response followed by a swifter decline (reaching the new steady state after about 8 quarters).

Figure A.15: Univariate process for y_t (MDS, 2019Q4)

(a) Real GDP growth

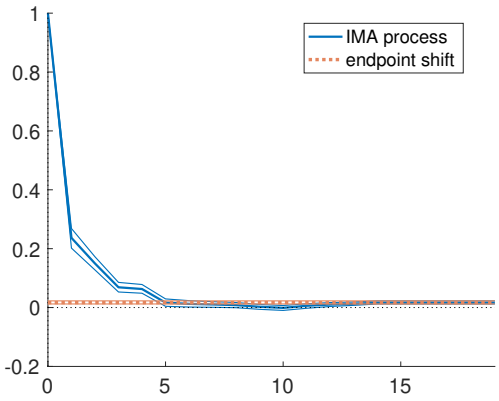

(b) Unemployment rate

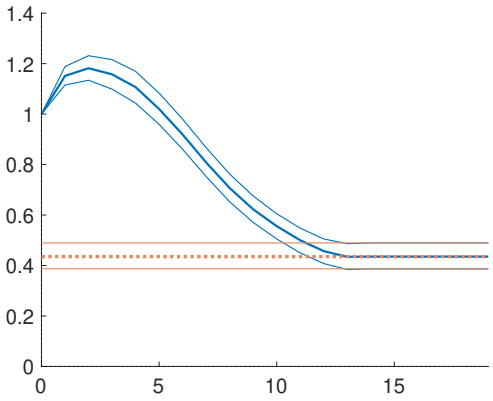

(c) CPI inflation

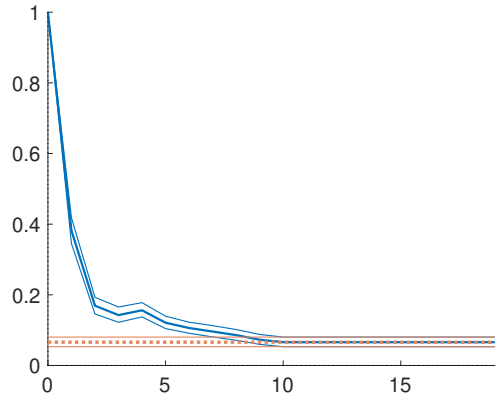

(d) GDP price inflation

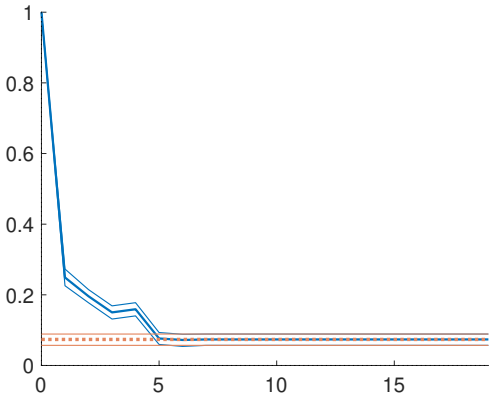

Notes: Impulse responses of univariate innovations representation for y_t implied by our state space for the MDS model. Posterior median and 68% uncertainty bands obtained from data through 2019Q4. The dashed (orange) line depicts the shift in endpoint induced by an innovation to y_t.

Figure A.16: Univariate process for y_t (MDS, 2024Q1)

(a) Real GDP growth

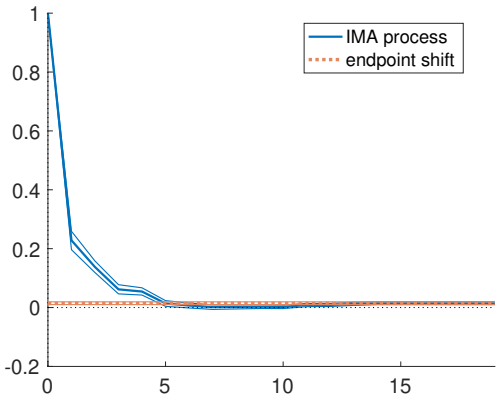

(b) Unemployment rate

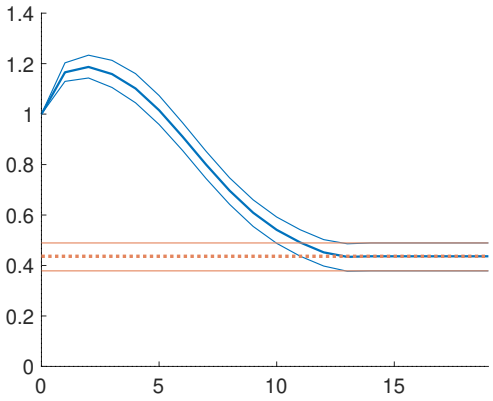

(c) CPI inflation

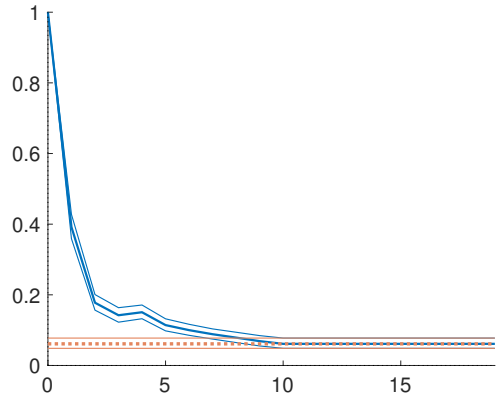

(d) GDP price inflation

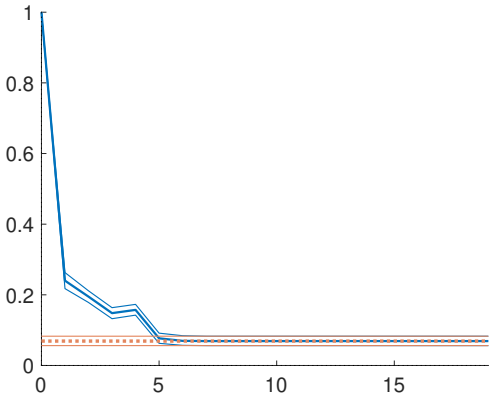

Notes: Impulse responses of univariate innovations representation for y_t implied by our state space for the MDS model. Posterior median and 68% uncertainty bands obtained from data through 2024Q1. The dashed (orange) line depicts the shift in endpoint induced by an innovation to y_t.

Figure A.17: Univariate process for y_t (VAR, 2019Q4)

(a) Real GDP growth

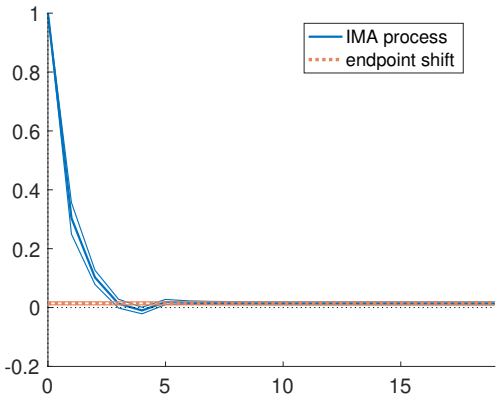

(b) Unemployment rate

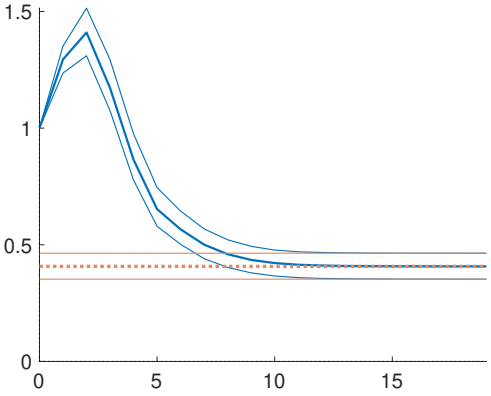

(c) CPI inflation

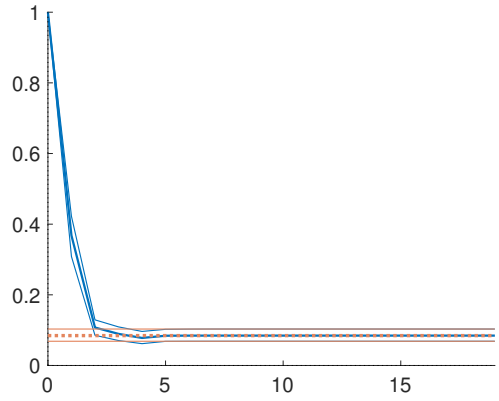

(d) GDP price inflation

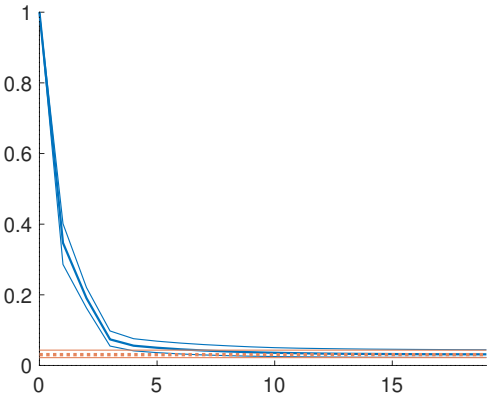

Notes: Impulse responses of univariate innovations representation for y_t implied by our state space for the MDS model. Posterior median and 68% uncertainty bands obtained from data through 2019Q4. The dashed (orange) line depicts the shift in endpoint induced by an innovation to y_t.

Figure A.18: Univariate process for y_t (VAR, 2024Q1)

(a) Real GDP growth

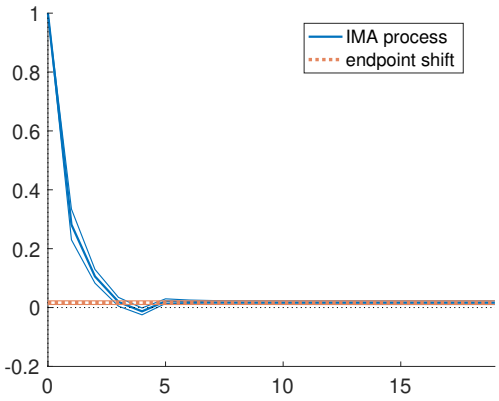

(b) Unemployment rate

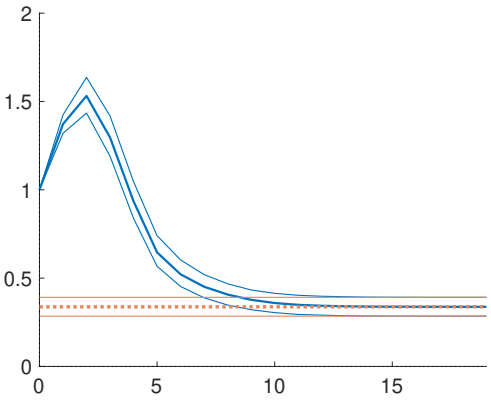

(c) CPI inflation

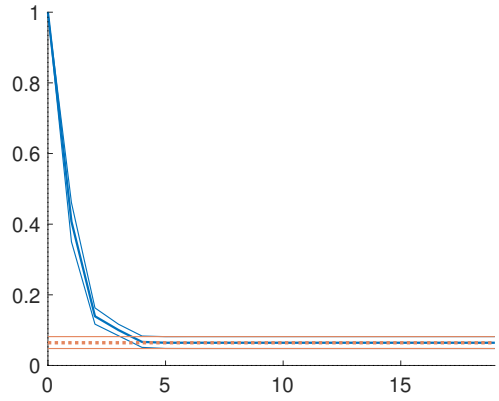

(d) GDP price inflation

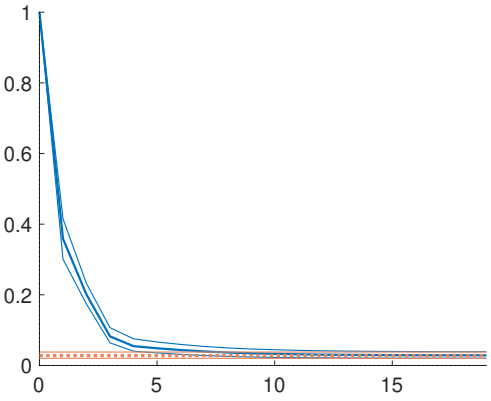

Notes: Impulse responses of univariate innovations representation for y_t implied by our state space for the MDS model. Posterior median and 68% uncertainty bands obtained from data through 2024Q1. The dashed (orange) line depicts the shift in endpoint induced by an innovation to y_t.

V Additional results

This section provides additional results, covering additional variables and further details that were not shown in the paper for the sake of brevity. These include: tables of results for a sample ending in 2019Q4, rather than the paper's sample end of 2023Q4, for Mincer-Zarnowitz predictability regressions (Tables A.7 and A.8, for models with and without noise), the relative accuracy of forecasts from the MDS and VAR models (Table A.9), and coverage rates (Table A.10). Those results are fairly similar to what is reported in the paper and above for data including the pandemic sample. In addition, Table A.11 complements the results for the VAR model reported in the paper (for the sample ending in 2023Q4), with similar results from the MDS model.

The results also include additional figures testing the uniformity of the empirical CDFs of PITs for forecasts of CPI and PGDP inflation (Figures A.19 and A.20) and comparing cumulative log scores — i.e., marginal likelihoods — of the MDS and VAR specifications (Figure A.21). In addition, Figure A.22 reports end-of-sample estimates, obtained from recursive out-of-sample forecast simulations, of the MDS model's shifting endpoints, y_t^*, for each variable, that track closely observed long-run forecasts from the SPF (these are 10-years-ahead average forecasts available for GDP growth and CPI inflation). Figure A.23 reports similar estimates generated from the VAR model.

Table A.7: Predictability of SPF point forecasts (pre COVID)

	intercept								slope							
	RGDP		UNRATE		PGDP		CPI		RGDP		UNRATE		PGDP		CPI	
Forecast	MDS	VAR	MDS	VAR	MDS	VAR	MDS	VAR	MDS	VAR	MDS	VAR	MDS	VAR	MDS	VAR
h = 0	−0.66	−0.49	−0.03	−0.08	0.04	0.13	−0.11	−0.11	1.17	1.16	1.00	1.02	0.94	0.92	1.03	1.08
	(0.43)	(0.39)	(0.07)	(0.08)	(0.11)	(0.11)	(0.44)	(0.43)	(0.16)	(0.15)	(0.01)	(0.01)	(0.05)	(0.05)	(0.18)	(0.18)
h = 1	−0.49	−0.15	−0.07	−0.01	−0.02	0.13	−0.01	0.09	1.14	1.03	1.01	1.00	0.98	0.95	0.97	0.96
	(0.35)	(0.33)	(0.09)	(0.09)	(0.08)	(0.08)	(0.16)	(0.14)	(0.12)	(0.12)	(0.02)	(0.02)	(0.03)	(0.04)	(0.07)	(0.06)
h = 2	−0.09	0.21	−0.10	−0.05	0.13	0.26	0.12	0.16	1.00	0.90	1.02	1.01	0.92	0.84	0.92	0.94
	(0.23)	(0.21)	(0.10)	(0.10)	(0.06)	(0.07)	(0.10)	(0.12)	(0.08)	(0.07)	(0.02)	(0.02)	(0.03)	(0.03)	(0.04)	(0.05)
h = 3	0.14	0.31	−0.13	−0.08	0.11	0.22	0.15	0.21	0.94	0.86	1.03	1.02	0.93	0.86	0.91	0.91
	(0.14)	(0.12)	(0.11)	(0.12)	(0.07)	(0.08)	(0.09)	(0.09)	(0.05)	(0.04)	(0.02)	(0.02)	(0.03)	(0.03)	(0.04)	(0.04)
h = 4	0.29	0.94	−0.18	−0.08	0.16	0.22	0.12	0.23	0.89	0.68	1.04	1.02	0.92	0.91	0.94	0.89
	(0.12)	(0.19)	(0.11)	(0.17)	(0.07)	(0.08)	(0.09)	(0.09)	(0.04)	(0.07)	(0.02)	(0.03)	(0.03)	(0.04)	(0.04)	(0.03)
y = 1	−0.24	−0.15	−0.17	−0.12	0.16	0.22	0.01	0.10	1.06	1.04	1.03	1.03	0.90	0.88	0.98	0.95
	(0.30)	(0.28)	(0.09)	(0.11)	(0.07)	(0.07)	(0.12)	(0.12)	(0.10)	(0.10)	(0.02)	(0.02)	(0.03)	(0.03)	(0.05)	(0.05)
y = 2	−0.19	−0.19	-0.27	−0.08	—	—	0.64	0.94	1.07	1.07	1.03	1.00	—	—	0.73	0.59
	(0.13)	(0.15)	(0.11)	(0.12)			(0.36)	(0.23)	(0.05)	(0.06)	(0.02)	(0.02)			(0.16)	(0.10)
y = 3	0.02	−0.10	0.52	−0.06	—	—	—	—	0.99	1.04	0.86	0.99	—	—	—	—
	(0.19)	(0.20)	(0.16)	(0.20)					(0.07)	(0.08)	(0.03)	(0.04)				

Notes: Estimated slope coefficients of Mincer-Zarnowitz regressions for model-based predictions of next-quarter's published values for SPF forecasts at different forecast horizons. Heteroskedasticity-consistent standard errors in brackets. Bold font distinguishes coefficient estimates significantly different from 0 (intercept) or 1 (slope) with a 10% confidence level. Evaluation window from 1990Q1 to 2019Q4 (and as far as data for SPF forecasts at the different horizons is available).

Table A.8: Predictability of SPF point forecasts (pre COVID, noise-free model)

	intercept								slope							
	RGDP		UNRATE		PGDP		CPI		RGDP		UNRATE		PGDP		CPI	
Forecast	MDS	VAR	MDS	VAR	MDS	VAR	MDS	VAR	MDS	VAR	MDS	VAR	MDS	VAR	MDS	VAR
h = 0	−0.66	−0.46	−0.03	−0.13	0.04	0.15	−0.11	−0.12	1.17	1.15	1.00	1.02	0.94	0.90	1.03	1.08
	(0.43)	(0.39)	(0.07)	(0.08)	(0.11)	(0.11)	(0.44)	(0.45)	(0.16)	(0.15)	(0.01)	(0.01)	(0.05)	(0.05)	(0.18)	(0.19)
h = 1	−0.49	−0.12	−0.07	−0.05	−0.02	0.09	−0.01	−0.01	1.14	1.02	1.01	1.01	0.98	0.94	0.97	0.99
	(0.35)	(0.32)	(0.09)	(0.09)	(0.08)	(0.09)	(0.16)	(0.14)	(0.12)	(0.11)	(0.02)	(0.02)	(0.03)	(0.04)	(0.07)	(0.06)
h = 2	−0.09	0.15	−0.10	0.00	0.13	0.12	0.12	0.17	1.00	0.93	1.02	1.00	0.92	1.01	0.92	0.92
	(0.23)	(0.22)	(0.10)	(0.13)	(0.06)	(0.10)	(0.10)	(0.10)	(0.08)	(0.08)	(0.02)	(0.02)	(0.03)	(0.05)	(0.04)	(0.04)
h = 3	0.14	1.74	−0.13	−0.16	0.11	1.10	0.15	0.61	0.94	0.35	1.03	1.04	0.93	0.41	0.91	0.75
	(0.14)	(0.15)	(0.11)	(0.24)	(0.07)	(0.07)	(0.09)	(0.18)	(0.05)	(0.06)	(0.02)	(0.05)	(0.03)	(0.02)	(0.04)	(0.07)
h = 4	1.65	1.76	−0.13	0.07	1.13	0.18	0.48	0.49	0.39	0.38	1.03	0.99	0.52	0.90	0.80	0.82
	(0.19)	(0.14)	(0.12)	(0.17)	(0.16)	(0.08)	(0.15)	(0.11)	(0.07)	(0.05)	(0.02)	(0.03)	(0.07)	(0.04)	(0.06)	(0.05)
y = 1	0.42	0.51	−0.16	−0.18	0.17	0.42	0.12	0.38	0.83	0.81	1.03	1.03	0.92	0.78	0.94	0.85
	(0.17)	(0.13)	(0.13)	(0.16)	(0.08)	(0.09)	(0.09)	(0.15)	(0.06)	(0.05)	(0.03)	(0.03)	(0.04)	(0.04)	(0.04)	(0.06)
y = 2	0.13	0.29	-0.33	−0.03	—	—	0.98	1.20	0.94	0.89	1.05	0.99	—	—	0.57	0.48
	(0.10)	(0.24)	(0.08)	(0.09)			(0.32)	(0.30)	(0.04)	(0.09)	(0.02)	(0.02)			(0.14)	(0.13)
y = 3	0.13	0.35	0.06	0.11	—	—	—	—	0.94	0.87	0.97	0.97	—	—	—	—
	(0.16)	(0.31)	(0.22)	(0.20)					(0.06)	(0.12)	(0.04)	(0.04)				

Notes: Estimated slope coefficients of Mincer-Zarnowitz regressions for model-based predictions of next-quarter's published values for SPF forecasts at different forecast horizons. Heteroskedasticity-consistent standard errors in brackets. Bold font distinguishes coefficient estimates significantly different from 0 (intercept) or 1 (slope) with a 10% confidence level. Evaluation window from 1990Q1 to 2019Q4 (and as far as data for SPF forecasts at the different horizons is available).

Table A.9: Relative Forecast Accuracy of MDS vs VAR models (pre COVID)

	RMSE				CRPS			
h	RGDP	UNRATE	PGDP	CPI	RGDP	UNRATE	PGDP	CPI
0	1.00	1.16	1.02	0.92*	1.00	0.96	1.01	0.94***
1	1.00	1.06	1.00	1.01	1.00	0.96	0.99	1.01
2	0.99	1.01	0.98	1.01	0.99	0.96	0.97	1.01
3	1.00	0.99	0.98	1.00	1.01	0.96	0.97	1.01
4	1.00	0.99	0.99	0.99	1.00	0.97	0.98	1.01
5	1.01	1.00	1.00	0.99	1.02	0.99	0.99	1.00
6	1.01	1.01	1.01	0.99	1.02	1.00	1.00	1.00
7	1.01	1.01	1.00	0.98	1.01	1.01	0.99	1.00
8	1.01	1.02	1.00	0.98	1.01	1.02	0.99	0.99
9	1.00	1.02	1.01	0.98	1.01	1.02	1.00	0.99
10	1.00	1.02	1.01	0.99	1.00	1.02	1.00	1.00
11	1.01	1.01	1.00	0.98	1.00	1.01	0.99	1.00
12	1.01	1.01	1.01	0.98	1.01	1.01	1.00	0.99
13	1.01	1.00	1.01	0.98	1.01	1.00	1.00	0.99
14	1.01	1.00	1.01	0.98	1.01	0.99	1.00	0.99
15	1.01	0.99	1.01	0.97	1.02	0.99	1.00	0.99
16	1.02	0.99	1.01	0.97	1.03*	0.98	0.99	0.99

Note: Relative RMSE and CRPS of VAR model (with MDS in denominator). Quarterly forecast horizons, h. Evaluation window from 1990Q1 through 2019Q4 (and as far as realized values are available). Significance assessed by Diebold-Mariano tests using Newey-West standard errors with $h + 1$ lags. ***, ** and * denote significance at the 1%, 5%, and 10% level, respectively.

Table A.10: Coverage rates (pre COVID)

	RGDP		UNRATE		PGDP		CPI	
h	68%	90%	68%	90%	68%	90%	68%	90%
PANEL A: MDS Model								
0	47.50***	77.50***	88.33***	98.33***	57.50**	87.50	66.67	90.83
1	52.94***	78.15***	84.03***	98.32***	62.18	88.24	60.50*	87.39
2	52.54***	80.51**	82.20***	96.61***	62.71	88.14	62.71	88.14
3	49.57***	81.20*	77.78	94.87	64.10	90.60	64.10	88.03
4	56.90**	84.48	71.55	93.10	61.21	89.66	70.69	89.66
5	58.26*	87.83	70.43	93.04	60.87	91.30	69.57	89.57
6	57.02**	86.84	71.05	93.86	61.40	90.35	70.18	89.47
7	59.29*	88.50	68.14	92.92	61.06	94.69**	69.91	91.15
8	62.50	86.61	62.50	91.96	64.29	95.54***	71.43	91.96
9	61.26	87.39	57.66	91.89	66.67	94.59**	73.87	91.89
10	61.82	87.27	56.36	90.91	65.45	98.18***	74.55	91.82
11	63.30	87.16	55.96	90.83	68.81	98.17***	75.23	92.66
12	68.52	90.74	58.33	89.81	71.30	97.22***	74.07	92.59
13	67.29	88.79	57.94	88.79	74.77	98.13***	76.64	93.46
14	66.04	90.57	58.49	88.68	78.30**	98.11***	77.36	93.40
15	67.62	89.52	56.19	86.67	79.05**	98.10***	77.14	94.29
16	69.23	91.35	58.65	87.50	77.88*	99.04***	78.85	94.23
PANEL B: VAR Model								
0	50.00***	81.67***	76.67*	96.67***	58.33**	87.50	66.67	92.50
1	56.30**	80.67***	79.83***	94.12	63.87	85.71	62.18	87.39
2	58.47*	83.90*	78.81**	95.76*	67.80	90.68	66.10	88.14
3	52.99***	82.91*	78.63*	94.02	67.52	91.45	67.52	90.60
4	57.76*	87.93	69.83	93.97	66.38	91.38	67.24	87.93
5	60.87	88.70	66.96	93.04	69.57	93.91	73.04	92.17
6	60.53	88.60	64.91	92.98	69.30	93.86	70.18	92.98
7	66.37	89.38	63.72	92.92	69.03	95.58**	70.80	92.92
8	64.29	88.39	60.71	91.07	71.43	94.64	74.11	91.96
9	64.86	87.39	56.76	90.99	72.97	92.79	72.07	92.79
10	65.45	89.09	56.36	89.09	71.82	96.36***	72.73	91.82
11	69.72	87.16	51.38**	87.16	76.15	97.25***	77.98	92.66
12	66.67	88.89	49.07**	86.11	75.93*	98.15***	75.93	93.52
13	72.90	88.79	47.66**	86.92	73.83	98.13***	76.64	92.52
14	70.75	91.51	48.11**	85.85	76.42	98.11***	76.42	93.40
15	68.57	91.43	46.67**	84.76	76.19	98.10***	76.19	94.29
16	71.15	91.35	46.15*	83.65	78.85*	99.04***	78.85	94.23

Note: Coverage rates for uncertainty bands with nominal levels of 68% and 90% for out-of-sample forecasts at quarterly forecast horizons, h. Evaluation window from 1990Q1 through 2019Q4 (and as far as realized values are available). Reflecting the availability of annual SPF forecasts, forecasts for inflation in CPI and GDP prices are evaluated only up to $h = 12$, and $h = 8$, respectively. Significance assessed by Diebold-Mariano tests using Newey-West standard errors with $h + 1$ lags. ***, ** and * denote significance at the 1%, 5%, and 10% level, respectively.

Table A.11: Coverage rates (full sample)

	RGDP		UNRATE		PGDP		CPI	
h	68%	90%	68%	90%	68%	90%	68%	90%
PANEL A: MDS Model								
0	48.53***	78.68***	86.76***	96.32***	55.15***	83.09*	66.18	88.97
1	52.59***	77.04***	82.22***	97.04***	60.00*	83.70	59.26**	84.44
2	52.99***	80.60***	79.85**	94.78*	60.45	83.58	60.45	84.33
3	50.38***	81.20*	75.94	92.48	61.65	85.71	61.65	84.21
4	56.82**	82.58	71.21	90.15	59.09**	84.85	67.42	85.61
5	58.02**	84.73	69.47	89.31	57.25**	86.26	65.65	84.73
6	56.15**	84.62	69.23	89.23	56.92*	85.38	65.38	85.38
7	57.36**	83.72	66.67	88.37	56.59**	89.15	65.89	86.82
8	60.16	82.03	61.72	88.28	60.16	90.62	66.41	86.72
9	58.27**	82.68	57.48	88.19	62.20	88.98	68.50	87.40
10	59.52*	82.54	56.35	87.30	60.32	92.06	69.05	87.30
11	60.80*	82.40	56.00	87.20	63.20	90.40	69.60	88.00
12	65.32	86.29	57.26	86.29	65.32	89.52	68.55	87.90
13	63.41	84.55	57.72	86.18	68.29	90.24	70.73	88.62
14	62.30	85.25	58.20	86.07	71.31	90.16	71.31	88.52
15	62.81	85.12	57.85	84.30	71.90	90.91	71.07	89.26
16	65.00	86.67	60.00	86.67	70.83	90.83	72.50	89.17
PANEL B: VAR Model								
0	50.00***	81.62***	76.47*	94.85**	55.88***	84.56*	66.18	91.18
1	55.56***	79.26***	77.78**	93.33	62.22	82.22**	60.74	84.44
2	58.21**	82.84**	77.61*	94.03	65.67	85.82	63.43	84.33
3	53.38***	82.71*	78.20*	91.73	64.66	86.47	64.66	86.47
4	56.06**	85.61	68.94	90.91	62.88	86.36	64.39	84.09
5	59.54	86.26	66.41	89.31	64.89	87.79	68.70	87.02
6	58.46**	86.15	63.85	88.46	64.62	87.69	66.15	88.46
7	64.34	86.05	62.02	88.37	64.34	89.92	65.89	87.60
8	62.50	84.38	60.16	87.50	65.62	88.28	68.75	86.72
9	62.20	83.46	56.69*	86.61	66.93	86.61	66.14	88.19
10	62.70	84.92	56.35*	85.71	65.87	89.68	67.46	87.30
11	66.40	83.20	52.00**	83.20	69.60	88.80	72.00	88.00
12	63.71	84.68	50.00**	82.26	69.35	89.52	70.16	87.90
13	69.11	84.55	48.78**	82.93	67.48	90.24	70.73	87.80
14	66.39	86.89	49.18**	82.79	69.67	89.34	69.67	88.52
15	64.46	86.78	48.76**	82.64	69.42	88.43	69.42	89.26
16	66.67	87.50	48.33*	81.67	71.67	90.00	71.67	89.17

Note: Coverage rates for uncertainty bands with nominal levels of 68% and 90% for out-of-sample forecasts at quarterly forecast horizons, h. Evaluation window from 1990Q1 through 2023Q4 (and as far as realized values are available). Reflecting the availability of annual SPF forecasts, forecasts for inflation in CPI and GDP prices are evaluated only up to $h = 12$, and $h = 8$, respectively. Significance assessed by Diebold-Mariano tests using Newey-West standard errors with $h + 1$ lags. ***, ** and * denote significance at the 1%, 5%, and 10% level, respectively.

Figure A.19: GDP price inflation PITs

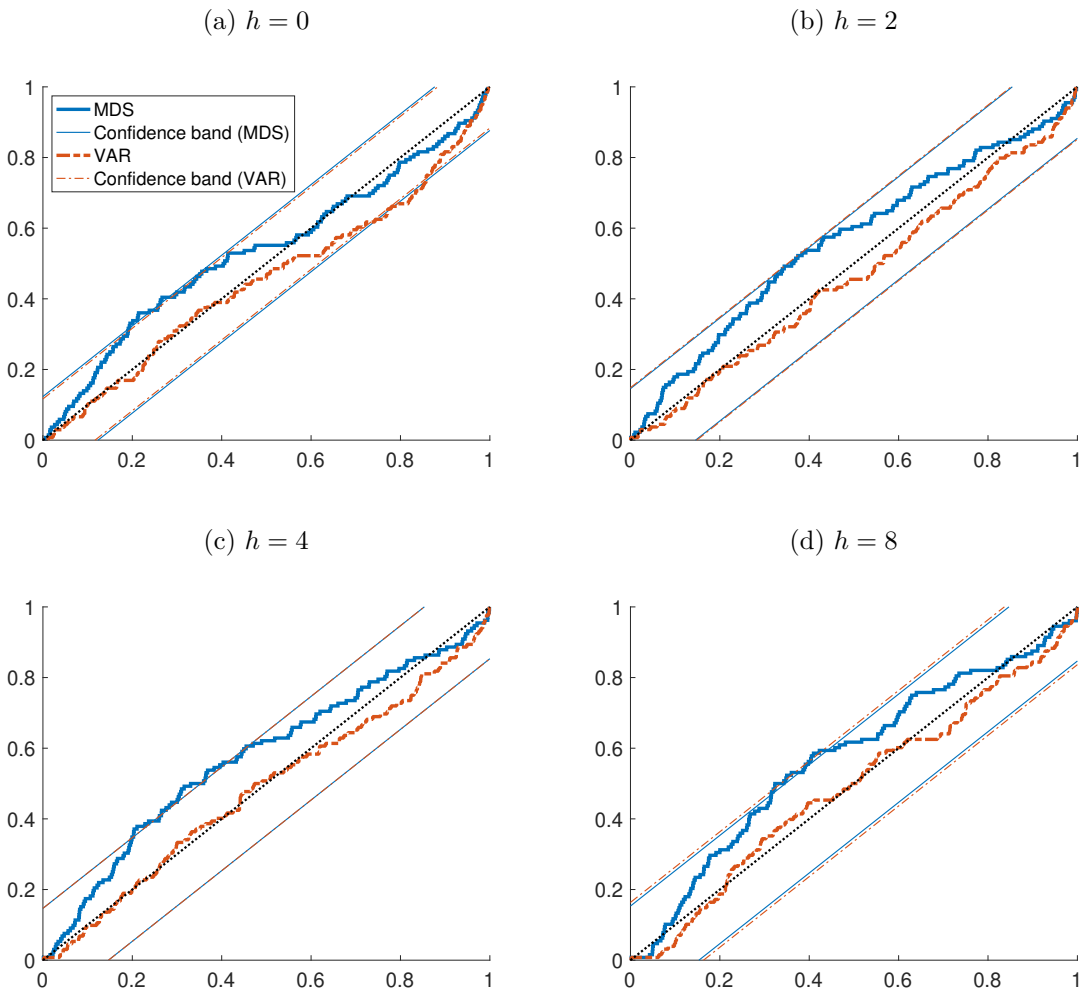

Notes: Empirical cumulative distributions of probability integral transforms (PITs) for inflation in the GDP price index at selected quarterly forecast horizons. All forecasts are generated out of sample by our MDS and VAR models, and evaluated over an evaluation window from 1990Q1 through 2023Q4 (and as far as realized values are available). 95% confidence bands for tests of correct calibration from Rossi and Sekhposyan (2019); computed separately for each model, but with nearly identical plot lines.

Figure A.20: CPI inflation PITs

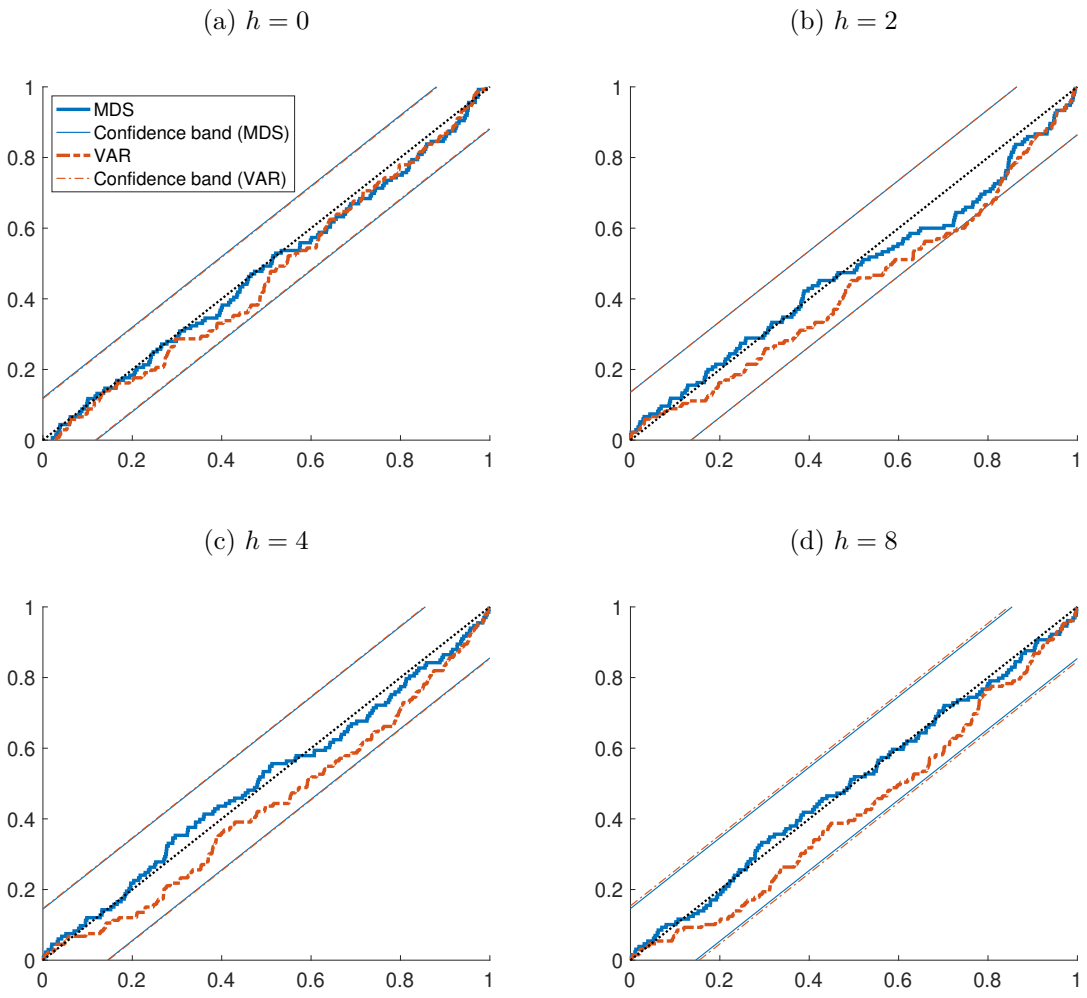

Notes: Empirical cumulative distributions of probability integral transforms (PITs) for CPI inflation at selected quarterly forecast horizons. All forecasts are generated out of sample by our MDS and VAR models, and evaluated over an evaluation window from 1990Q1 through 2023Q4 (and as far as realized values are available). 95% confidence bands for tests of correct calibration from Rossi and Sekhposyan (2019); computed separately for each model, but with nearly identical plot lines.

Figure A.21: Log scores

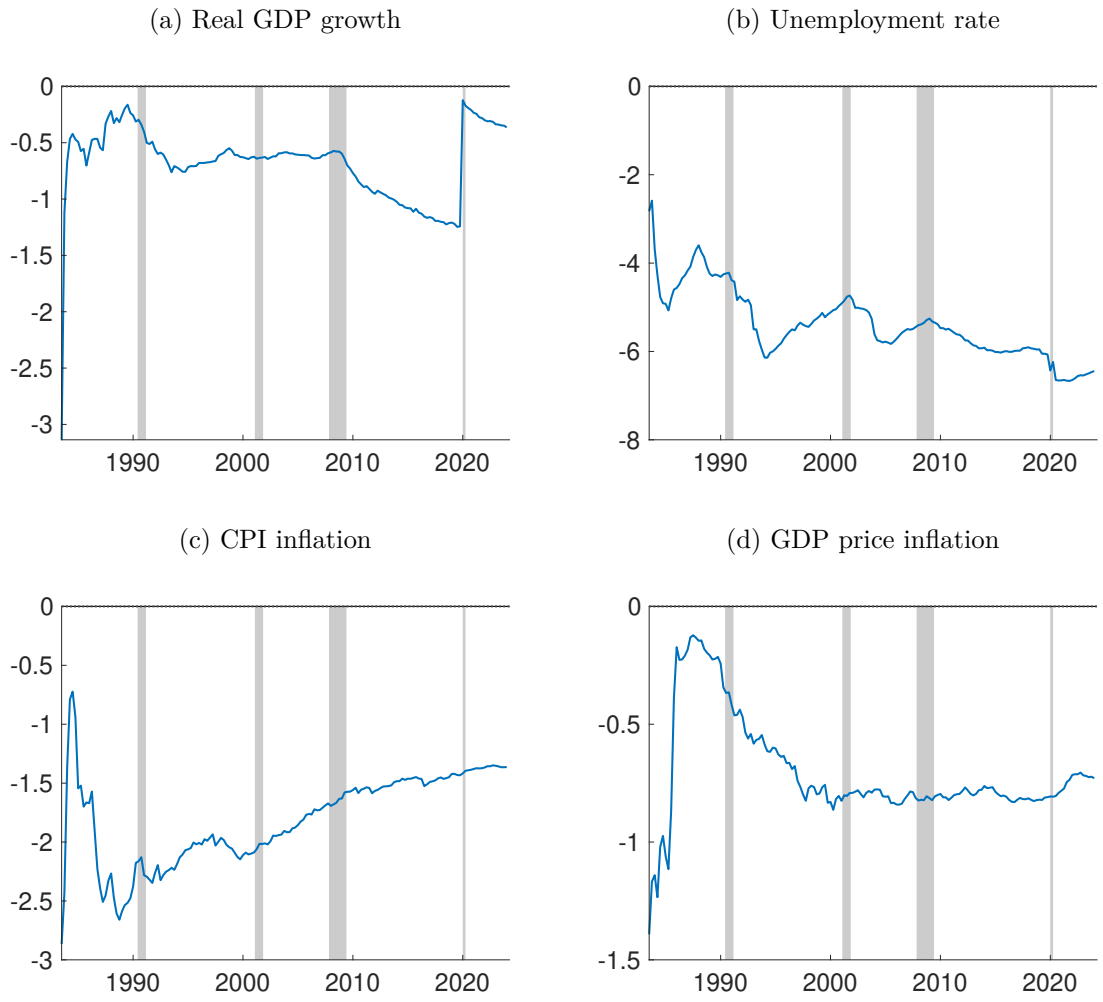

Notes: Figures show recursive means (across time) of the differences in 1-step-ahead log predictive scores for the MDS less the VAR model (negative entries mean the MDS model has the better score). These score differences are closely related to differences in log marginal likelihoods; the likelihoods equal sums of 1-step-ahead log predictive scores. Shaded areas depict NBER recessions.

Figure A.22: Endpoint estimates (MDS)

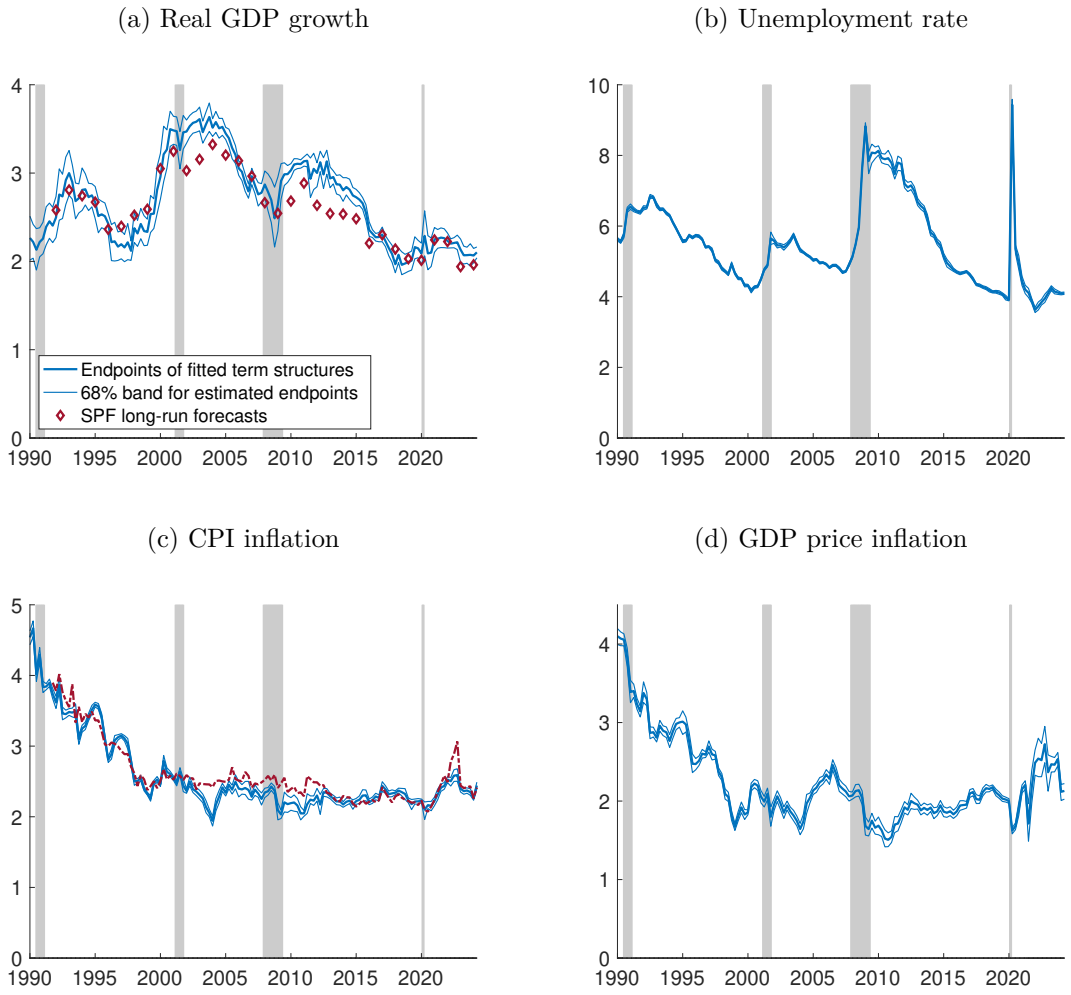

Notes: End-of-sample estimates of endpoints, y_t^*, for the MDS model. Estimates reflect posterior means and 68% bands, obtained from MCMC model estimates over growing samples (all using data since 1968Q4), as used in our out-of-sample forecast simulations. For GDP growth and CPI, corresponding long-run forecasts from the SPF (for 10-year ahead average growth) are shown as well.

Figure A.23: Endpoint estimates (VAR)

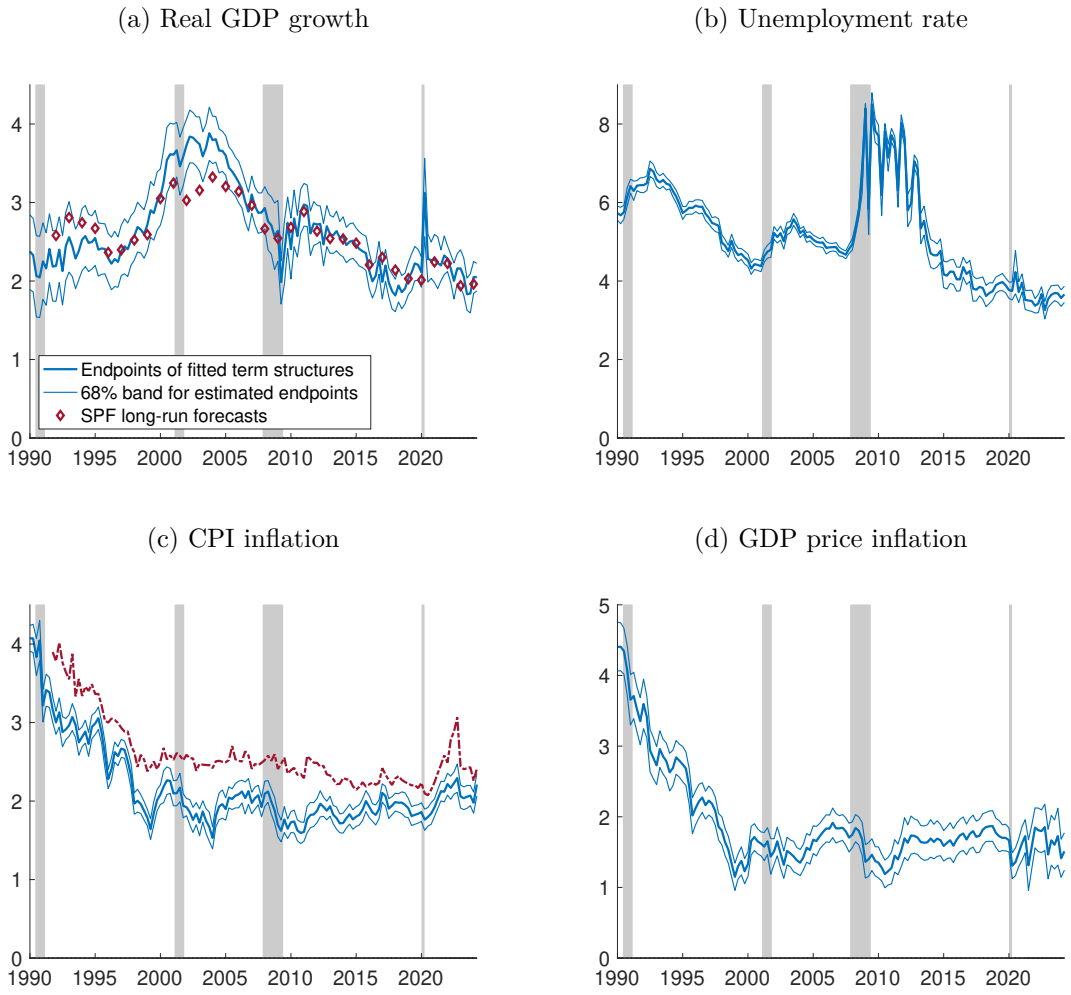

Notes: End-of-sample estimates of endpoints, y_t^*, for the VAR model. Estimates reflect posterior means and 68% bands, obtained from MCMC model estimates over growing samples (all using data since 1968Q4), as used in our out-of-sample forecast simulations. For GDP growth and CPI, corresponding long-run forecasts from the SPF (for 10-year ahead average growth) are shown as well.

References

Angeletos, George-Marios, Zhen Huo, and Karthik A. Sastry (2021), "Imperfect macroeconomic expectations: Evidence and theory," NBER Macroeconomics Annual, 35, 1–86, https://doi.org/10.1086/712313.

Aruoba, S. Boragan (2020), "Term structures of inflation expectations and real interest rates," Journal of Business & Economic Statistics, 38, 542–553, https://doi.org/10.1080/07350015.2018.1529599.

Carriero, Andrea, Joshua C. C. Chan, Todd E. Clark, and Massimiliano Marcellino (2022a), "Corrigendum to: Large Bayesian vector autoregressions with stochastic volatility and non-conjugate priors," Journal of Econometrics, 227, 506–512, https://doi.org/10.1016/j.jeconom.2021.11.010.

Carriero, Andrea, Todd E. Clark, and Massimiliano Marcellino (2016), "Common drifting volatility in large Bayesian VARs," Journal of Business & Economic Statistics, 34, 375–390, https://doi.org/10.1080/07350015.2015.1040116.

——— (2019), "Large Bayesian vector autoregressions with stochastic volatility and non-conjugate priors," Journal of Econometrics, 212, 137–154, https://doi.org/10.1016/j.jeconom.2019.04.024.

Carriero, Andrea, Todd E. Clark, Massimiliano Marcellino, and Elmar Mertens (2022b), "Addressing COVID-19 outliers in BVARs with stochastic volatility," Review of Economics and Statistics, forthcoming, https://doi.org/10.1162/rest_a_01213.

Carvalho, Carlos M., Nicholas G. Polson, and James G. Scott (2010), "The horseshoe estimator for sparse signals," Biometrika, 97, 465–480, https://doi.org/10.1093/biomet/asq017.

Chan, Joshua C. C. (2020), "Large Bayesian VARs: A flexible Kronecker error covariance structure," Journal of Business & Economic Statistics, 38, 68–79, https://doi.org/10.1080/07350015.2018.1451336.

Chan, Joshua C. C., and Ivan Jeliazkov (2009), "Efficient simulation and integrated likelihood estimation in state space models," International Journal of Mathematical Modelling and Numerical Optimization, 1, 101–120, https://doi.org/10.1504/IJMMNO.2009.03009.

Chib, Siddhartha, and Ivan Jeliazkov (2006), "Inference in semiparametric dynamic models for binary longitudinal data," Journal of the American Statistical Association, 101, 685–700, https://doi.org/10.1198/016214505000000871.

Clark, Todd E., Michael W. McCracken, and Elmar Mertens (2020), "Modeling time-varying uncertainty of multiple-horizon forecast errors," The Review of Economics and Statistics, 102, 17–33, https://doi.org/10.1162/rest_a_00809.

Clark, Todd E., and Francesco Ravazzolo (2015), "Macroeconomic forecasting performance under alternative specifications of time-varying volatility," Journal of Applied Econometrics, 30, 551–575, https://doi.org/10.1002/jae.2379.

Coibion, Olivier, and Yuriy Gorodnichenko (2015), "Information rigidity and the expectations formation process: A simple framework and new facts," American Economic Review, 105, 2644–2678, https://doi.org/10.1257/aer.20110306.

Crump, Richard K., Stefano Eusepi, Emanuel Moench, and Bruce Preston (2023), "The term structure of expectations," in Handbook of Economic Expectations eds. by Rüdiger Bachmann, Giorgio Topa, and Wilbert van der Klaauw: Academic Press, chap. 17, 507–540, https://doi.org/10.1016/B978-0-12-822927-9.00025-2.

Del Negro, Marco, and Giorgio E. Primiceri (2015), "Time varying structural vector autoregressions and monetary policy: A corrigendum," Review of Economic Studies, 82, 1342–1345, https://doi.org/10.1093/restud/rdv024.

Durbin, J., and S.J. Koopman (2002), "A simple and efficient simulation smoother for state space time series analysis," Biometrika, 89, 603–615, https://doi.org/10.1093/biomet/89.3.603.

Hayashi, Fumio (2000), Econometrics, Princeton, NJ: Princeton University Press.

Jacquier, Eric, Nicholas G. Polson, and Peter E. Rossi (2004), "Bayesian analysis of stochastic volatility models with fat-tails and correlated errors," Journal of Econometrics, 122, 185–212, https://doi.org/10.1016/j.jeconom.2003.09.001.

Kadiyala, K. Rao, and Sune Karlsson (1997), "Numerical methods for estimation and inference in bayesian VAR-models," Journal of Applied Econometrics, 12, 99–132, https://doi.org/doi.org/10.1002/(SICI)1099-1255(199703)12:2<99::AID-JAE429>3.0.CO;2-A.

Kim, Sangjoon, Neil Shephard, and Siddhartha Chib (1998), "Stochastic volatility: Likelihood inference and comparison with ARCH models," The Review of Economic Studies, 65, 361–393, https://doi.org/10.1111/1467-937X.00050.

Makalic, Enes, and Daniel F. Schmidt (2016), "A simple sampler for the horseshoe estimator," IEEE Signal Processing Letters, 23, 179–182, https://doi.org/10.1109/LSP.2015.2503725.

Mariano, Roberto S., and Yasutomo Murasawa (2003), "A new coincident index of business cycles based on monthly and quarterly series," Journal of Applied Econometrics, 18, 427–443, https://doi.org/10.1002/jae.695.

Mertens, Elmar (2023), "Precision-based sampling for state space models that have no measurement error," Journal of Economic Dynamics and Control, 154, p. 104720, https://doi.org/10.1016/j.jedc.2023.104720.

Omori, Yasuhiro, Siddhartha Chib, Neil Shephard, and Jouchi Nakajima (2007), "Stochastic volatility with leverage: Fast and efficient likelihood inference," Journal of Econometrics, 140, 425–449, https://doi.org/10.1016/j.jeconom.2006.07.008.

Patton, Andrew J., and Allan Timmermann (2011), "Predictability of output growth and inflation: A multi-horizon survey approach," Journal of Business & Economic Statistics, 29, 397–410, https://doi.org/10.1198/jbes.2010.08347.

Prüser, Jan (2021), "The horseshoe prior for time-varying parameter VARs and monetary policy," Journal of Economic Dynamics and Control, 129, https://doi.org/10.1016/j.jedc.2021.10418.

Rossi, Barbara, and Tatevik Sekhposyan (2019), "Alternative tests for correct specification of conditional predictive densities," Journal of Econometrics, 208, 638–657, https://doi.org/10.1016/j.jeconom.2018.07.008.